ATTENUATED TOTAL REFLECTION ENHANCED PHOTOEJECTION FROM CATHODES

By:

E. Robert Schildkraut

Dr. Tomas Hirschfeld

Final Report

15 June 1969

Contract No.: NAS 2-4661

Contract Monitor: William D. Gunter, Jr.

Prepared For:

NASA AMES RESEARCH CENTER
Moffett Field, California 94035

BLOCK ENGINEERING, INC.
19 Blackstone Street
Cambridge, Massachusetts 02139

ATTENUATED TOTAL REFLECTION ENHANCED PHOTOEJECTION FROM CATHODES

By:

E. Robert Schildkraut

Dr. Tomas Hirschfeld

Final Report

15 June 1969

Contract No.: NAS 2-4661

Contract Monitor: William D. Gunter, Jr.

Prepared For:

NASA AMES RESEARCH CENTER
Moffett Field, California 94035

BLOCK ENGINEERING, INC.
19 Blackstone Street
Cambridge, Massachusetts 02139

TABLE OF CONTENTS

LIST OF FIGURES

LIST OF FIGURES (CONT'D)

LIST OF FIGURES (CONT'D)

LIST OF FIGURES (CONT'D)

ACKNOWLEDGMENT

Block Engineering, Inc. wishes to acknowledge the support of the NASA Ames Research Center in its research on the subject of Attenuated Total Reflection and its application to efficient photocathodes. We would particularly like to thank our Contract Monitor, William D. Gunter,Jr. for his continued cooperation and valuable suggestions throughout the duration of this program. His patience, in particular, has been most welcome.

ATR ENHANCED PHOTO-EJECTION FROM CATHODES

FINAL REPORT

I. Summary

Since January of 1968 Block Engineering, Inc. has been involved in a systematic investigation of Attenuated Total Reflection Enhanced Photocathodes. The ATR cathodes have exhibited significantly improved quantum efficiency due to their very high absorption of incident radiation in an extremely thin (and consequently highly efficient) photo-emissive layer. The Fresnel optical equations governing the interaction between radiation and an interface of two different media have been investigated theoretically and confirmed by experiment. The work was carried on using pure metallic cathodes in the ultra violet region of the spectrum and later proceded to an investigation of the alkali metals, extending the spectral sensitivity of the cathodes into the blue-visible regions of the spectrum. Quantum efficiency gains from 2 to a factor of 10 have been observed and partial confirmation of the theoretical absorption of incident radiation vs. incidence angle have been obtained.

II. Attenuated Total Reflection - An Introduction

The application of Attenuated Total Reflection (ATR) to the fabrication of highly efficient photocathodes is a new technique developed at Block Engineering, Inc. For the benefit of those who are not familiar with internal reflection phenomena as applied to photocathodes, a simplified schematic diagram is shown in the first figure (1).

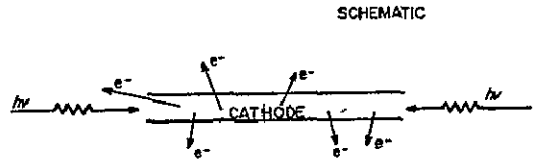

The technique is based upon decoupling the functions of absorption of a photon and emission of an electron. This has been accomplished schematically by (a) injecting photons edgewise into a very thin cathode, resulting in large absorption of incident radiation, and (b) ejection of most electrons through the cathode surface along the short dimensions. Thus, the probability of escape is improved since fewer collisions occur as the photo-electron leaves the medium along the short dimension.

The actual mechanism is more sophisticated although the fundamental geometry shown in the next figure (2) is also practical.

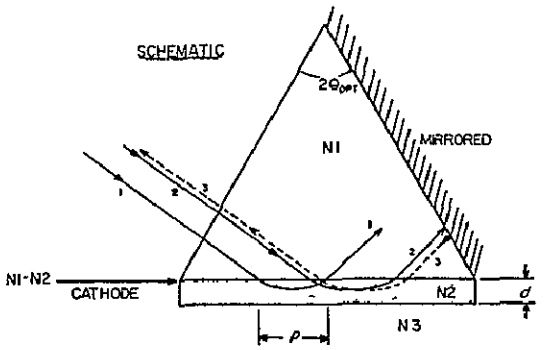

Light rays incident on a boundary between two media are totally reflected at or above the critical angle θ_{c_1}, depending on the relative refractive indices of the two media[1]. During total reflection, the ray actually penetrates a fraction of a wavelength into the second medium and is deflected back into medium 1. By appropriate coating thickness control, the apparent absorption path length in the second medium (p) can be made large compared to the thickness (d) of medium 2, i.e.

$$\frac{p}{d} \gg 1$$

The primary reason for this enhanced absorption is the large value of the electric field vector in the x and y directions at the interface. If medium 2 is an absorbing material of appropriate refractive index, then the radiation is attenuated while traveling along the coating and we have Attenuated Total Reflection $(ATR)^2$.

The ratio $\frac{p}{d}$ is of fundamental conceptual importance since this effect is primarily responsible for the improvement in quantum efficiency of the cathode. Using the ATR phenomenon a very thin cathode can be made to absorb most of the incident radiation (normally this would require a very thick cathode)

but it can still remain thin enough so that there is a very high probability that any photoelectron generated will reach the surface. In fact, the collision/capture probability can be made so low that many or most of the electrons with initial velocities toward the n_1 n_2 (substrate) interface can still escape into vacuum after being reflected at n_1 n_2 and traveling back through the cathode[3]. Weakly absorbing photoemitters, heretofore useless as cathodes, can be used in the ATR mode.

Note that in this illustration (2) light ray #2 penetrates the ATR cathode on its way toward the mirrored surface of the prism, is reflected from it (ray 3 shown displaced), and passes a second time through the ATR cathode before it is lost to the system. This type of simple reflection can further increase the efficiency of such a cathode. More complicated multiple reflection geometries have also been devised and their effect on aperture and imaging criteria have been studied[4].

Although many workers have been experimenting in the field of multiple reflection and interference photocathodes[5,6], the work up to now has consisted primarily of specialized geometrical optical modifications of standard commercially available photocathodes[5]. The large angular restriction and reduced field of view which result from the use of these geometries [7] are just two of the many disadvantages inherent in this approach. We have attempted, in our work, to investigate the performance of optimized Attenuated Total Reflection (ATR) photocathodes, which are manufactured specifically for ATR use. Since these new cathodes are on the order of few atomic layers thick, an accurate and stable method for the manufacture and control of such oligatomic films[8,9] had to be devised and implemented.

Fabrication[10] of the actual experimental cathodes had to be controlled within extremely precise tolerances through the use of Fizeau fringe techniques and fringes of equal chromatic order (FECO)[11]. We were able to maintain coatings of heavy metals 10 to 50Å in thickness with ± 5Å accuracy.

The optical step caused by a deposited film on a polished optical test flat was measured with specially built interferometric instrumentation[12], since no commercial devices can resolve steps below 100Å with the required accuracy. A typical fringe step pattern illuminated by Sodium light $\bar{\lambda}$ = 5890Å is shown in the next figure (3) and in the Figure 1 on the next page.

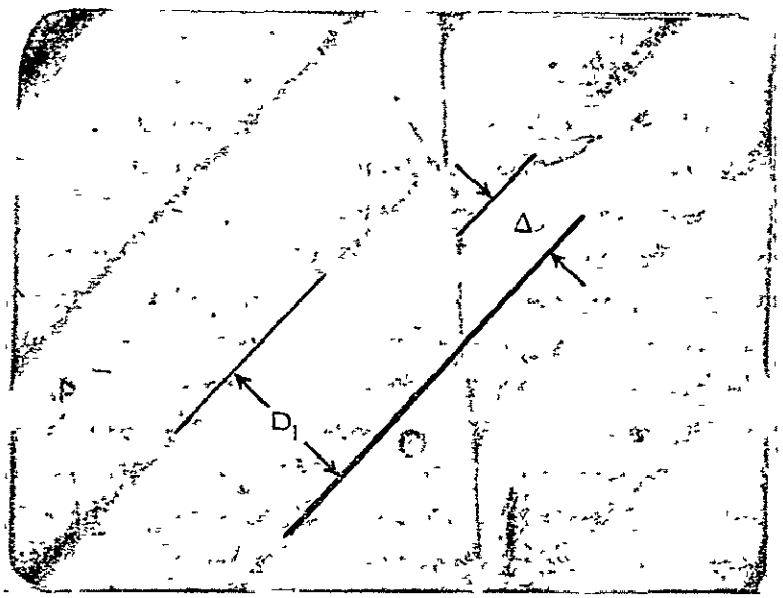

The step height (h) can be easily evaluated as it is related to fringe displacement D_1

$$h(\text{Å}) = \frac{\Delta}{D_1} \times 2945\text{Å}$$

for Sodium illumination.

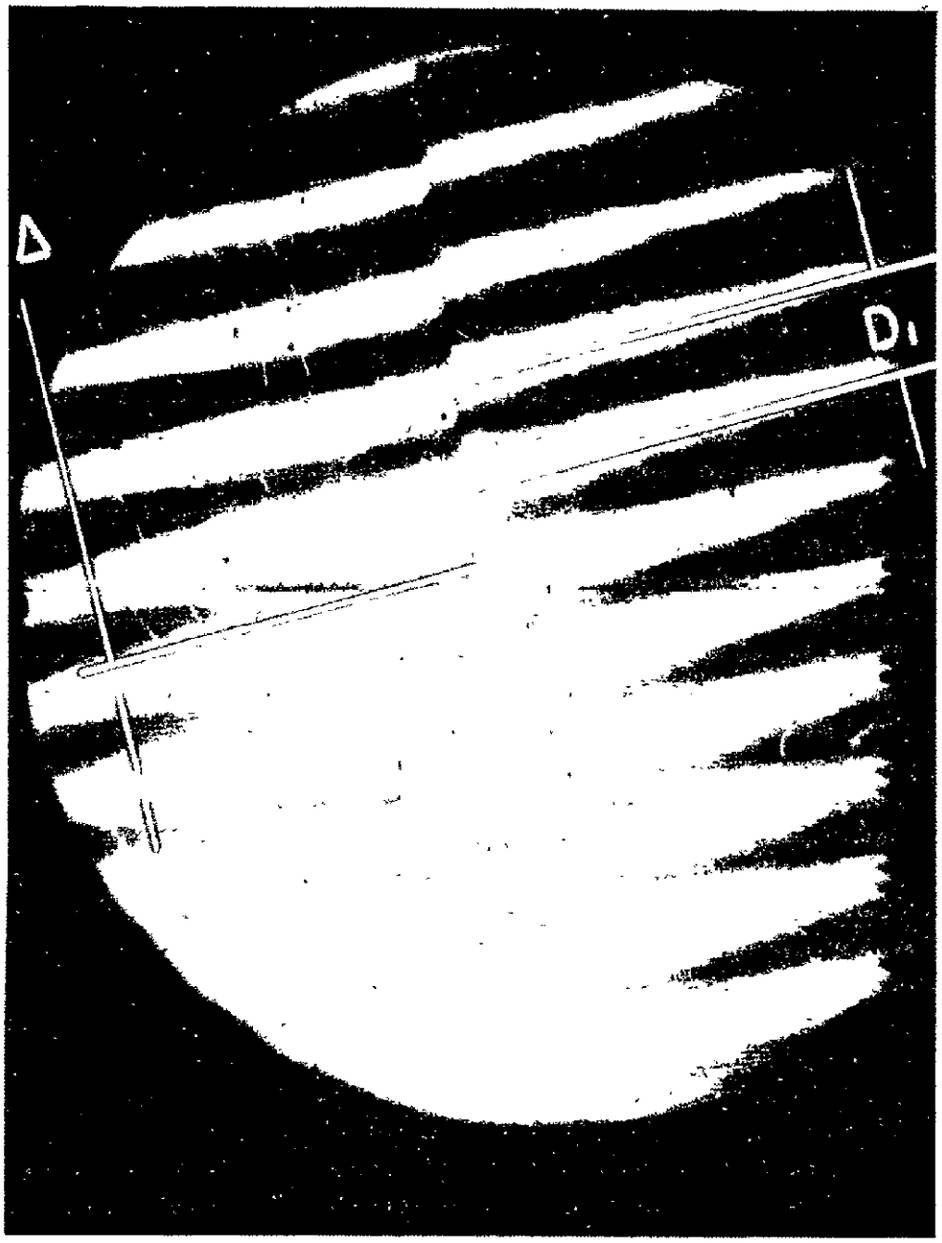

Figure 1
Fizeau Interferometer
Step Measurement

Mass deposit monitors of the resonant crystal or microbalance type cannot be used for absolute calibration since the density ρ of the coatings for films of 100Å and below may not bear any relation to the bulk density of the material[13,14]

Our first experiments, used spectroscopically pure gold as a solar blind photocathode, because of the ease with which it can be evaporated as a thin film and because of its resistance to contamination. The absorption data indicate agreement with the theoretical predictions, although we have not confirmed the theory in enough detail. The purpose of this report is to delineate our final results under this contract.

III. An Introduction to Present Work

The phenomenon of Attenuated Total Reflection and its application to enhanced photoemission from cathodes has been explored to some extent by Gunter, Hirschfeld and several other workers[15,16]. In most cases standard photodetectors were modified by the use of an ATR "prism" optically attached to the surface of a standard commercial detection device.

Unlike previous investigations, Block has pursued an essentially new approach by tailoring photocathodes specifically for Attenuated Total Reflection behavior. We have attempted to achieve a large field of view (at least 20° for 2 to 4 reflections), large aperture area, and a collection of geometries suitable for use in specific experiments. The geometries include a multiple reflection uniline system, a two reflection prism scheme, a unipoint rosette system for use with small spot cathodes, and a multiple internal reflection prism* as examples. Standard internal reflection elements as described by Harrick[17] have also been contemplated during the course of the experiments in order to illustrate the wide variety of multiple reflection geometries compatible with the technique.

Over the period of this work we have attempted to tailor specific metallic and alkali metal photocathodes[18] for use in the ultra violet and blue-visible regions of the spectrum in Attenuated Total Reflection mode. The extremely thin cathodes required, and the particular procedures necessary for optimizing photoemission[19] in this spectral region are one of the subjects of this study.

---

* Suggested by W.D. Gunter, Jr.

Preliminary investigations by Dr. Hirschfeld indicate that the various metallic and alkali coatings to be used as cathodes must be applied to the substrate in extremely thin controlled films whose dimensions and properties tax present state-of-the-art measuring devices[20]. Our basic apparatus consists of an ultra-high vacuum evaporator system with provisions for electron beam, filament thermal evaporation, and sputtering. The system is capable of low rate and flash evaporation techniques. It has been reworked specifically for ultra thin film coatings of few angstroms thickness but can be used for the evaporation of almost any material(s) in practically any thickness desired. The necessary design criteria pertinent to the system which enable highly controlled thin films to be attained are covered in detail in a separate technology report. Specific techniques for obtaining ultra pure thin films and for calibration have also been reported in great detail separately in technical notes for use by NASA in separate publications if desired.

Special cleanliness procedures have been necessitated by the contaminating effect of extremely small amounts of Mercury[21] and other (hard to control) contaminants. The danger of microscopic contamination has necessitated specialized handling procedures. We feel these would be of general interest to all those working in thin films.

Our procedure in brief is to manufacture the ultra thin coating on the necessary substrate and measure the thickness as it is being deposited in the vacuum. We immediately subsequently test the quantum efficiency and absorption of incident radiation vs. angle of the cathode. The thin film

cathode is then tested without being removed from its holder and without breaking vacuum (absolutely necessary in the case of alkali metals), using a photometer system which can measure the optical parameters* of the coating necessary for evaluation. The sample cathode, if it is of stable material, may later be removed from the vacuum chamber and placed on a goniometer for confirmation of absorption vs. angle measurements. A light source and monochromator with a collection of several gratings, blazed for different regions of the spectrum, provide ultra violet and visible radiation for the photometer. These are also used as the source in testing the efficiency of the photocathode produced on the substrate. An auxiliary electron multiplier string is used adjacent to the cathode and forms a photomultiplier whose output is connected to a synchronous amplifier for measurement of the extremely low currents expected. Such an open structure photomultiplier enables testing of the cathode in a geometry similar to that which will be used in any practical application.

---

* Primarily absorption and polarization.

IV. System Configuration and Description

In the block diagram of the system Figure 2, the basic system functions are outlined. The high vacuum system is necessary for both coating and the testing operation. Ultra-high vacuum is necessary in order to keep the absorption rate of residual gases low enough so that low deposition rates can be used without the danger of forming a monolayer[22] of residual gas on the substrate surface. Pressures in the low 10^{-7} and 10^{-8} Torr range can be achieved in our system with a liquid nitrogen optically blind cold trap. Low ambient pressures are also necessary in view of the fact that extremely high voltages are used on the dynode string and the presence of significant numbers of generated ions in the chamber could cause destructive bombardment of the dynodes or the cathode itself.

The substrate is located on a rotatable control fixture which enables stabilization and control of its temperature, if necessary, in order to achieve some measure of adjustment in the crystallite growth rate[23] on the surface.

The source and monochromator are used for both the photometer system and the photocathode efficiency measurements in conjunction with the photoemission electronics (synchronous amplifier) and the electron multiplier structure.

The thickness monitor is used during evaporation to control both the rate and the final thickness of the deposit. The electron gun and thermal or sputtering sources are used alternately to heat the sample material to be coated or to heat the substrate itself prior to coating.

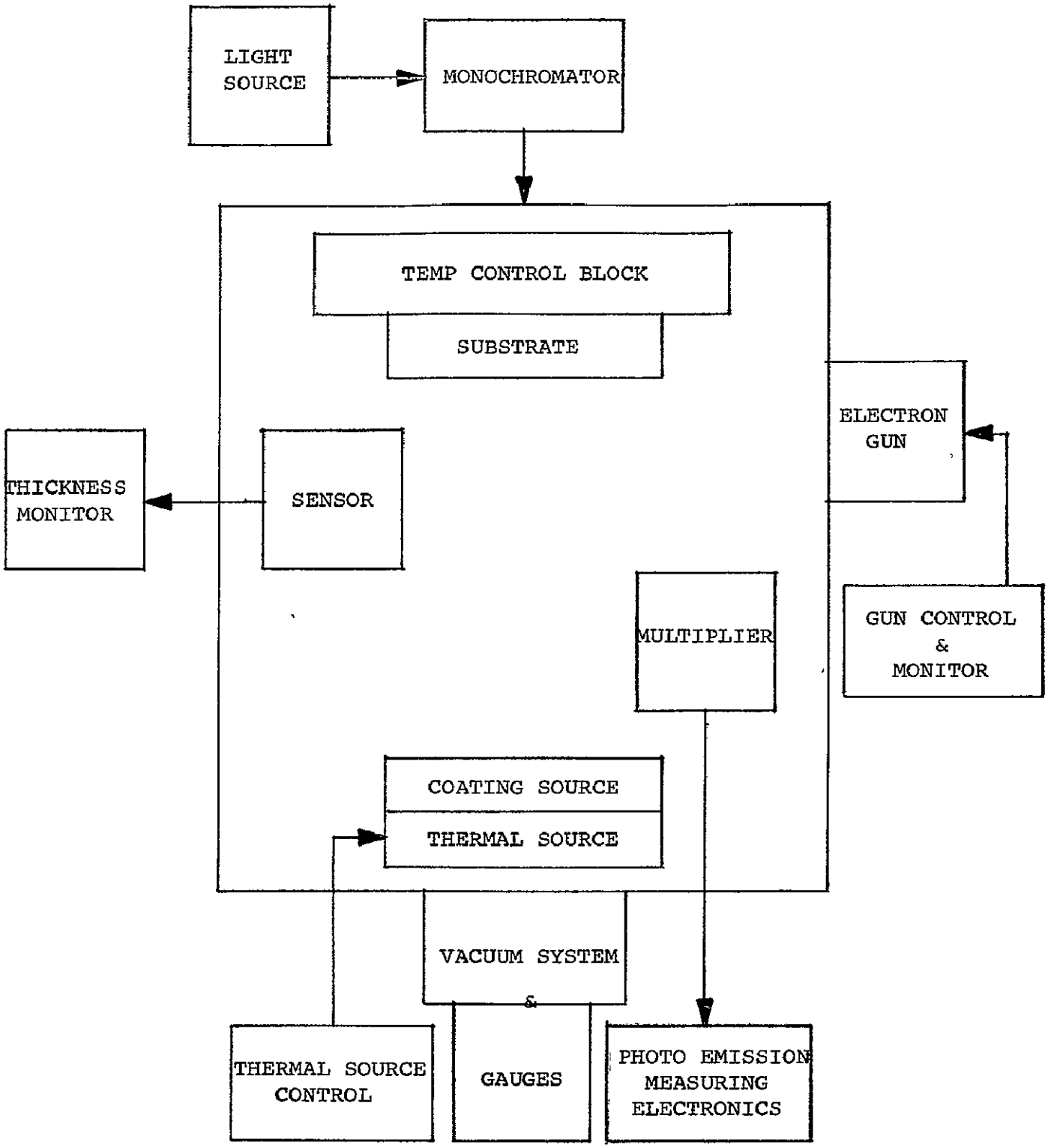

BLOCK DIAGRAM I

Figure 2
System Block Diagram

V. Vacuum System

A water cooled crucible holder is installed to improve the coating control during Platinum evaporation.

A quartz lamp substrate heater and a thermocouple substrate temperature monitor are attached to provide correct substrate temperature for alkali deposition. However, it was found that an increased temperature of the substrate was not beneficial or harmful during alkali deposition and consequently this extra step in the procedure was eliminated. Substrate temperature within wide limits does not seem to affect the rate of deposition of the cathode material or its effective quantum efficiency.

BLOCK DIAGRAM

The schematic functional diagram in Figure 3 illustrates the various manipulations and controls available for handling the cathode while inside the system. Although the present system is particularly suited to the manufacture of ultra thin cathodes, it has sufficient flexibility to coat practically any usable geometry and will allow coating almost any known material in any commonly used coating environment. A substantial amount of time was required to modify the vacuum system with all necessary gauges, safety cutouts and monitor functions for ultra thin film control. The rapid pump down time is necessitated by the fact that rapid recycling of the system is desirable in order to manufacture and test a wide variety of cathodes and cathode thicknesses. It is also necessary to have rapid pump down to prevent buildup of an

SCHEMATIC FUNCTIONAL DIAGRAM II

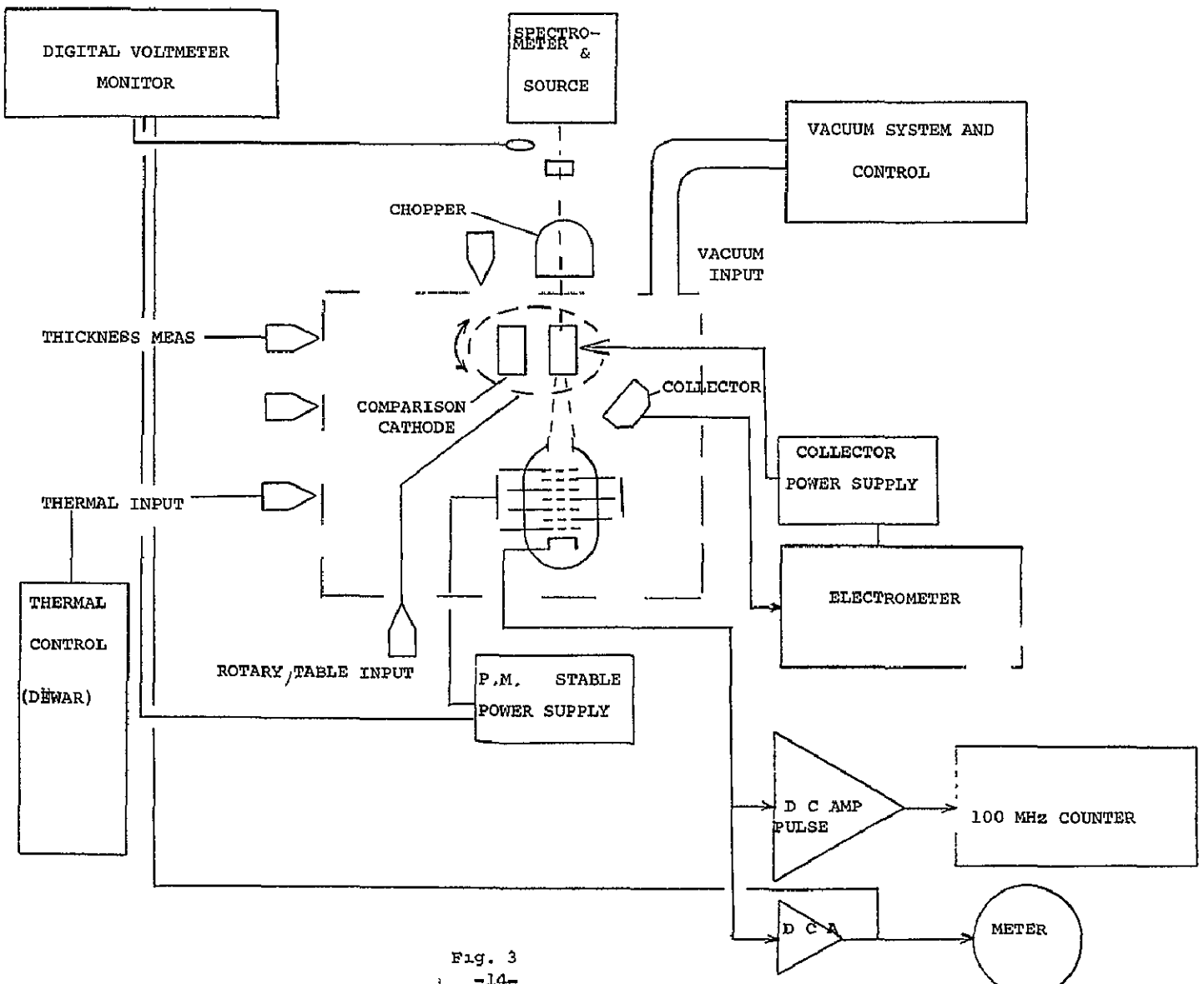

Fig. 3

adsorbed gas layer between the time when glow discharge cleaning ceases and coating begins.

The electron gun, in particular, was overhauled and redesigned for low current (small spot size) operation at a precisely controlled intensity level. Typical electron guns are far too large and uncontrollable for accurate rate control of deposition.

A new Jarrell-Ash ¼ meter monochromator was installed and calibrated using an 1180 line per millimeter grating blazed at 3000Å for the UV work and a similar grating blazed at 6000Å for the blue-visible spectral region. We have available a 1.2μ blazed grating for use on cathodes sensitive in the red and infrared regions of the spectrum.

A tremendous amount of difficulty was encountered in obtaining a suitable system geometry which allows for a coating of the test cell substrate (without coating primary sensors and windows) and which also permitted subsequent testing of the absorbtion of incident radiation by the cathode and its quantum efficiency.

All of the windows and optics used are special quality Lithium Fluoride or quartz. Since Lithium Fluoride cannot be easily cleaned of any deposit, it is necessary to carefully baffle the system such that no deposit arrives at the Lithium Fluoride surfaces in the first place. A suitable manipulator was finally designed which allows motion of the dynode to and away from the cathode while the unit is still in vacuum. A lateral cathode positioner, which can select different areas of the cathode for illumination and testing presents a check on nonuniformity.

Several electron multiplier (dynode) strings have been purchased for use with the cathode. These units are calibrated using a small β-ray source with a half life of approximately 15 years. The β-ray source produces a known quantity of high energy primary electrons which serve to check the gain of the tube with the exception of the first dynode. The first dynode cannot be checked using this method since the high energy electrons produce secondaries not characteristic of those which would be obtained from low velocity primary photoelectrons produced by the cathode.

A complete collection of thermal evaporation electrodes and fixtures was fabricated in order to determine the optimum configuration for controlled coating of these materials in the form of cathodes. Flat plates, discs, boats, crucibles, and capillary evaporation tubes are all available and were investigated with the various metals which were used during the program.

Optics such as polarizers, light choppers and sources have been obtained which enable testing from the vacuum ultra violet region of the spectrum down into the near infrared.

Extensive use was made of coating technology avialable in the immediate geographical area and continuous contact with local coating vendors has enabled us to proceed without the necessity for completely relearning technology which is well known in the field.

The coating has proceeded using the inert precious metals first due to their ease of handling and immunity from contamination and progressing toward the alkali metals which are far more difficult to handle and much more sensitive to contamination and impurity.

Procedure for Calibration, Coating and Testing

Summary

1. Calibrate mass deposit monitor for the material to be deposited. Details are noted in calibration section. Particular attention is paid to films below 50Å in thickness for work in the ultra violet and films from 50 to 250Å in thickness for the blue-visible region.

2. Deposit the necessary thickness of material on a prepared hemicylinder which has been thoroughly cleaned. The cleaning procedure is covered in the cathode formation section.

3. Measure absorption vs. angle for useful response wavelengths of the cathode.

4. Test the cathode for relative quantum efficiency vs. angle and relative quantum efficiency vs. wavelength. Establish the maximum response angle and measure the absolute quantum efficiency for operation at this angle. This will establish the actual enhancement due to the ATR technique. These results are then compared to theoretical predictions for absorption improvement and are related to quantum efficiency enhancement.

5. Determine, by calculation, the optimum thickness of material for single pass geometry using the same cathode material and the same substrate. Multiple pass geometry optimum thickness should be calculated using multipass substrate.

6. Coat a multiple path prism with the calculated optimum thickness cathode. The thickness of the deposited cathode will be established using previously determined optimum thickness and correcting for the multiple pass optical path.

Complete Procedure

The following section outlines in detail the procedures used during the entire program for coating and testing of the cathode materials.

I. Prepare and coat substrate.

1. Use standardized washing methods and glow discharge bombardment to thoroughly clean the substrate prior to coating.

NOTE: Substrate is never left in vacuum with the liquid nitrogen cold trap off.

2. System in coating configuration.

a. Place shutters over all windows to protect surfaces.

b. Position thickness monitor.

c. Substrate cell rotated into coating position with its flat face in the downward direction.

d. Coating shutter closed during evaporate preheat.

e. Total reflection mask in place over a small section of the cathode.

f. All dynode and external monitor electronics are turned off (ion gauge, dynode string, bias mesh, discharge source, etc.).

g. Thickness monitor checked and stabilizing at temperature.

h. Determine substrate temperature and control substrate as necessary.

i. Use electron beam or thermal source for evaporation of cathode.

j. Monitor coating thickness and rate of deposit of the cathode material. Coatings will be uniform across the face of the cathode except for a small section which will be masked by a plate which is not in contact with the cathode substrate. This will leave an area where total reflection occurs and no cathode material is present as a comparison area on the cathode substrate.

3. Test cathode.

a. Evaporate coating shutter closed.

b. Electron gun off.

c. All vacuum gauges turned on.

d. Thickness monitor turned off but remaining in position.

e. Move substrate from coating position to test position.

f. Move dynode multiplier string from shielded position (during the coating sequence) into test position immediately behind the cathode at the optimum distance.

g. Rotate all shutters to uncover windows and the dynodes.

h. Check calibration of dynode string by moving the β-ray source in and out of the photomultiplier field.

4. Illuminate and monitor primary photoelectron current at the cathode using a electrometer if possible.

a. Check photoelectron current vs. angle using the previously calibrated photomultiplier dynode chain.

b. Check for ion feedback.

c. Obtain quantum efficiency estimate.

d. Using the calibrated dynode string obtain an estimate of quantum efficiency vs. wavelength.

e. Using the input beam I without mirror H determine the relative quantum efficiency vs. angle of illumination with the substrate. Subsequently determine quantum efficiency vs. wavelength of the incoming radiation at all convenient points. Absolute calibration of the absorption photometer is carried on using an ultra violet light source powered by radio active Krypton gas which has a half life of approximately 5 years.

5. Check absorption of the incident light.

a. As a function of angle.

b. As a function of thickness of the cathode.

c. As a function of the polarization of the incident light.

d. As a function of the wavelength of the incident light.

6. Strip and recoat the substrate.

NOTE: After several strippings substrate will probably need repolishing. Surface is to be maintained to $\frac{1}{4}\lambda$ or better in the Helium yellow line.

VI. System Optics

A hemicylindrical cathode substrate was selected since it allows rotation about its θ-axis while maintaining a constant optical path independent of angle[24]*.

The cathode is coated on the flat face of the quartz hemicylinder and its response to and absorbtion of incident radiation vs. angle can be determined. Optical paths are selected such that parallel light intersects the cathode surface.

A retro-reflecting quadrant mirror is used in conjunction with the hemicylinder to redirect the light back through the hemicylinder anti parallel to the input beam and then out of the system to the photometer. See Figure 5.

A multiple internal reflection element is also used (without the retro-mirror) to examine absorbtion in a multi-reflection geometry.

Details on these optical components and their manufacture are found in Appendix I.

Figure 4 illustrates an optical diagram of the system. The optical path is as follows: A selected wavelength from the monochromator/source (a) is incident on the first surface prism (b) through a collimating/converging lens (c), and window. Light then reflects from the first surface fixed mirror (e) into a lens (not shown) and is incident on the hemicylinder/cathode. The beam is reflected at an equal angle with the normal and thence to a curved roof retro-reflecting mirror placed immediately outside the hemicylinder. The beam is displaced laterally and re-enters the cell at where it is again incident, this time on an uncoated section of the substrate.

---

* See theoretical analysis.

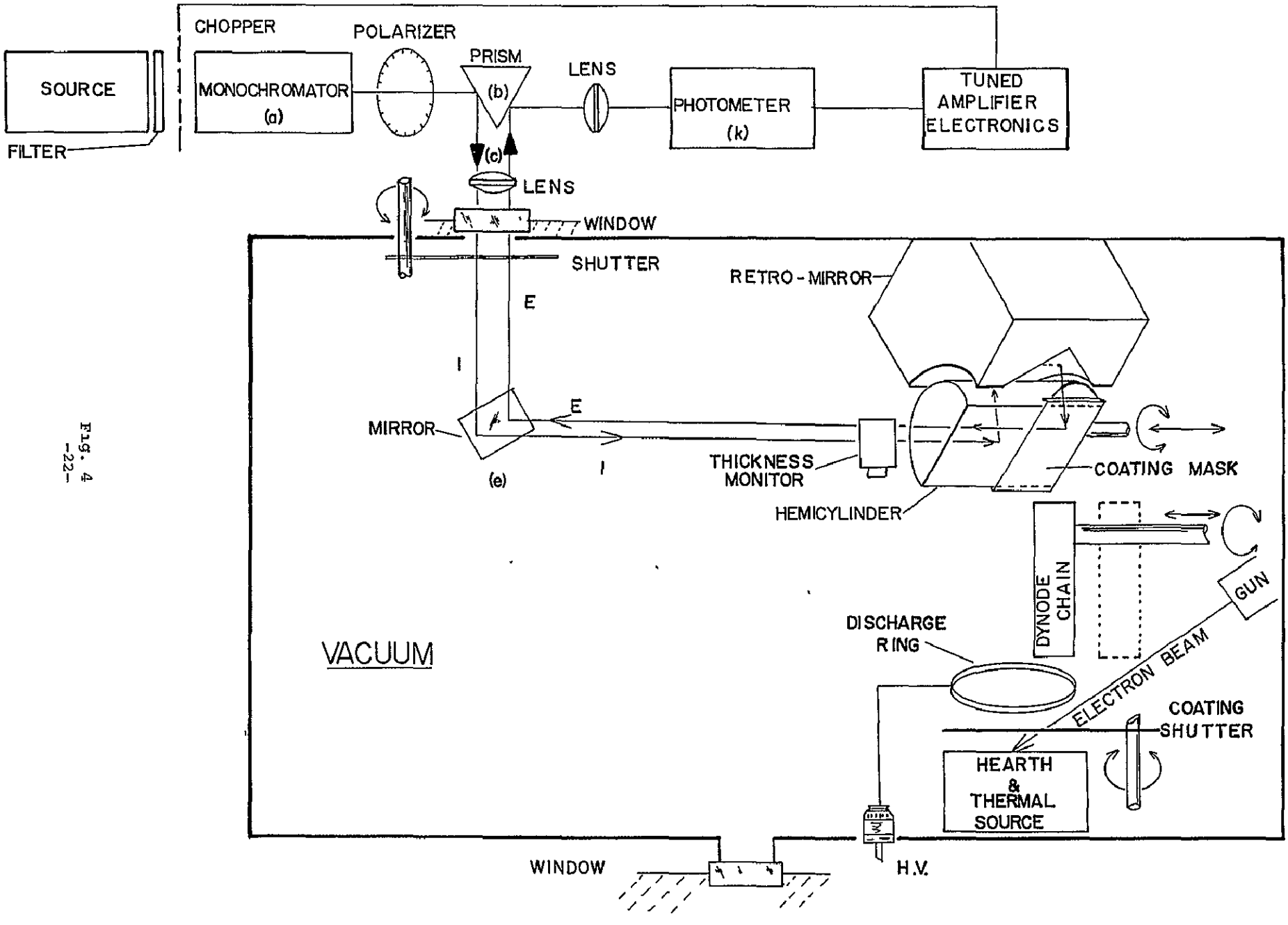

Fig. 4
-22-

A T R COATING/EVALUATION SYSTEM

Total reflection occurs at the uncoated surface and the beam next exits the hemicylinder for a second time exactly parallel to the incident beam (I). The exit beam (E) is reflected from mirror (e) and passes again through the view port and lens (c) displaced laterally from the incident beam. The radiation hits the opposite face of the prism (b) and is reflected through appropriate optics to the photometer (k).

The beam separation is adjustable by moving the retro-reflector along the z-z axis or by rotating mirror (e). Due to the hemicylindrical design, the optical path is constant regardless of the input angle of the light beam. Zero absorption calibration is possible by moving the cell along the z-z axis until incident and return beams both intersect the uncoated area of the substrate (beneath the coating mask) resulting in total reflection of the beam. This is the zero absorption calibration point. By subsequently moving the cell on the z-z axis to different areas of the coating it is possible to determine the magnitude of any inhomogeneities which may result in the cathode deposit.

Polarizers may be inserted between (a), (b), (e), or (k) to investigate the effect of polarization on the absorption and to closely check the theory which predicts strikingly different absorptions of the perpendicular and parallel polarized ray, as described in the theoretical section of this report.

The diagram on p. 25 and Figure 6 illustrate the photometer/absorption measurement arrangement. Note particularly:

1. Chopper blade (extreme left).
2. Angular control wheel for cathode angle positioning.

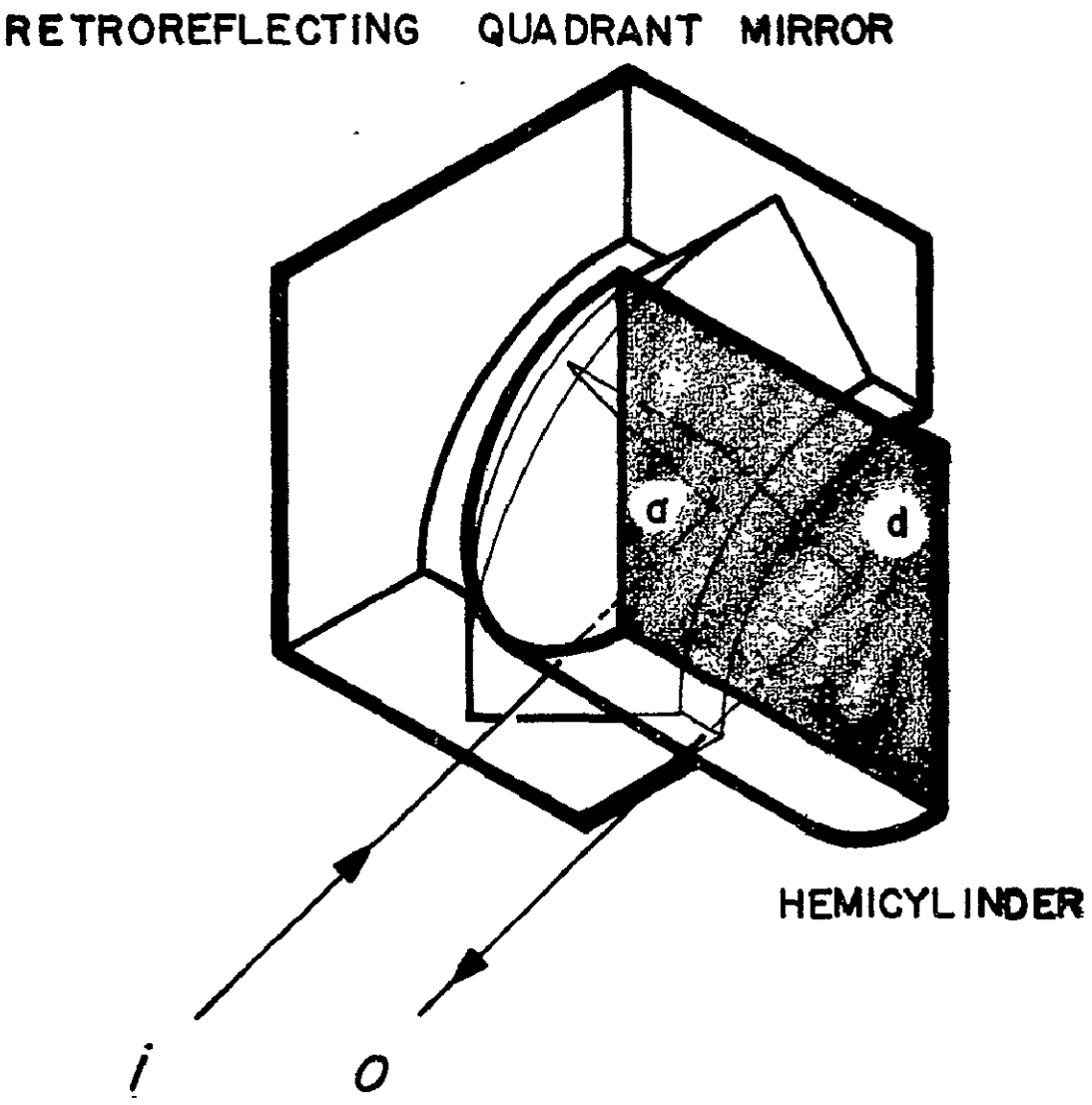

Figure 5
Retroreflecting Quadrant
Mirror

3. Entrance/exit mirror prism (center right) which obscures the view of the window.

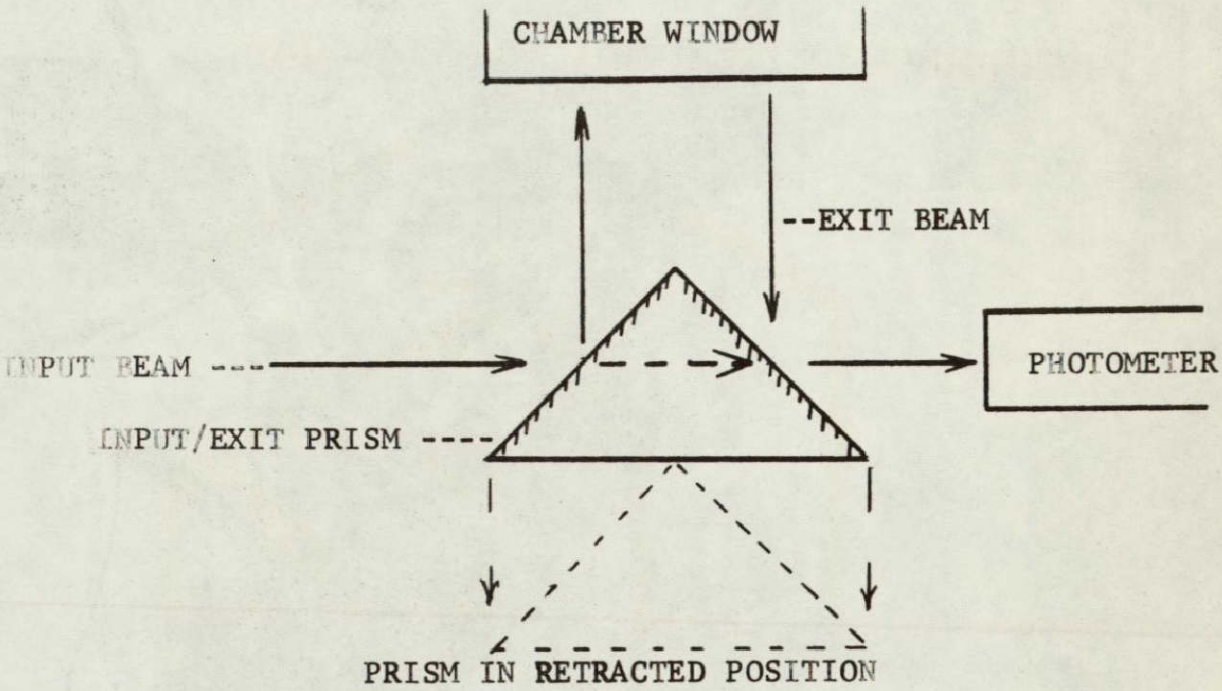

4. Photometer housing and alignment manipulator. (Black tube at center right). By removing entrance/exit prism, the input beam can be measured directly with photometer.

Since light sources for the visible region of the spectrum are considerably brighter than those in the ultra violet region, the problem of signal to noise in the photometer is diminished and a closer degree of correlation between the theoretically predicted absorption of the cathode and the measured values possible. Separation of polarizations is also practical*. The

* Polarizers for the UV are inefficient and expensive.

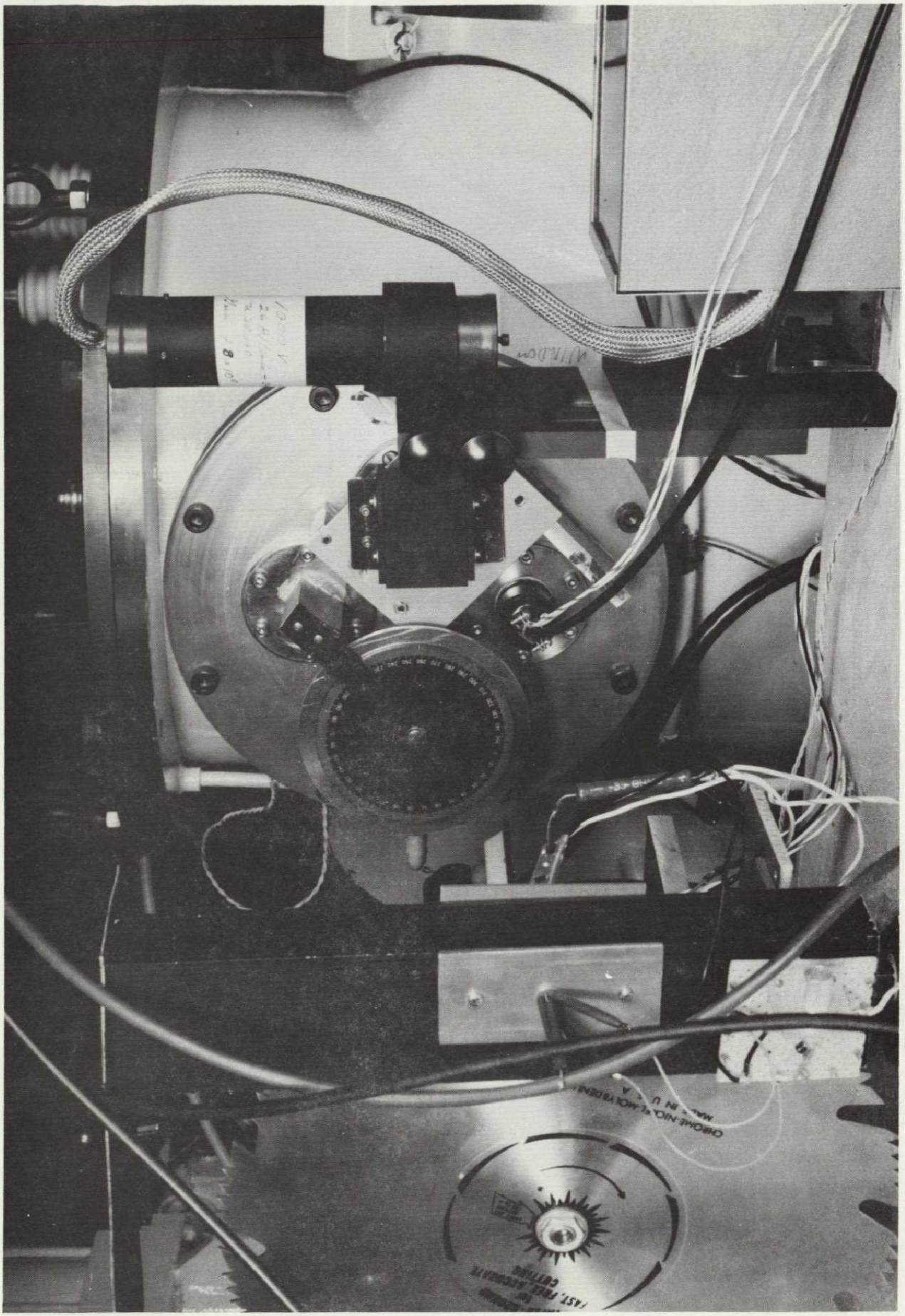

Figure 6
Chopper and chamber
entrance window

actual photo currents from the cathode will have to be kept small due to the intrinsically high surface resistance of ultra-thin cathodes. This is no disadvantage in any typical application of an ultra sensitive device.

The position of the reflection photometer photomultiplier tube has been changed in order to take advantage of the higher exit beam intensity available inside the chamber. There is now the option of placing this photomultiplier tube inside the chamber and remotely introducing a mirror into the beam to measure the incident radiation; the option of using the original system which measures the radiation incident upon the vacuum chamber window is retained.

VII. Details of Micro-Manipulators and Fixtures Used to Manufacture and Test The Photocathodes

Manipulators were designed which permit close control of the position of the photocathode with respect to the incident light beam. In previous designs the cathode could be manufactured and then tested in the chamber without breaking vacuum, but the lateral and rotational motions of the cathode/dynode chain assembly were somewhat limited. The new arrangement permits complete shielding of the dynode chain* during the evaporation cycle and manipulation of the cathode/dynode assembly over the complete range of angles from 0 to 90° with the normal. Due to optical limitations, of course, the range from 0 to 10° and from 80 to 90° are relatively useless since the input light beam diameter has finite size and becomes vignetted as the hemicylinder approaches either of these angles. At one extreme, the vignetting is caused by the edge of the hemicylinder (80 to 90°) and at the other limit the vignette is caused by the edge of the retro-reflecting quadrant mirror encroaching upon the light beam (0 to 10°). Both vignetted regions are of no interest in ATR cathode experiments.

The geometry of the system requires that the hemicylinder and cathode under test be rotated 90° from the test position to the evaporate position. This is accomplished by means of a D.C. motor (tested for outgassing under high vacuum). Microswitch actuated pilot light indicators provide position readout of hemicylinder.

A remote, manually operated, precision traverse mechanism is used to provide retraction of the dynode string when the hemicylinder is in the deposition/coat position.

---

* More critical now in view of the reactive evaporants involved and their higher inherent vapor pressures.

A turntable, with manual remote control, is used with a precision angular read-out disc and cursor.

A linear motor driven actuator (cam operated) is incorporated into the existing system carrier; and moves the cathode carrier and dynode assembly laterally with respect to the incoming light beam. The lateral position is read to 0.010" from a 1" travel linear potentiometer.

Drawings on the following pages, and photographs illustrate the essentials of the mechanism.

In Figure 7 the dynode and photocathode manipulator assembly is illustrated at close range. The dynode assembly is shown on a precision slide mounting which enables it to travel forward and backward toward and away from the cathode; the cathode hemicylinder is shown in vertical position, ready for testing. The large cylindrical object in the left foreground is the motor which rotates the cathode from coating position into test position. The retro-reflecting quadrant mirror is shown at the right side of the picture and the electrical mechanism for moving the dynode string toward and away from the cathode is shown on the upper left quadrant of the picture. The linear actuator is visible in the upper right corner of the photograph.

The dynode slide is racked completely forward, toward the cathode. Slip clutches are used on all motors to prevent damage to the components and to eliminate the necessity for electro-mechanical readouts of these two motions. Mechanical stops are used to limit the travel in both directions for both coating and testing. Independent control of the lateral motion of the dynode string and rotary motion of the cathode holder is obtained

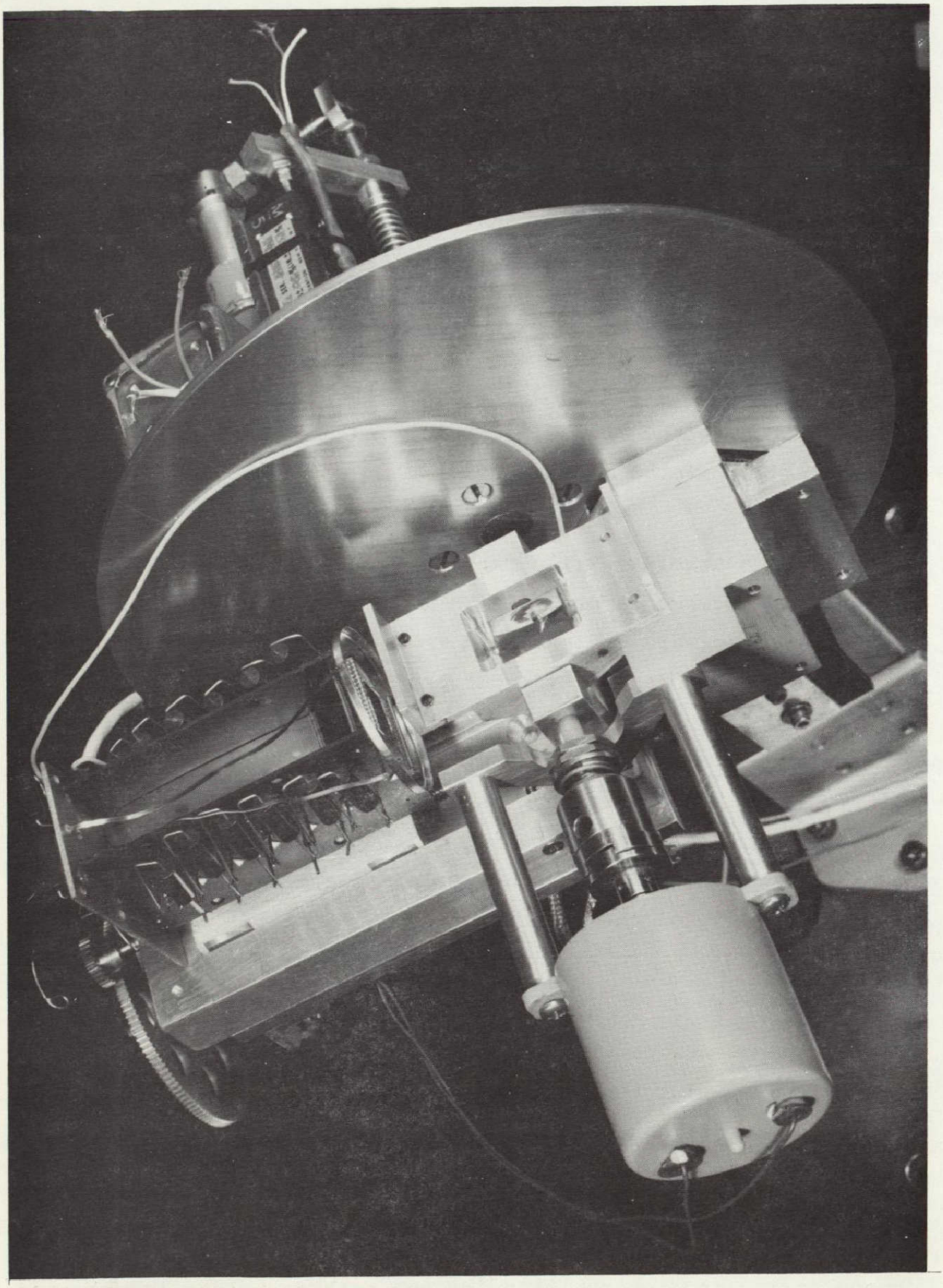

Figure 7
Rotation Plate - cathode
in test position

through the use of two independent motors. The cathode itself is isolated by means of machined lava insulator blocks so that it can be maintained at 4000 volts negative potential with respect to the anode and ground. Grounded anode operation is always preferred, if possible, due to the elimination of the coupling capacitor (always a source of noise) between the anode and the preamplifier.

Figure 8 illustrates the dynode/cathode assembly rotated into the cathode coating position. The evaporation baffles have been removed for visibility in order to illustrate the mechanisms. During use, the baffles would be in place to prevent alkali materials from coating the motor, the dynode string, or any portion of the retro-reflecting quadrant mirror. The perspective seen in the photograph is an off axis view but is close to that seen from the position of the evaporation source used to coat the cathode face. The convex portion of the hemicylinder is facing upward and away from the observer in the picture. A comparison of this photograph with the previous photograph will illustrate that the cathode has been rotated 90° and that the dynode string in this picture is in the extreme retracted position in order to allow for the rotation of cathode mounting fixture. A coating mask is shown covering the retro-reflecting mirror.

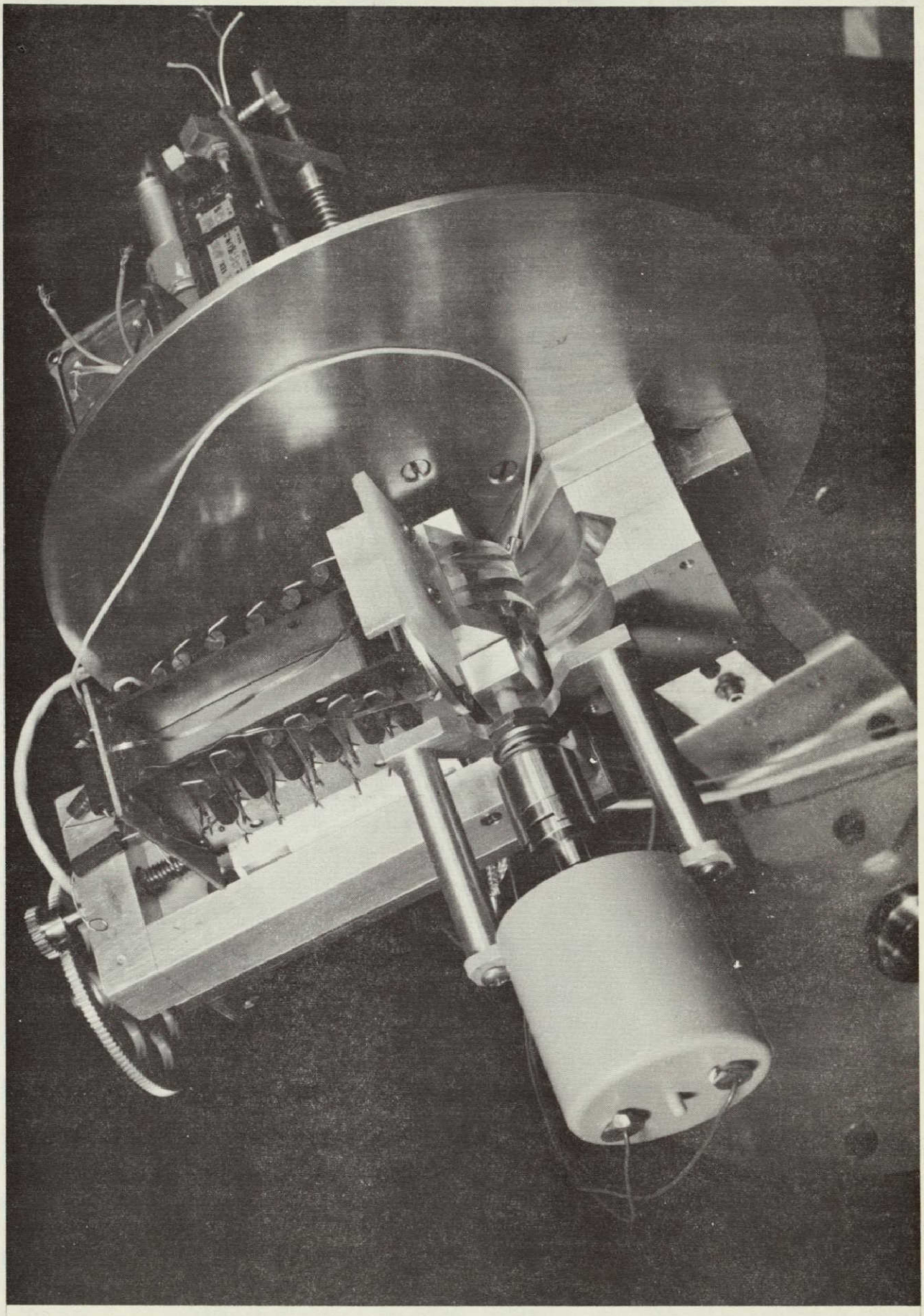

Figure 8
Rotation Plate - cathode
in coating position

In Figure 9 the entire rotational assembly is illustrated in the 90° incidence position; the cathode and dynode are not clearly visible, however the mechanism for moving the dynode string and rotation of the cathode are seen. The mechanism shown on the vertical axle is a linear actuator used to traverse the entire assembly along the axis of rotation (in this view-up and down) so that different areas of the cathode can be excited by the incident light beam. The lateral motion is accomplished by means of a linear actuator and exact position readout is obtained by means of a linear potentiometer which reads accurately to 1/100". The incident light beam travels from left to right in the picture and the prism assembly can be seen on the outside of the metal vacuum plate at the left. The manual rotary angle indicator for adjusting incidence angle is shown at the upper left in a side view.

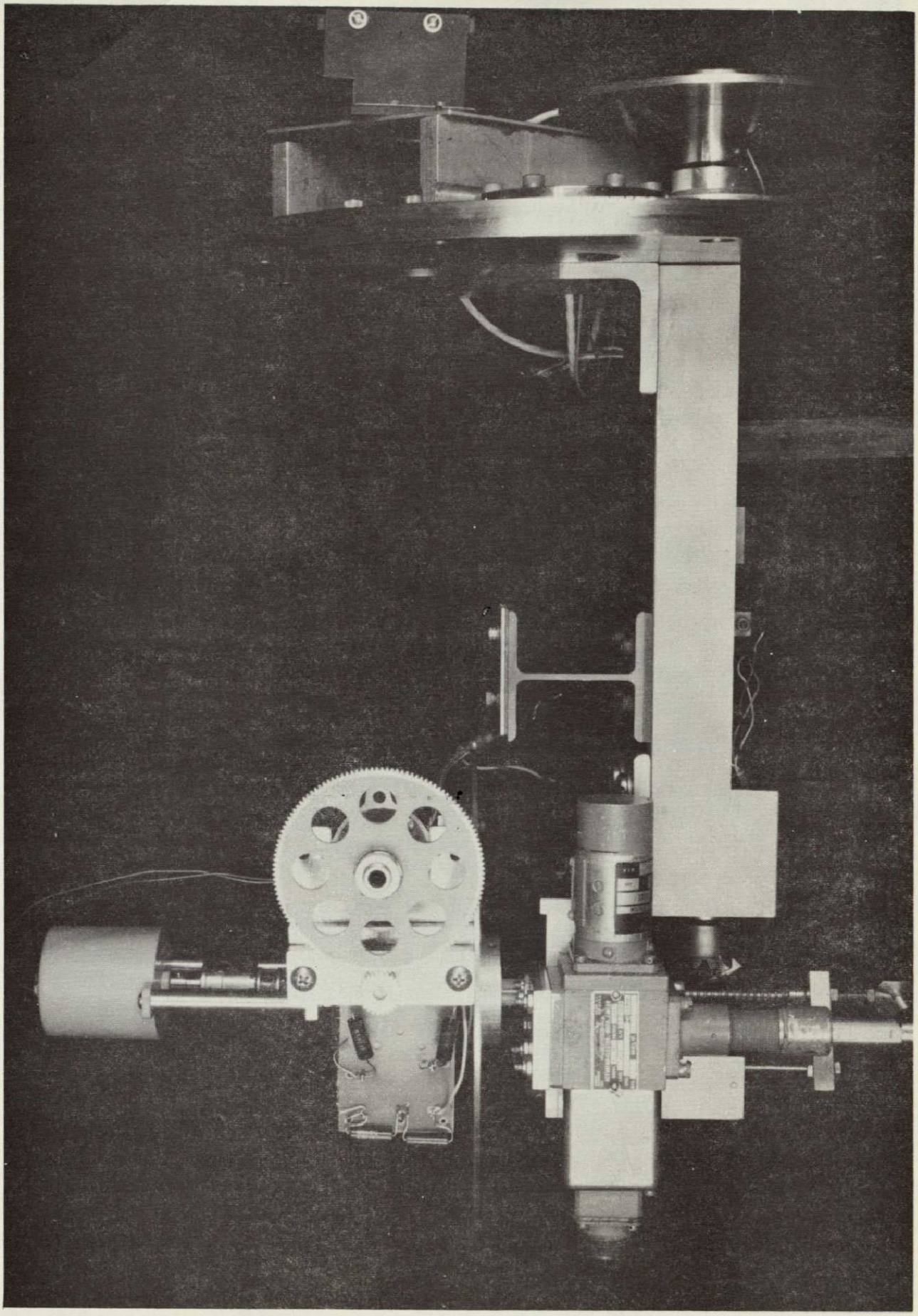

Figure 9
Optical Arm Assembly -
rotated to 90° incidence
with cathode

VIII. Cathode Formation - Substrate Preparation

In the formation of cathodes, both thermal and electron beam evaporation were used. The table below outlines the methods we found most suitable for each material. The criteria for suitability were ease of rate control and purity of the ultra thin layer.

Material	Melting Point/ Boiling Point	Evaporation Method
Gold	1063/1405	Wire-filament
Platinum	1774/1765	Electron beam bomb
Silver	961/1105	Wire-Filament
Magnesium	651/600*	Filament/Basket
Cesium	28.5/705°**	Reaction Capillary
Sodium	97.7/883°	Reaction Capillary
Potassium	63.7/774°	Reaction Capillary
Calcium	842/630	Basket-Crucible
Rubidium	39°/696°	Boat/Crucible

Substrate Preparation

A standard cleaning procedure has been established which provides the best deposit adherence for most films. This procedure is a consolidation of those obtained from other workers in this field and vendors in our area. It has been experimentally determined that this procedure yields the most uniform results and it is followed as a preparation to all of our in-house coating work.

A. Strip previous coating and fingerprints with Acetone and Trichlorethylene rinse.

---

* Sublimes

** Obtained from reaction mix.

B. Soak in hot 10% Chromic Acid/Nitric Acid distilled water solution at 190°F for 30 minutes.

C. Rinse in distilled water.

D. Heat in Alconox or surface active detergent solution for 15 minutes with mild scrubbing using a lint free cotton cloth which has been previously washed in detergent.

E. Rinse in room temperature distilled water.

F. Wipe with a thick paste of Calcium Carbonate and de-ionized water until an unbroken film of de-ionized water will run over the surface.

G. Immediately blow off surface water with filtered prepure ionized dry Nitrogen which removes residual static charge from the surface.

H. Place face down on lint free cloth, not paper.

NOTES:

Do not use Q-tips, cotton swabs or industrial wipers as these all contain vegetable oils in the fibers.

Do not use lens tissue or any other material wiped across surface after final Nitrogen blast.

I. Place in vacuum chamber and energize glow discharge in Argon at 50-100μ pressure for 10 minutes immediately prior to evaporation. This drives off any residual adsorbed gases.

NOTE: Use only Aluminum discharge rings since Aluminum has a very low sputtering coefficient due to easy oxide formation on its surface.

Noble Metals

Gold and Platinum are easily coated in thin films and represent no particular problem except for the very high temperatures necessary for Platinum deposition. Sputtering of Platinum takes place at a lower temperature but at such high gas pressures that gaseous inclusions in a relatively porous cathode result. The consequent contamination represents a significant fraction of the molecules present in the cathode and cannot be tolerated.

Magnesium

Magnesium was most successfully evaporated from pure ribbon placed in a solid Tantalum basket which was then heated to incandescence. Deposits up to 1500Å showed excellent homogeneity and reflectivity in the visible. This material sublimes during evaporation.

Formation of Alkali Cathodes

First attempts at forming ultra-thin layers of Potassium and Cesium were conducted using an indirect chemical reaction[25], due to the reactivity of Cesium and Potassium metals. A combination of Cesium Chromate and Aluminum or Potassium Chromate and Aluminum, (all of which were stable at room temperature and in atmosphere), were thoroughly mixed and combined as a fine powder and placed in the bore of a small Tungsten or Tantalum capillary tube. The tube is then gripped at each end by an electrical conductor block; a current through this fixture then heats the mixture to incandescence or reaction temperature. When the current ceases and the Tungsten begins to cool, there will be sufficient conduction of heat away from the Exothermic mass within the tube to stop the reaction. In the absence of such a metal tube, the Thermit type of reaction would continue explosively on its own, producing an uncontrollable film thickness, or at least, contaminating the walls of the chamber. A picture of the capillary evaporation source, constructed especially for this work, is shown in Figure 10.

While it is extremely difficult to obtain Molybdenum, Tungsten, and Tantalum tubing of the desired size, the degree of control gained by using such a crucible and heating scheme is well worth the effort. The expected evaporation temperatures are 400-500°C (onto a cold substrate) for Cesium. For Potassium, the temperatures can be correspondingly higher (up to 700°C).

In commercial photomultiplier tubes where the thickness of the cathode is not nearly as critical, a less exotic crucible can be used, since the reaction continues to exhaustion. In

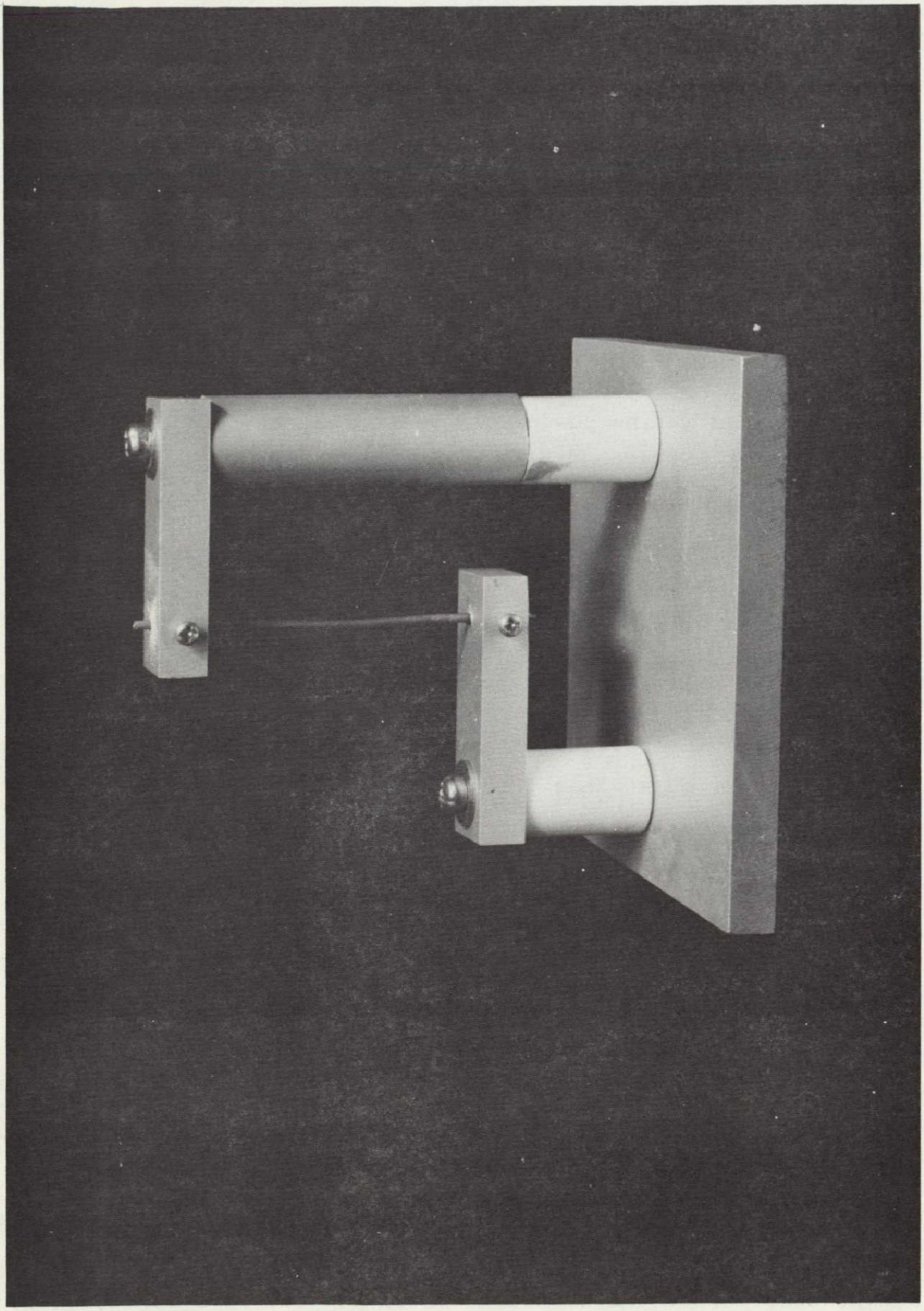

Figure 10
Capillary evaporation
fixture

fact, these crucibles are usually built right into the tube itself and are made of Aluminum or Nickel. Induction heating would be of no benefit in this application since the reaction rate is the critical factor; the method of heating to initiate the reaction is irrelevant. The critical design consideration is that sufficient heat must be carried away from the Exothermic reaction to stop it when further deposition of the alkali metal is no longer desired.

Formation Reactions

In this section we describe the various chemical reactions used to obtain the alkali metal cathodes. The various pitfalls involved in using these chemical reactions are noted. It should be mentioned at the outset that pure alkali metals are not used as evaporation materials due to the relatively low purity in which these metals can usually be obtained in raw form and the great difficulty in handling and evaporating them successfully in a complex vacuum system. The control of chemicals such as Cesium (liquid at elevated room or body temperature) in a nonglass vacuum system which must be used for other purposes (including electronic testing), is extremely difficult; the chance of contamination when large amounts of Cesium are used is very great. Contamination of diffusion pump fluid is always a possibility.

Various Chromate and catalytic reactions were tried in order to improve the purity of the deposited product and uniformity of the evaporation. In all cases a shuttering system was used in order to prevent the possibility of a runaway thermit reaction from producing a cathode too thick to be useful. The procedure was essentially the same in all cases: (1) the reaction was started after a complete bakeout of components at a low temperature,

(2) as the reaction proceeded the shutter was opened during a period of reasonably uniform evaporation, (3) the coating thickness was monitored on the deposit thickness monitor and, (4) the shutter was closed at the conclusion of the thickness buildup-as required. The current input to the reaction basket was then decreased and, in most cases, the reaction stopped immediately. The cathode deposit was then allowed to thoroughly cool in high vacuum on the substrate before over coating the alkali metal with Aluminum in the case of a calibration run. The system is then backfilled and the substrate removed for thickness determination. After each calibration coating, a second filament containing Aluminum was energized and an overcoating of Aluminum was placed over the test step to protect the reactive cathode material beneath. The overcoating of Aluminum was used only during the calibration phase and was necessary since a highly reflective coating is required for accurate measurements using the Fizeau Fringe Interferometer.

During cathode formation on a test hemicylinder, no overcoating is used and testing proceeds immediately after coating as itemized in the procedure.

All reactions were conducted in Tantalum or Molybdenum tubes which were used themselves as the heating elements by passing a current through them. Although the capillary size of these containers was relatively large (3 to 5mm inside diameter), the reaction stopped upon elimination of the current, and the heat transfer to the vessel is assumed adequate. Extremely small amounts (less than 1gm) of the reactants were used so that runaway reactions were not a serious possibility.

It was established, however, through chemical testing that the thermit reaction which was used, deposited a quantity of Chromium or Chromate of Aluminum which could slightly contaminate an efficient cathode. We have determined that the large bore Tantalum basket used for the early reactions did not carry away sufficient heat to prevent the reaction from "thermal runaway" and depositing by-products at the higher temperature. We are now packing the mixture into 1mm bore capillary tubing** as originally planned and are heating to 700°C[26]. The larger surface area to volume ratio of the 1mm bore tube should keep the reaction from free running and should also lower the production of by-products.

The following reactions were tried and the results of these reactions are summarized.

Potassium Chromate Reaction

$$3K_2CrO_4 + 8Al \xrightarrow{\Delta} 4Al_2O_3 + 3Cr + 4K \uparrow$$

Stoichiometric Proportion:

2.698:1 = Potassium Chromate: Aluminum.

Use excess Potassium Chromate so that no Aluminum is evaporated.

Trial 1: The ratio used in Molybdenum basket for evaporation was 2.7:1 = Potassium Chromate: Aluminum.

* Trial II: The ratio used was 2:1 Aluminum: Potassium Chromate by weight.

**Use of a hypodermic needle with a Luer tip as a micro funnel aids in the packing operation.

Cesium Chromate Reaction

$$3Cs_2CrO_4 + 8Al \xrightarrow{\Delta} 4Al_2O_3 + 3Cr + 6Cs\uparrow$$

Stoichiometric Proportion:

5.306:1 = Cesium Chromate: Aluminum.

Initially excess Cesium Chromate was used so that no free Aluminum was left to evaporate. This procedure was later found to be incorrect and a second mixture (Trial II) was used for tests.

Trial I: The actual ratio used in Tantalum basket was 5.31:1 = Cesium Chromate: Aluminum.

*Trial II: The ratio used was 2:1 Aluminum: Cesium Chromate by weight.

NOTE: Aluminum powder comes finely divided but the various chromates are relatively granular. Crushing the mixture after proportioning is dangerous and not very successful. We recommend finely crushing the chromate separately in an Agate crucible and then mixing the finely divided powders together. Good mixing is essential to a complete reaction with few by-products (contaminants).

Raney Nickel Reaction

$$3K_2CrO_4 + 8Al \xrightarrow[\Delta]{\text{Raney Nickel}} 6K + 3Cr + 4Al_2O_3$$

also

$$3Cs_2CrO_4 + 8Al \xrightarrow[\Delta]{\text{Raney Nickel}} 6Cs + 3Cr + 4Al_2O_3$$

Proportion of catalyst is variable.

* The 2:1 excess of Aluminum powder proved to be the more successful mixture and is, in fact, a commonly used mixture[27].

Chemical Testing

After the vaporized material was collected on a glass slide, tests were run in order to establish presence of Potassium.

First H_2O was dropped on glass. No noticeable amount of H_2 was evolved. However, when phenolphthalein solution was added, it showed presence of a base (probably KOH). A flame test was done which did not show any violet color (Potassium).

A distinct green color was seen on the slide indicating a possibility of Cr contamination.

Further tests to examine purity, (eliminate green indicator color) were conducted during the tests.

Upon examining the coatings produced from the Trial II mixtures (excess aluminum) no chromate green color appeared. A flame test for sodium indicated positive as did a test for potassium. The cesium flame test was inconclusive but may have been due to the extremely small quantities of cesium present and washing by a slight sodium yellow induction. All test substrates indicated the presence of a basic metal after evaporation. The use of nickel other than tantalum or tungsten capillaries also improves control of evaporation rate.

IX. Theoretical Analysis

The following analysis is appropriate to the test geometry which was used during this study.

If we assume a polarized, collimated light bundle incident on a hemicylinder of index n_1 coated on its plane surface with a cathode material a few atomic layers thick, (index n_2, k_2) we can see in this illustration an exaggerated idea of the path such a bundle will follow.

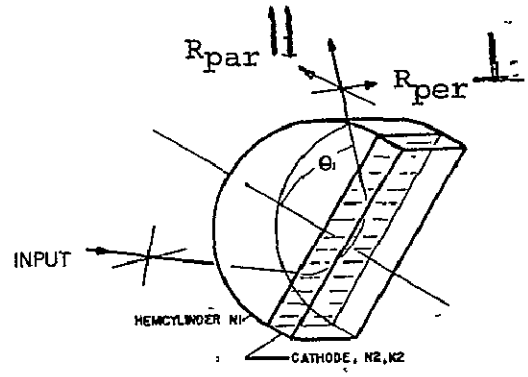

The beam is incident on the cathode at an angle θ_i or θ_1 with the normal. It is deflected in the second medium n_2 back toward the first medium where it can exit the system or be reflected by mirrors for a second or third pass through the cathode before it is lost to the system. The apparent absorption path length* p of the light ray through the cathode will be much greater than the thickness of the cathode coating d

$$\left(\frac{p}{d} \gg 1 \right).$$

* The increased absorption is due to the high values of the electric field vector at the interface. Dissipation in an absorbing medium is proportional to the electric field vector amplitude squared.

It is this effect which allows high absorption in extremely thin cathodes. The probability of escape of any photoelectrons generated within this extremely thin layer is very high, since only a few collisions will occur.

Since the concept of Attenuated Total Reflection (ATR) is familiar to most workers, the fine details of the theory and the appropriate Fresnel[28,29] equations for calculating absorption will not be included here. Rather the appropriate theoretical results will be illustrated. The exact Fresnel equations optimizing the thickness of the coating appropriate to this simple single pass geometry[30] are related to the complex indices of the substrate and the cathode material. Their extremely tedious nature lends itself to automatic data processing with the following interesting results. Note the illustrated sense and direction of the polarization vectors shown in the last drawing; these are appropriate to the next illustration. In the first graph is a plot of the reflected intensity of the parallel polarized light ray exiting the hemicylinder.

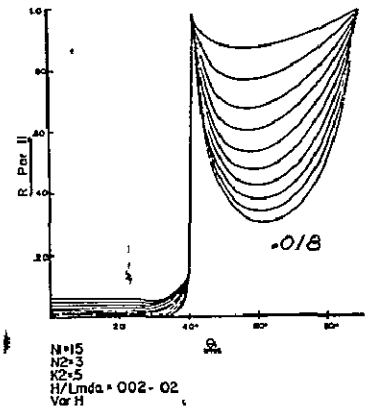

H/λ varies from 0.002 to 0.02 steps of 0.002.

R_{par} is plotted versus angle of incidence with the cathode. This particular family of curves corresponds to a substrate index of $n_1 = 1.5$ which corresponds closely to the quartz material used for the hemicylinder. The n_2 and k_2 appropriate to the cathode are 3 and 0.5 respectively. Our initial estimates of the cathode constants were made using data from other workers in ultra thin films[31]. The values are those formerly obtained with gold in the ultra violet region of the spectrum. The family of curves is generated by varying h/lamda (h/λ) or the ratio of cathode thickness-h to lamda, the wavelength. Although it is not possible to see from this graph, due to the bunching of lines near the critical angle, the peak absorption enhancement corresponds to h over lamda equal to .018*. For cathode thickness below and above this optimum, the absorption decreases. This enhancement reversal occurs at different thicknesses for different cathode indices. The higher the cathode index, the thinner the coating at which enhancement reversal occurs. A later curve will illustrate the behavior of peak absorption versus cathode thickness at the optimum angle and the reversal behavior will become clear. For parallel polarization, peak absorption occurs when $\theta_i = 62°$ or approximately 20° higher than the critical angle for quartz.

In the next graph we see data plotted for the perpendicular polarized ray reflected from the cathode.

---

* This can be read from the numerical print-out obtained simultaneously with the graphs.

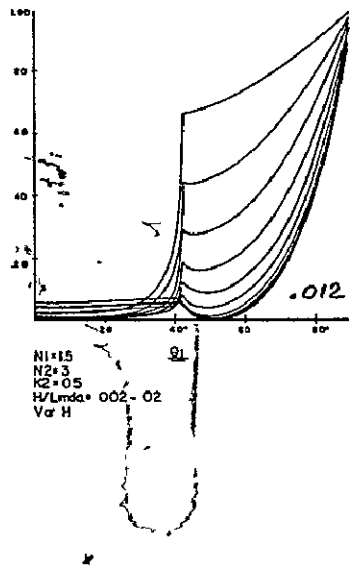

In R_{per} family, the enhancement reversal is a little more clearly visible. However the next graphs will demonstrate behavior of absorbtion versus cathode thickness. For optimum coating thickness in this family $h/\lambda = 0.012$ and the peak absorbtion occurs near 50° which is approximately 8° larger than the critical angle.

The next graph is a plot of the intensity of the perpendicular polarized reflected ray versus the cathode thickness h/λ.

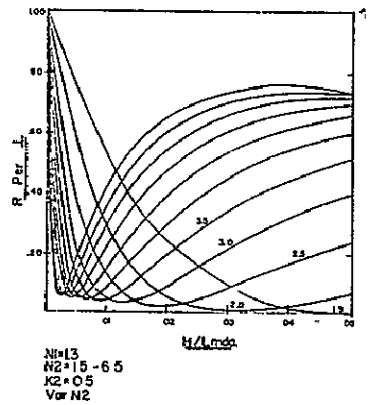

For best absorption*, the optimum cathode index corresponds to $n_2 = 2$. As seen from the graph, this line represents the greatest and broadest absorption. For $n_2 = 3$ (we estimate this index for Gold in UV) the peak absorption occurs at $h/\lambda = 0.012$. Note, as before, that for very thin cathodes, the absorption increases with thickness up to an optimum point and decreases rapidly above this point. For higher index cathodes this reversal or absorption maximum occurs at thinner coatings. In our case the optimum coating thickness for perpendicular polarized ray absorption is approximately 30Å.

The next graph shows behavior of the parallel polarized ray with cathode thickness.

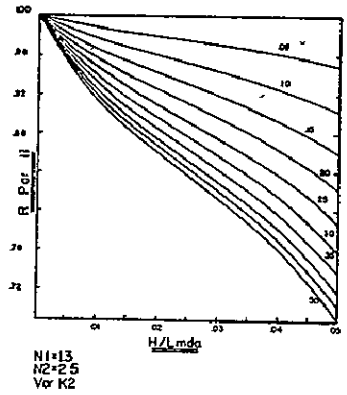

We can see that the behavior for R_{par} is not nearly as strong a function of h/λ as for R_{per}. The absorption maxima are quite weak and for single reflections will not contribute significantly to the design considerations. For a cathode index of 2.5 the absorption versus cathode thickness from 25 to 75Å thickness in the UV remains essentially constant within 10%. Note as k_2 increases the absorption increases as expected.

---

* Least reflection.

The next set of curves illustrates the reflection of the perpendicular polarized ray versus cathode thickness where the family is generated as above by varying k_2, the absorption constant of the cathode.

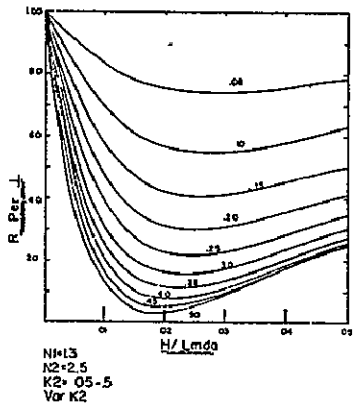

Again, the absorption increases with the increasing k_2. The index of the cathode is = 2.5 but similar curves result for $n_2 = 3.0$. Note the existence of weak but observable absorption maxima here which were not present for parallel polarized ray. For randomly polarized illumination, the behavior of the cathode to the perpendicularly polarized component is most important and the optimum cathode design thickness would be primarily based on response to R_{per}.

In the next graph a plot of the perpendicular polarized reflected ray (R_{per}) versus cathode thickness is shown. The family is generated by varying the angle of incidence θ.

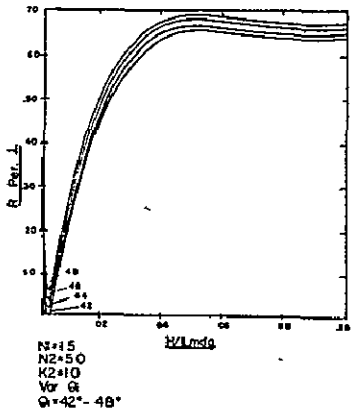

Clearly the optimum angle for perpendicular polarization is the critical angle 42° (when $n_2 = 5$). However the absorption is still greater than 90% at 48°.

In the next graph we see typical behavior for the parallel polarized ray (R_{par}) where 48° is the optimum angle of incidence and the 42° curve does not have a significant minimum at all. The spread in angular absorption maxima tends to broaden the angular response of the cathode (field-of-view) at the expense of some sensitivity.

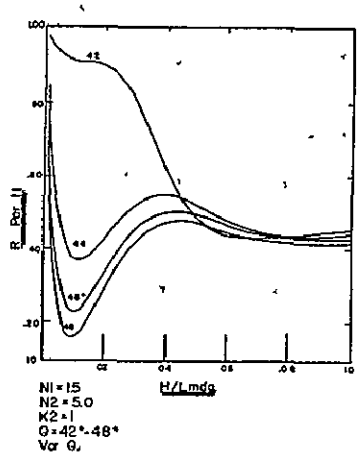

Noble Metals

The following Figure 11, shows the tehroetical prediction of reflection of the s and p-polarized* light waves from a 25Å coating of Gold on a material with an index of 1.5 at 2500Å. The two polarizations are averaged to obtain the predicted reflection for randomly polarized light which was used in the initial experiments. Note here, the average peak absorption occurs at the 55° incidence angle. This corresponds to within 3° of our experimental peak enhancement angle for the Gold cathode. The actual measured value of absorption cannot be accurately correlated with this curve, since the calibration of the reflection photometer is not yet considered adequate for complete confirmation.

---

* s wave = R_{per}

p wave = R_{par}

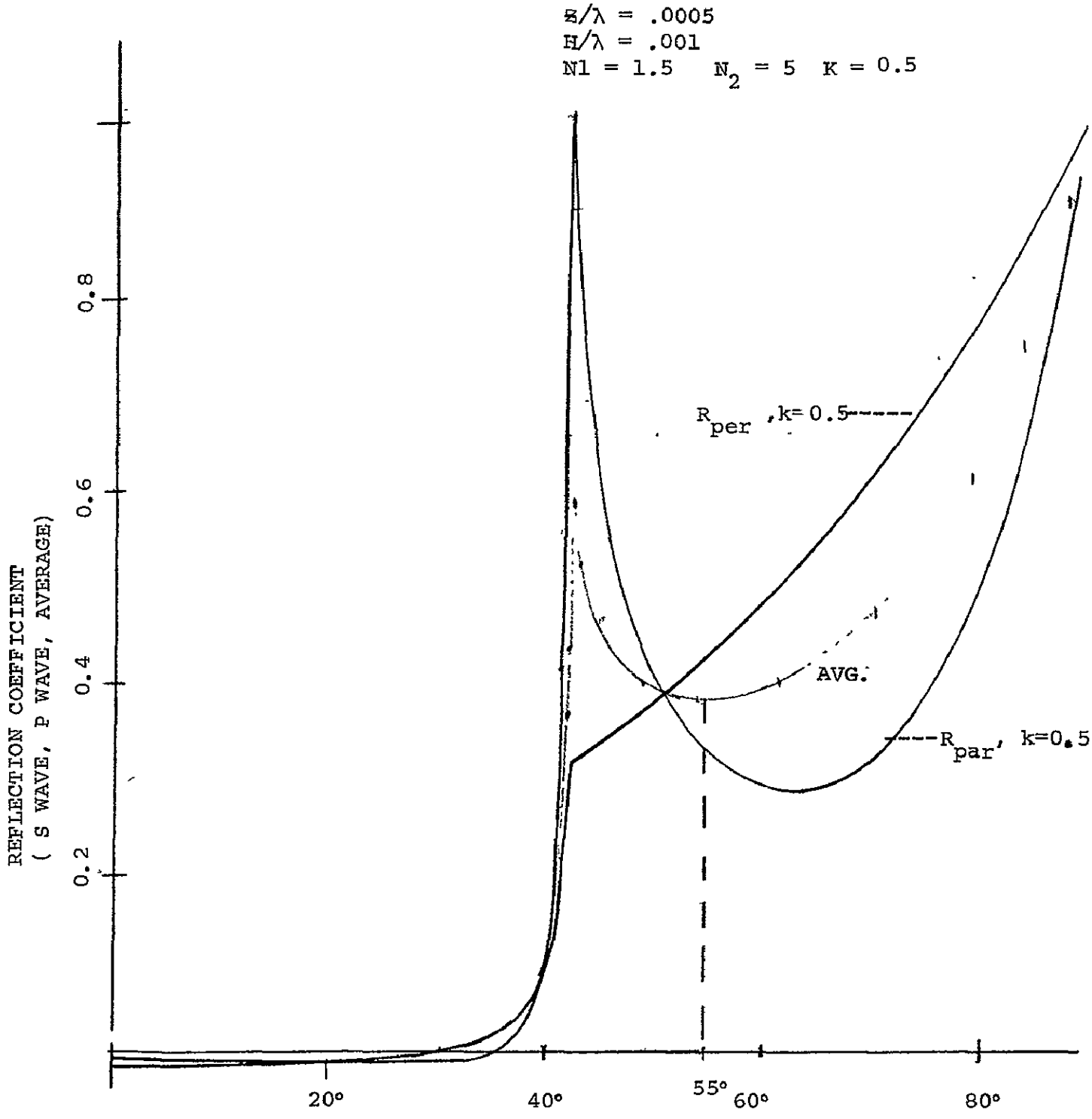

Figure 11
Average Reflection
Coefficient versus
Angle of Incidence

The next graphs illustrate computer printout of absorption data for a thin UV photoemissive coating of index 3. Figure 12 is appropriate to the parallel poarized reflected ray and: the Figure 13 family illustrates the reflection of the perpendicular polarized ray.

The equations pertinent to the reflected waves for perpendicular $\perp$ and parallel // polarization are:

$$r_{\perp} = r_{\perp\ 12} = \frac{\mu_2\ \xi_1 - \mu_1\ \xi_2}{\mu_2\ \xi_1 + \mu_1\ \xi_2} \qquad 32$$

where $\xi_j = \hat{n}_j \cos \theta_j$ after Hansen[33]

and $r_{//} = r_{//\ 12} = \frac{\hat{\epsilon}_2\ \xi_1 - \epsilon_1\ \xi_2}{\hat{\epsilon}_2\ \xi_1 + \epsilon_1\ \xi_2}$

The complex indices which must be used for absorptive coatings make calculation by computer almost a necessity. Several expected types of behavior become clear by observation of the curves.

1. Absorbtion is enhanced in thinner coatings up to an optimum point.

2. Lowering k decreases absorption (observed from vary k_2 curves).

3. Critical angle remains primarily dependent upon n_1 (in our case 1.54 for G-E #151 quartz).

4. A peak average absorption ($\perp$ and // rays) occurs in the vicinity of 53-58 degrees.

   a. peak $\perp$ absorption lies near 50°

   b. peak // lies near 62°

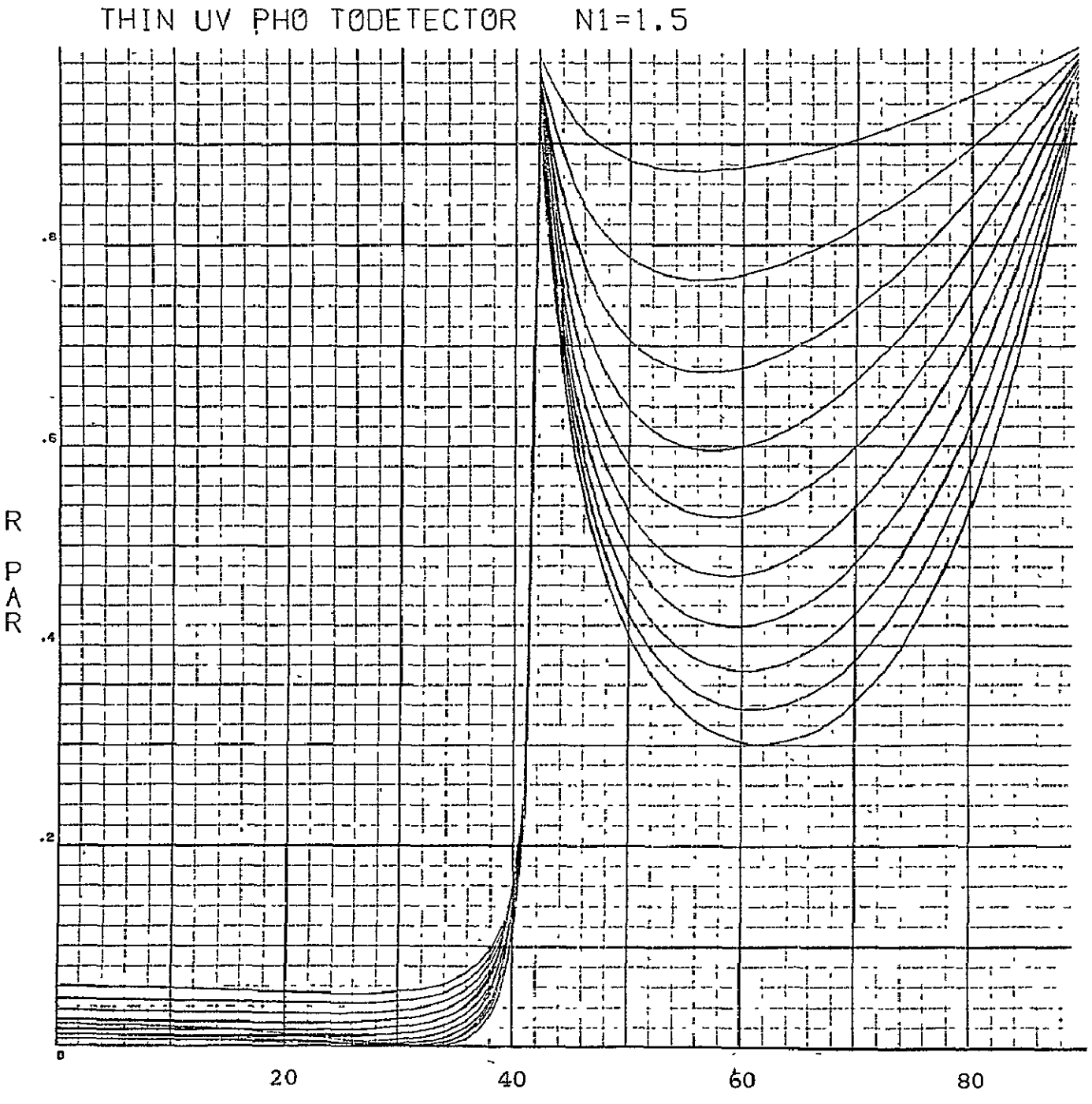

n_2=3, k=.5,

H/λ = .002~.020

.002 steps

Figure 12
R_{par} versus
Angle of Incidence,
N_1 = 1.5, N_2 = 3, k = 0.5

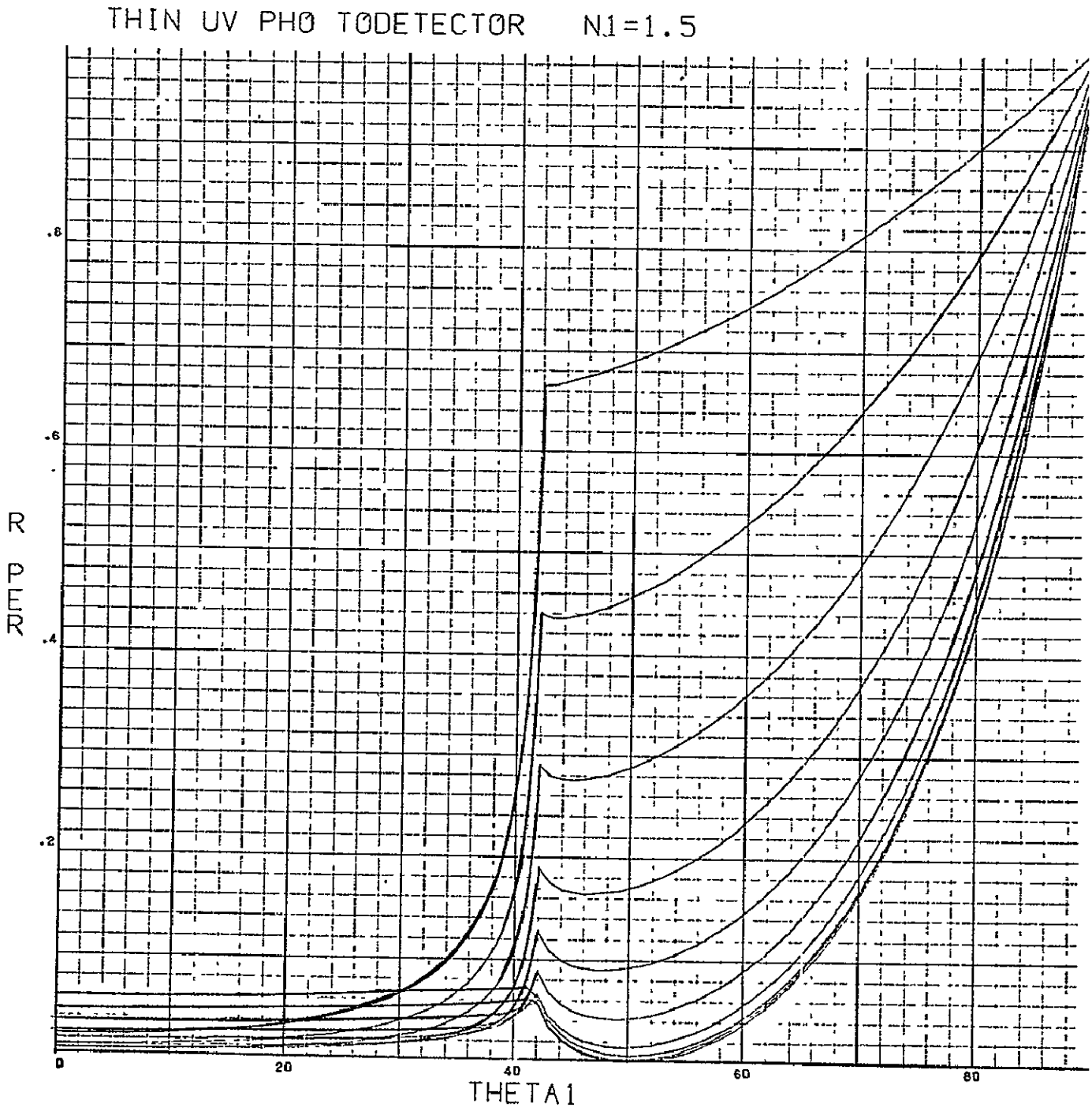

ANGLE OF INCIDENCE (in degrees)

n_2=3, k=.5, H/λ =.002-.020

Figure 13
R_{per} versus
Angle of Incidence,
N_1 = 1.5, N_2 = 3, k = 0.5

5. A higher index n_1 window or substrate is desirable (see Figure 14 - "vary n_1" graph) in order for:

a. More nearly perpendicular incidence

b. Broadening the angle over which enhancement occurs

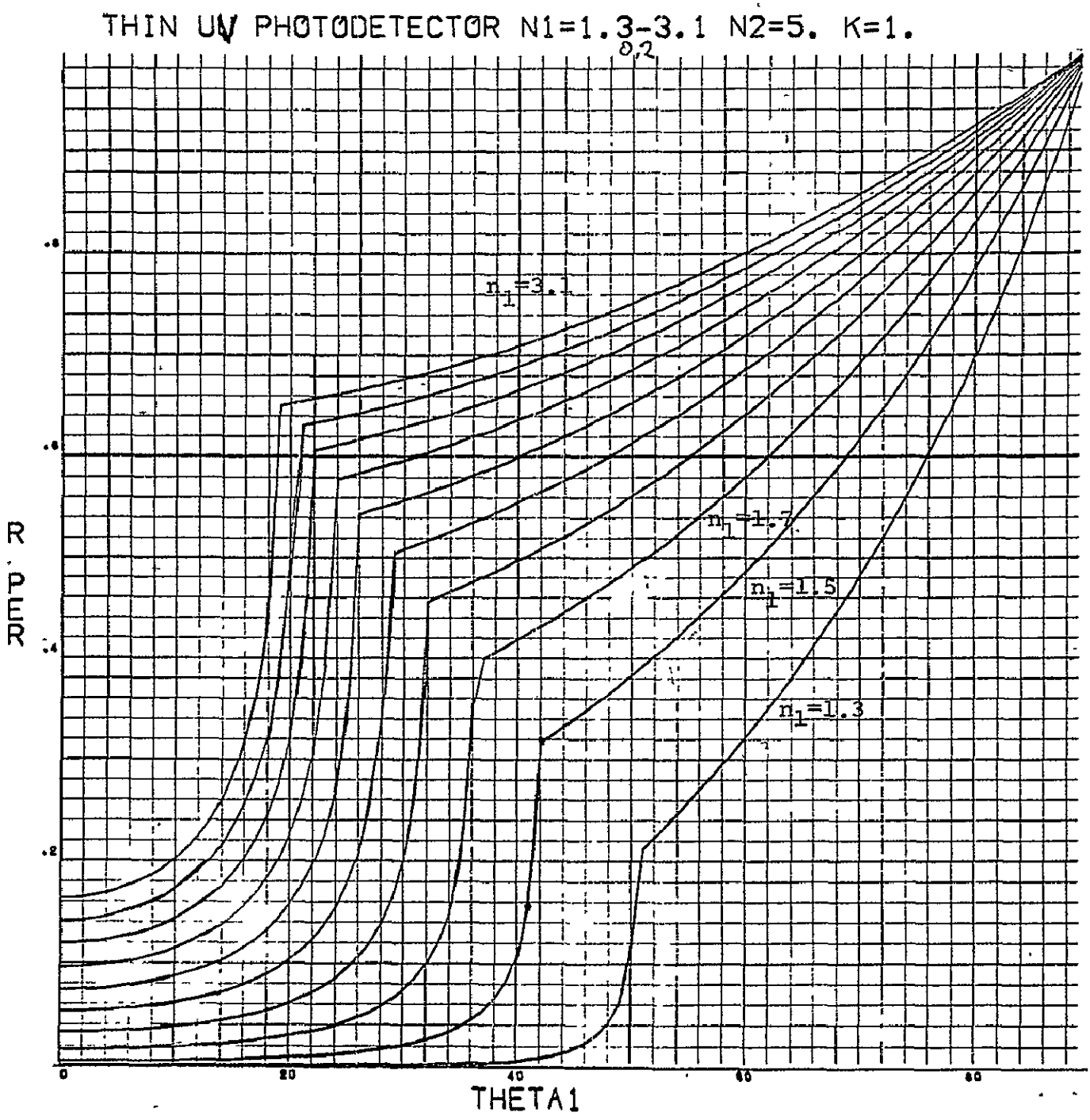

ANGLE OF INCIDENCE (in degrees)

N_1 varies in 0.2 steps, $H/\lambda = 0.001$

Figure 14
R_{per} versus
Angle of Incidence, Vary N_1

Gold Cathodes

Figure 15 illustrates expected theoretical transmission + absorption (1-Reflectivity) for a 50Å Gold coating. In the region below the critical angle (42°) almost all of the incident illumination is transmitted, while in the region between 42° - 90° a large portion of the radiation is absorbed. The exact values for absorption and transmission have been evaluated theoretically and the inaccuracy of calibration of our reflection photometer has not enabled us to obtain sufficiently accurate data for comparison. The significant point is, of course, the peak of absorption (~54°) which correlates very well with our peak QE enhancement. The correlation of this curve with the Quantum Efficiency enhancement curves included in the results is excellent.

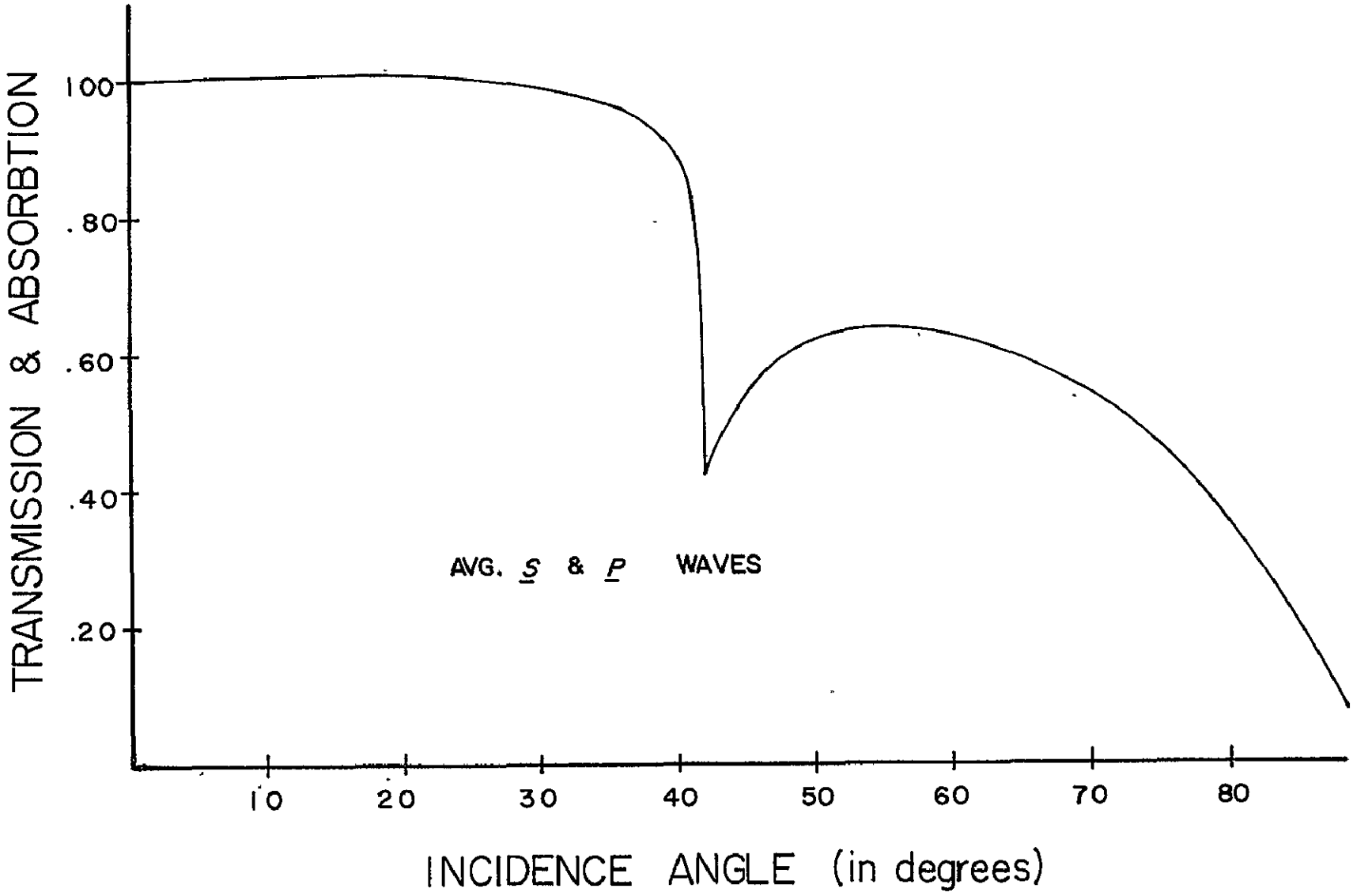
Z/λ = .0005
H/λ = .001 = 25A°
N1 = 1.5, N2 = 5, K2 = .1
TRANSMISSION & ABSORBTION
100
.80
.60
.40
.20
AVG. S & P WAVES
10
20
30
40
50
60
70
80
INCIDENCE ANGLE (in degrees)

Fig. 15

Introduction to The Alkali Metals

The following represents relevant theoretical analysis for alkali metals and their behavior as photocathodes in the ATR mode. The analysis is necessary in order to predict the average behavior of materials, whose precise optical indices are not known accurately enough when the materials are prepared in ultra thin films. Not only are the indices not accurately established, but their behavior with respect to wavelength is even less well known. The analysis is therefore required in order to approximately estimate the best thickness for each type of cathode made from alkali metals. A haphazard approach toward the optimum thickness by successive approximations would be very time consuming and costly.

Various materials such as Cesium, Potassium, Sodium, Calcium, and Magnesium all have indices which vary from very high value at the plasma frequency[34] to a relatively low value ; and then this value slowly increases as the wavelength increases. The absorption or attenuation[35] constants vary similarly with respect to wavelength*. Both effects serve to enhance each other in the ATR mode which consequently results in a cathode of stable behavior and wide band sensitivity, (with respect to wavelength) as will be shown.

---

* The graphical behavior is roughly analogous to that obtained in a parallel resonant electrical circuit. The absorption coefficient vs. wavelength behaves similarly to the magnitude of the impedance and the index vs. λ behaves similarly to the phase angle of such a network.

When the optical index is low, the moderate optical mismatch between the substrate and the cathode creates an intense electric field at the interface which enhances the absorption of radiation. The higher value of the attenuation constant at points where the index is low, however, compensates for the fact that the electric field at the boundary does not assume such extremely high values as would result if the index of the coating were very large. At wavelengths where the attenuation constant drops to a relatively small value, the index of refraction is sufficiently large to create an optical mismatch* and the concurrent electric field intensities and absorption enhancement. This high value of the electric field compensates for the low absorption constant of the cathode material-particularly for extremely thin cathodes.

Theoretical Predictions for Alkali Metal Cathodes

Typical optical properties of alkali metals[36] exhibit extremely high values of n and k at the plasma frequency[37] with the absorption coefficient k slowly increasing toward the infrared. The refractive index has less spectacular behavior and typically progresses from 0.5 in the UV to 1.5[38] in the blue-visible region of the spectrum. Lower absorbtion coefficients are typical in the ultra violet and higher n and k are prevelant for the alkali metals in the visible region. For most purposes, the minimum cathode refractive index will be 0.5 (a reasonable estimated value) and the typical index of refraction will vary from 1 to 1.5 for the cathodes in the visible region. All curves included here are calculated assuming a glass or quartz substrate index of 1.5 ($n_1 = 1.5$).

---

* Large electric field vector.

The following graph Figure 16 illustrates the wide range of n and k over which significant absorption enhancement occurs. The curves are plotted for the index of refraction of glass at a 45° incidence. Good absorption is obtained for the parallel polarization only (curve 1B) as can be seen from the minimum h/λ line 0.05. Here 90% absorption occurs in one reflection and almost total absorption occurs for two reflections. The variation of absorption of the parallel polarized ray with thickness is not significant, and occurs over a wide range of indices of the cathode. The enhanced absorption behavior for the perpendicular polarized ray (Figure 16) is far less important in this case and unfortunately occurs for a much higher range of indices of the photocathode. This higher range of indices makes the behavior of the perpendicular polarized ray less important here.

In these plots as the index increases, the performance of the cathode improves up to a maximum index value of approximately 0.8, which is very close to the expected value for alkali cathodes in the visible region of the spectrum. Peak absorption occurs in these cases for $h/\lambda = 0.05$ in the case of the parallel polarized ray (cathodes approximately 250Å thick). We could also typically obtain 90% absorption in two reflections for a 15Å layer with an index of 0.2 as shown on this second graph Figure 17.

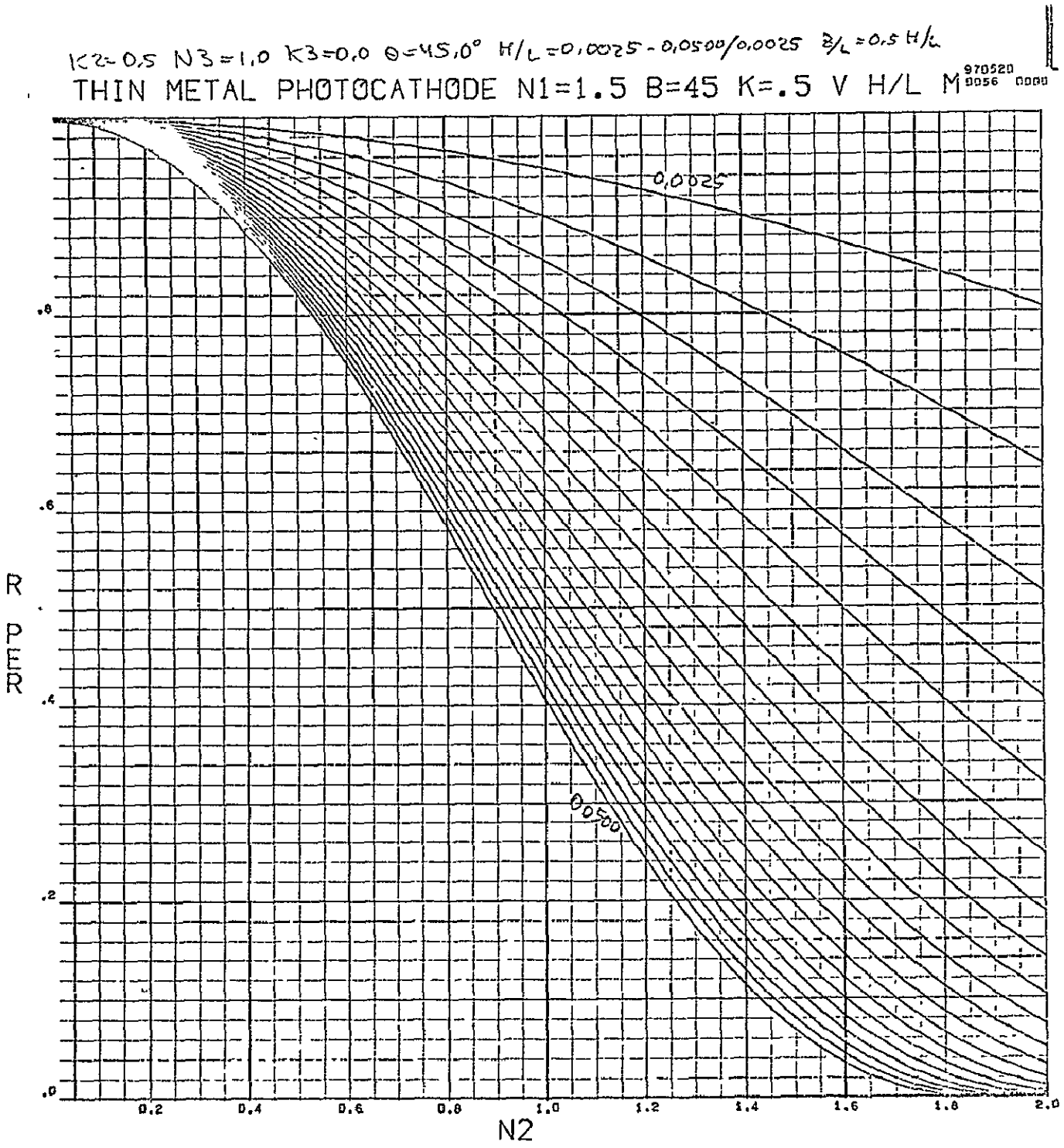

Figure 16

R_{per} versus N_2

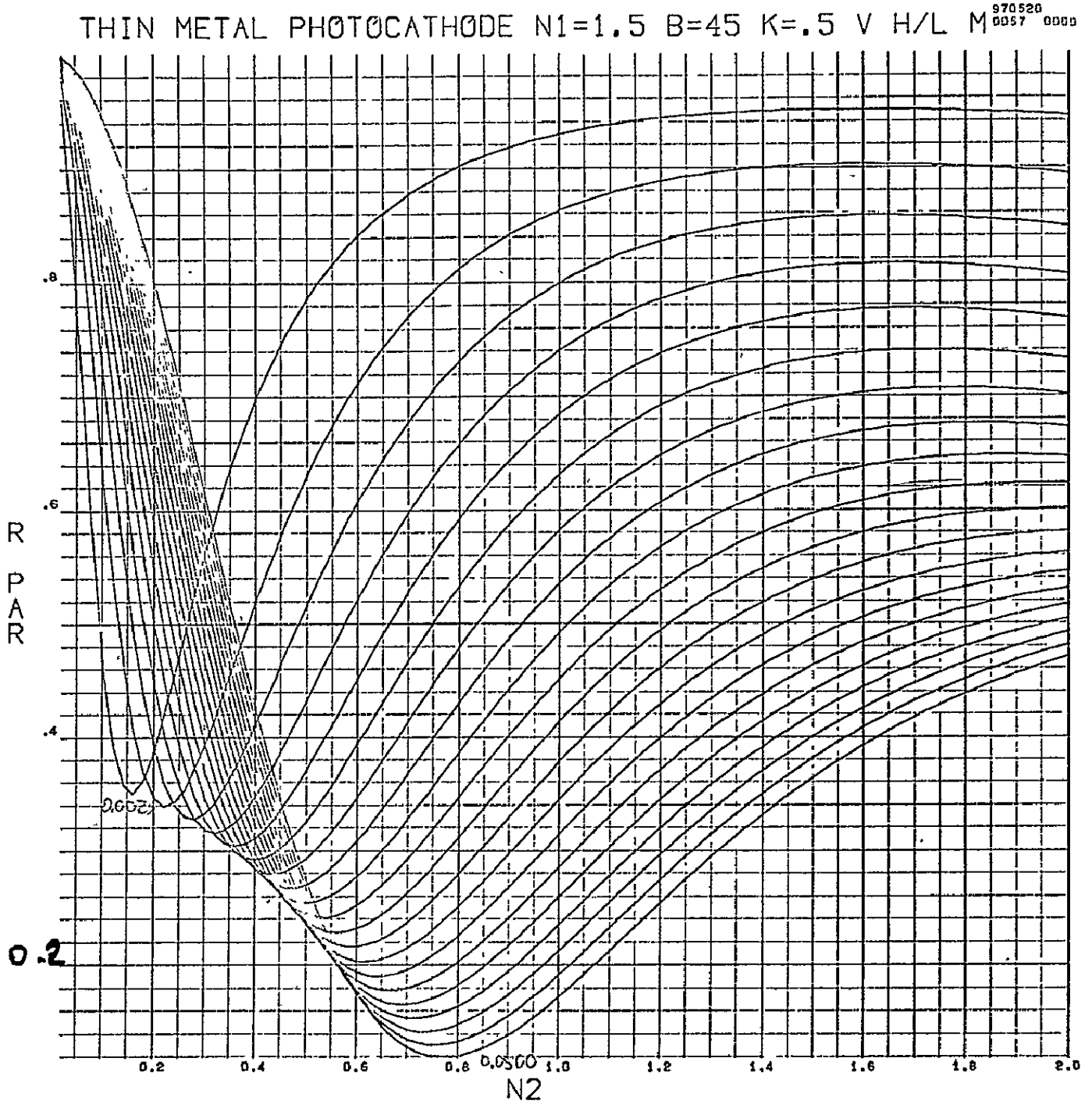

Figure 17

R_{par} versus N_2

Figures 18 and 19 illustrate the fact that one can use a material with a low index plus a low absorption coefficient and yet still obtain large enhancement in the ATR mode. Here the index of the cathode n_2 is estimated at 0.5 which is a reasonable value for the visible portion of the spectrum. We vary the absorption constant k and notice for a value of k = 0.5 or greater we have significant absorbtion. Below a value of k = 0.5 (parallel polarized ray graph) we have no inversion of absorption as we do when k increases to a value of approximately 1.2. This absorption inversion is one of the peculiarities of the ATR cathode and indicates most directly that the equations predict a <u>decrease</u> in the absorption of radiation as a cathode passes an optimum thickness and becomes heavier. For the parallel polarized ray, with $h/\lambda = 0.045$, we can obtain 100% absorption with a 200Å thick layer in a single reflection, (k is = to 1.2 and n = 0.5).

Note that when k is less than 0.7 the parallel polarized ray is not sufficiently absorbed unless two reflections are used*. For the perpendicular polarized ray, the optimum absorption is approximately 48% as indicated on the R_{per} graph. Throughout the analysis it is obvious that the perpendicular polarized ray and the parallel polarized ray cannot be simultaneously optimized for alkali metals in the visible region of the spectrum. It is also obvious that the parallel polarized ray almost always exhibits significantly higher absorption over a wider range of values of n and k for the cathode. Consequently, it will be standard procedure to optimize the response and thickness of the alkali cathode for the parallel polarized ray unlike the procedure for very high index metallic cathodes in the UV, where the opposite procedure is true.

---

* The criterion for good absorption of incident radiation is about 90% corresponding to about 10% reflection on the graph.

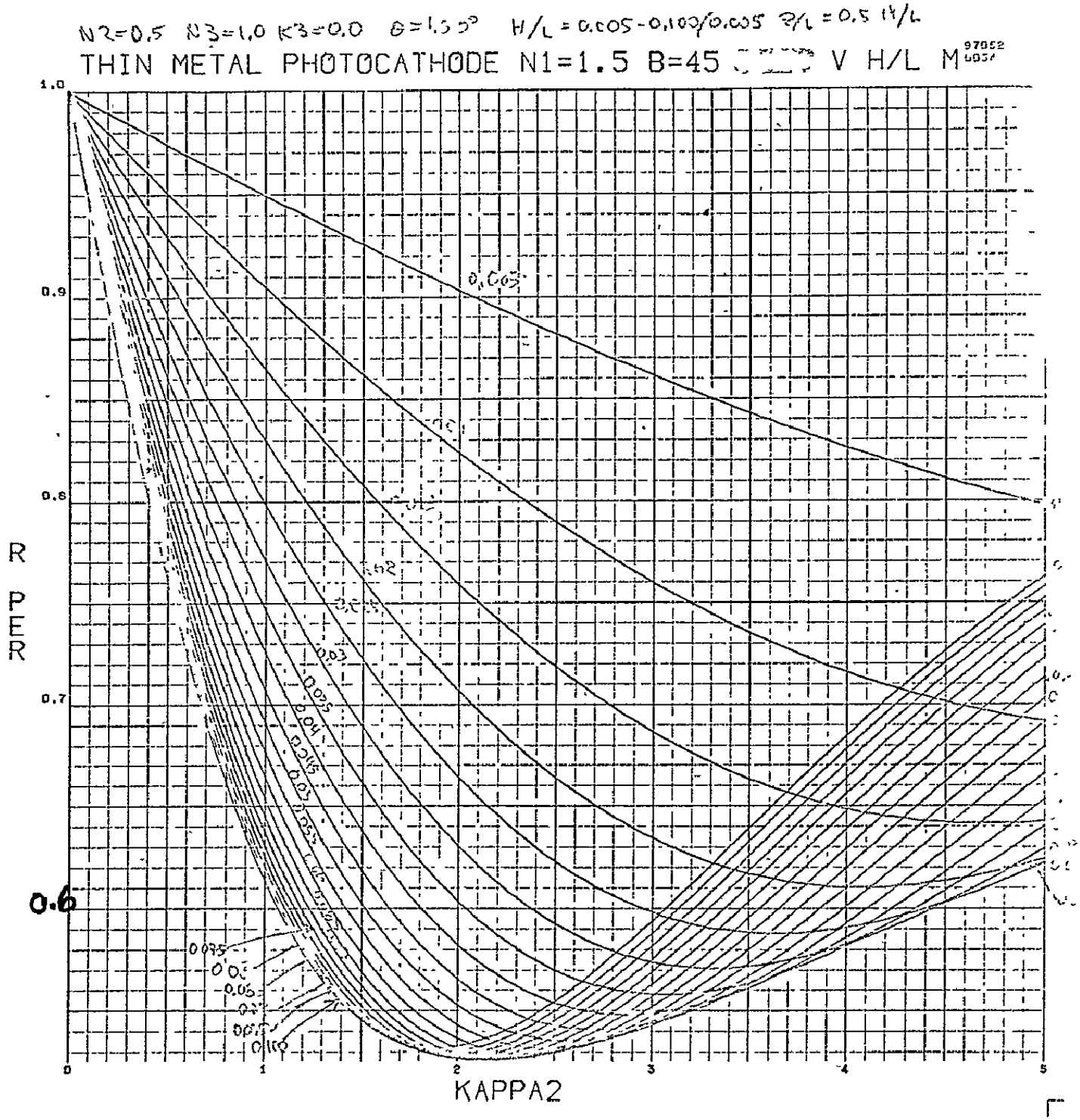

Figure 18

R_{per} versus k_2

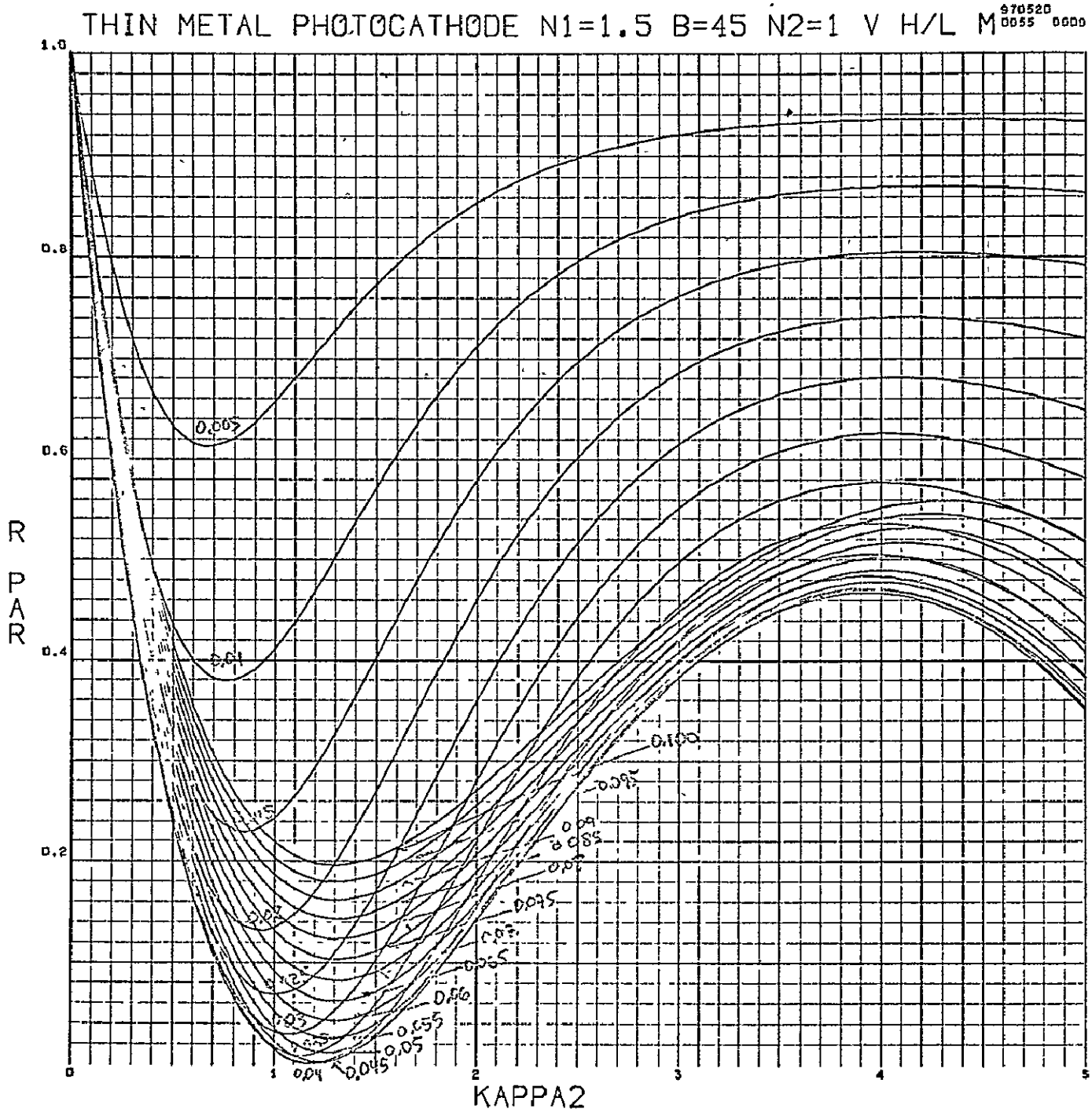

Figure 19

R_{par} versus k_2

Angular Dependence (Figures 20 and 21)

In the next two graphs we notice that the angular region of enhancement shrinks drastically as large thicknesses of the cathode are approached. For the perpendicular polarized ray we obtain an inversion of absorption at approximately $h/\lambda = 0.0225$ which corresponds to approximately 115Å cathode thickness and a cathode index of 0.5. For a low thickness cathode, the angular width of acceptable radiation in the substrate would be approximately 15° (2.5 in air). For larger thicknesses the angle is reduced to approximately 5° (7.5 in air) and becomes almost useless for very large input aperture detectors. Although the transparency of these cathodes is low, we could obtain good angular response from materials of high transparency.

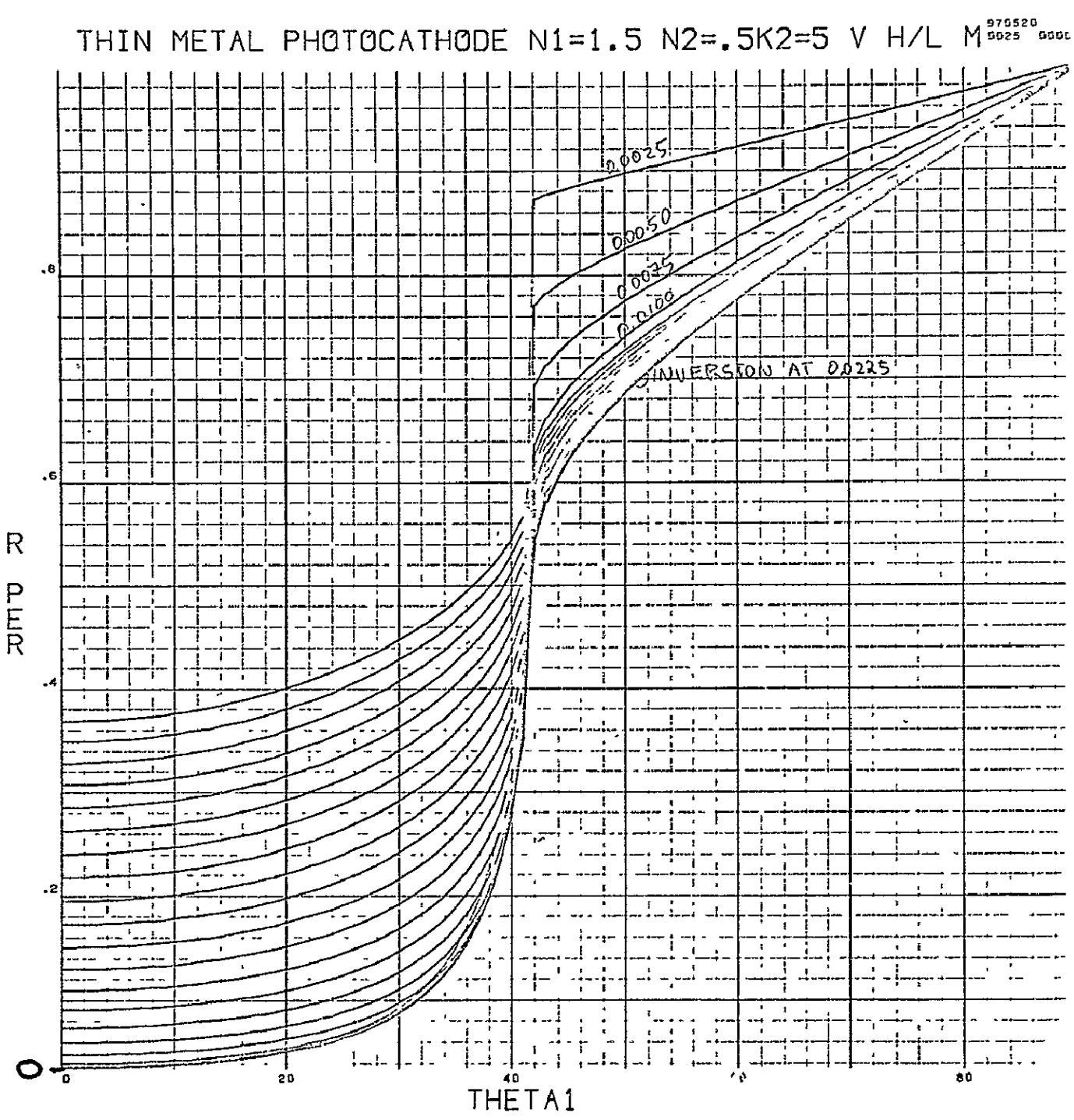

Figure 20
R_{per} versus
Angle of Incidence,
$N_1 = 1.5$, $N_2 = 0.5$

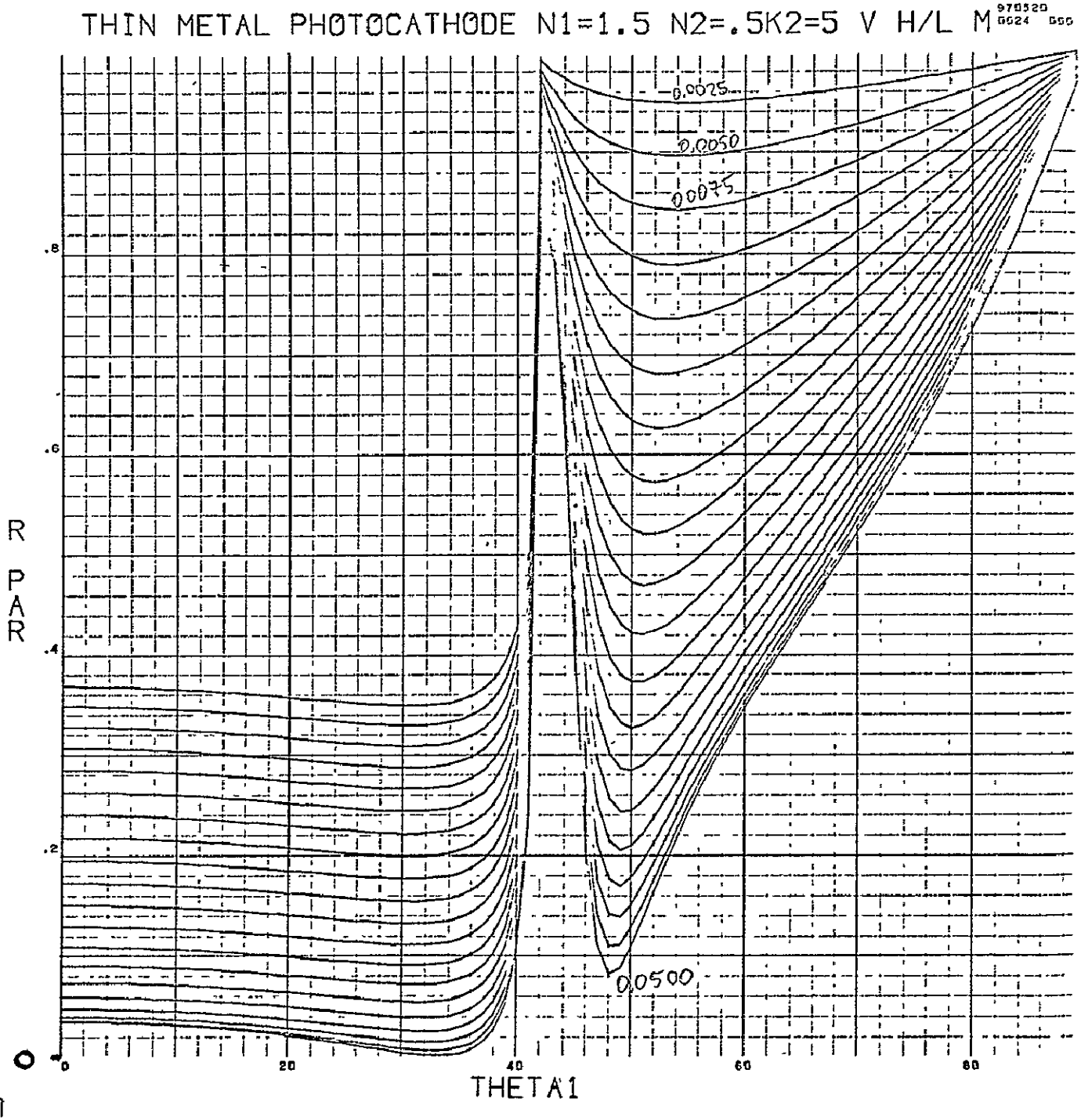

Figure 21
R_{par} versus
Angle of Incidence,
$N_1 = 1.5$, $N_2 = 0.5$

Absorption Inversion With k (Figures 22 and 23)

The index of the cathode is again 0.5 and we notice for the first time an inversion of absorption in these plots as k varies. For the perpendicular polarized ray the absorption has a maximum when k is in the region 2.5 to 2.0; the absorption is less (for a given thickness cathode coating) for both higher and lower values of the absorption coefficient. In the next graph (Figure 23) notice the absorption inversion with k is even more interesting. Here, however, the optimum values of k vary between 0.9 and 1.2 with an absorption maximum occurring near $h/\lambda = 0.04$. This corresponds to a cathode thickness of approximately 200Å for (cathode index of 0.5). The perpendicular polarized ray has an absorption maximum of approximately 48%; to achieve this value of absorption would require a cathode with an index of 0.5, an absorption coefficient of 2.0 and a thickness of 400Å. Two reflections from such a cathode would result in approximately a 75% absorption of the incident energy. After four reflections* all but 7% of the incident energy would be absorbed. For the parallel polarized ray, (Figure 23), a material with an index of 0.5, an absorption coefficient of 1.0, and a thickness of only 200Å will absorb 100% of the incident radiation. Here it makes most sense to optimize the cathode for the parallel polarized ray.

The range of k over which absorption is almost independent of both k and h/λ is striking in both of these graphs. Both the perpendicular and parallel polarized ray exhibit rather weak dependence upon k and h/λ, greater than 98% absorption of the input radiation in the parallel polarization can be obtained

* This many reflections precludes the use of an imaging device.

over an octave of the spectrum. Note that the thicknesses here are approximately 200Å and these are well within the state of the thin film art particularly at Block Engineering, Inc. Values of k which can be easily obtained range from 0.5 to 2.5. Outside this region the absorption decreases to less than 75% in one pass and multiple reflections become necessary.

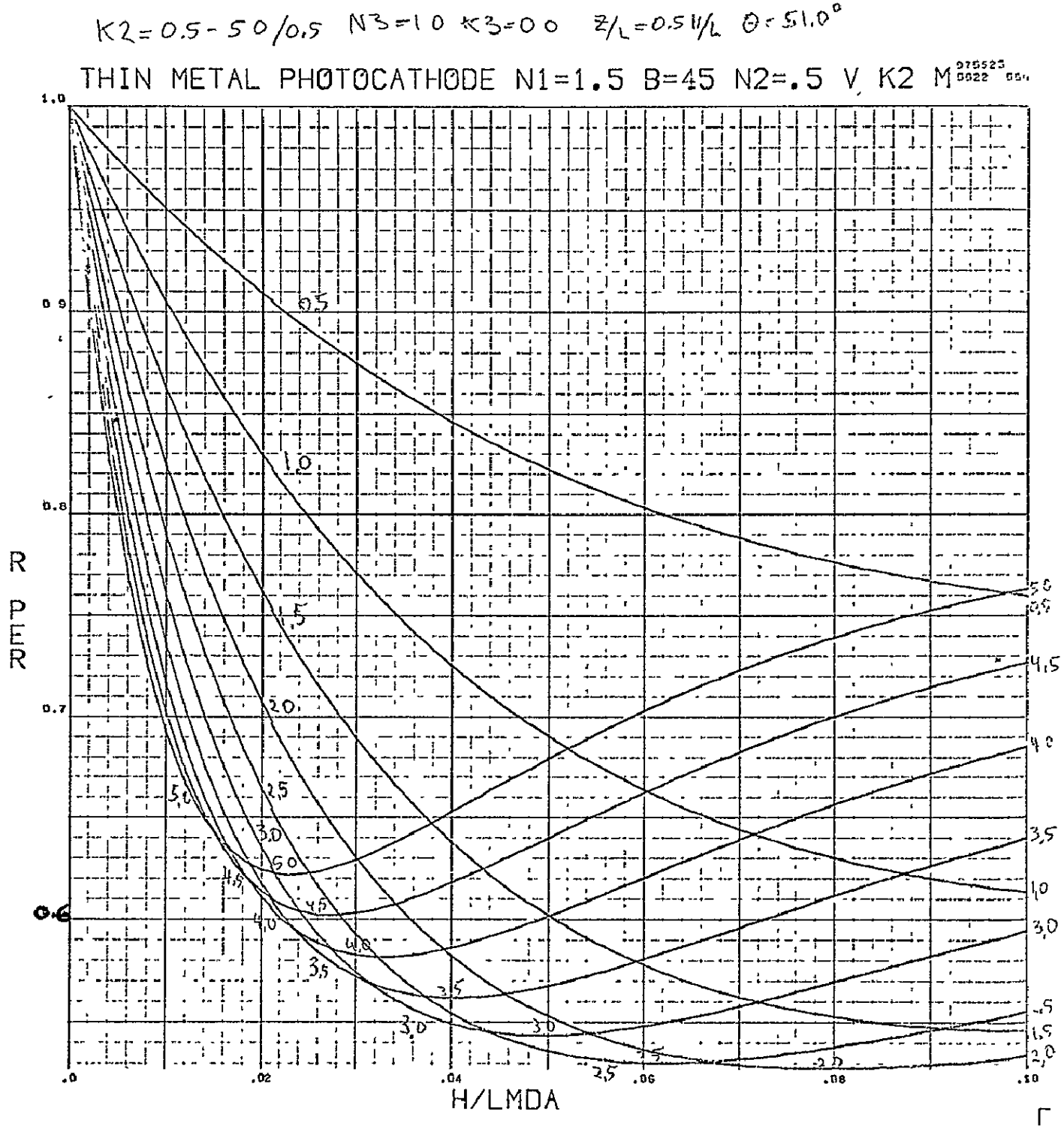

Figure 22

R_{per} versus H/Lamda, Vary k_2

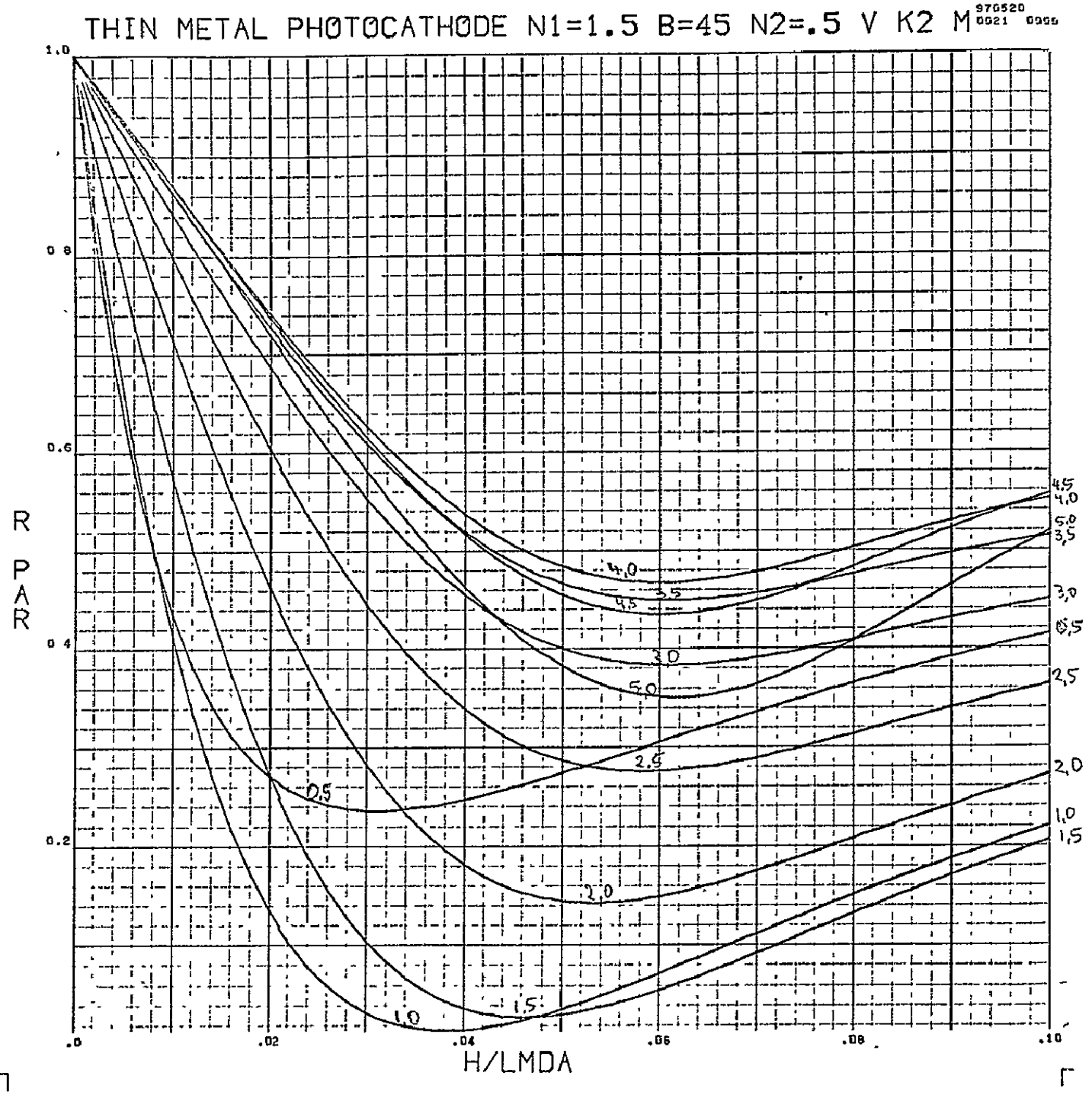

Figure 23

R_{par} versus H/Lamda, Vary k_2

On Figure 24 the absorption of perpendicular polarized radiation is not particularly high for low index cathodes and becomes only fair as the cathode index approaches 1. There is, however, an absorption inversion in the vicinity of moderate ($n_2 = 2.0$) index cathodes. For an index of 2.0 and a coating thickness of approximately 200Å, almost 100% of the radiation will be absorbed (perpendicular polarization) for a single pass of radiation. As the index of the cathode is increased, the angular region over which the enhancement occurs becomes rather narrow and the optimum cathode thickness also decreases rapidly. For 200Å thick cathodes, the region of enhancement for 90% absorption (in a single pass) extends over 1 octave in wavelength.

Particular attention should be paid to the parallel reflected ray absorption illustrated in Figure 25. Note for extremely thin cathodes there is a peak in absorption when the cathode index approaches 0.2 and another peak in absorption as the cathode index approaches 4.0, although the peak at 0.2 illustrates significantly greater absorbtion (63%) for a single pass of radiation. The absorption enhancement at 4.0 (42% abs.) is primarily caused by the large electric field vector in the Y direction parallel* to the cathode substrate interface. The value of the electric field vector in the Z direction has relatively small values for high cathode index as seen from Figure 26 where the values E_z^2 for indices higher than 0.6 are all slightly above the horizontal line near the 0 axis (not clearly defined on plot). For a cathode index of 0.2, however, the value of the electric field in the Z direction reaches an extremely large peak as illustrated by the 0.2 spike on the E_z^2 curve. This extremely intense electric field vector in the Z

* X and Y are parallel to the interface the Z vector is perpendicular to the interface.

direction is responsible for the enhanced absorption of radiation of both polarizations in extremely thin cathodes of relatively low index.

As a corollary advantage it should be mentioned that photoelectrons generated in the presence of an extremely intense Z field are emitted perpendicular to the plane of the cathode and have practically no velocity component in the tangential direction. The advantage of this type of emission is obvious. With an extremely low velocity component in the Y or the X direction, the chances of inter-action between the photoelectron and the cathode material are minimized. Secondly, for such extremely thin cathodes, the electron is emitted either toward the vacuum or toward the cathode substrate interface (where it is totally reflected); almost no electron optics are necessary in such a photomultiplier to assure all the electrons will be emitted in one direction-toward the first dynode*. It is true that such behavior results for a relatively narrow band of wavelengths, however, this band of wavelengths, as with all of our ATR work, can be tailored to the specific region of interest.

---

* A third advantage is the possibility of spectral selection as a function of primary photoelectron energy.

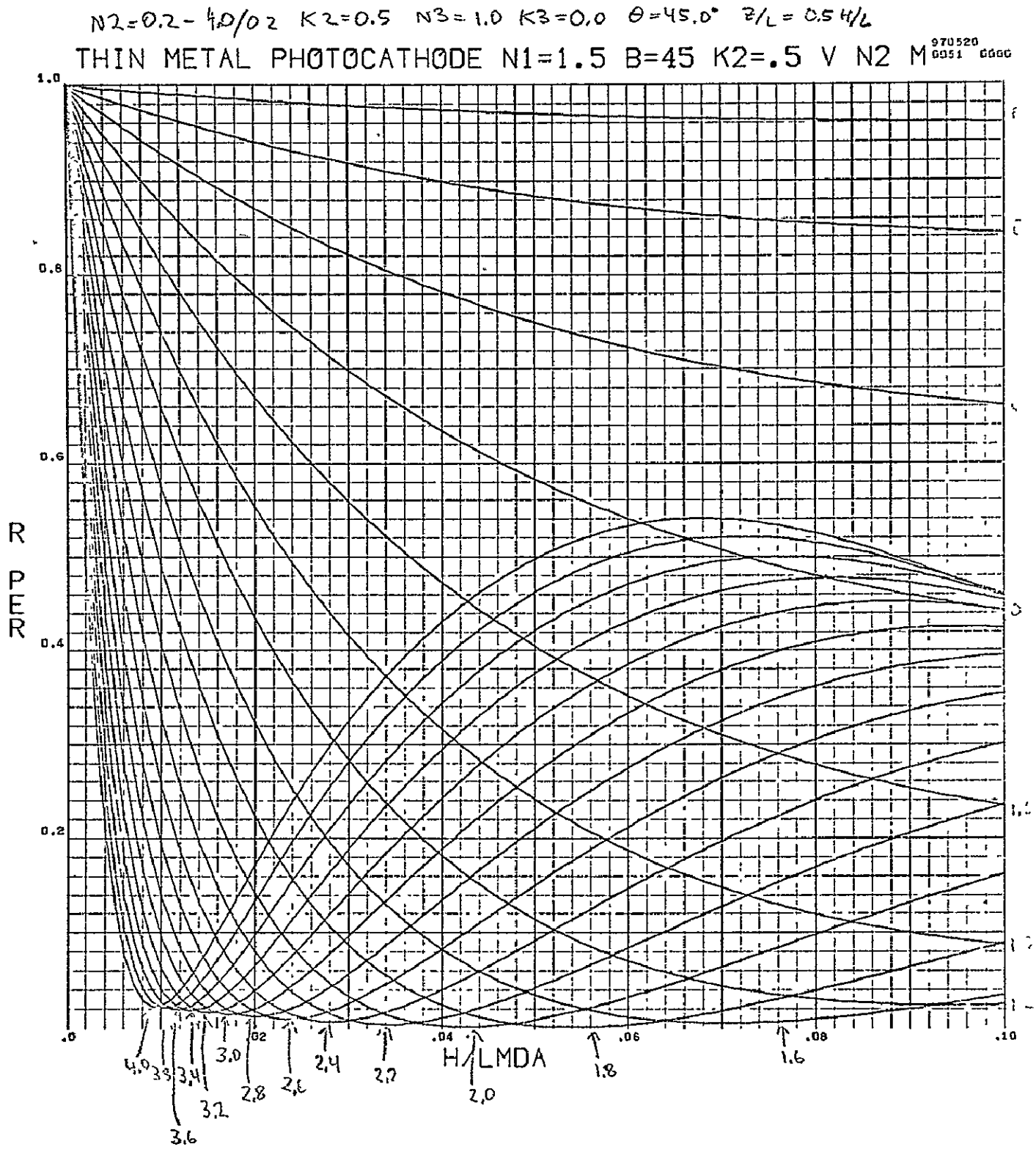

Figure 24

R_{per} versus H/Lamda, Vary N_2

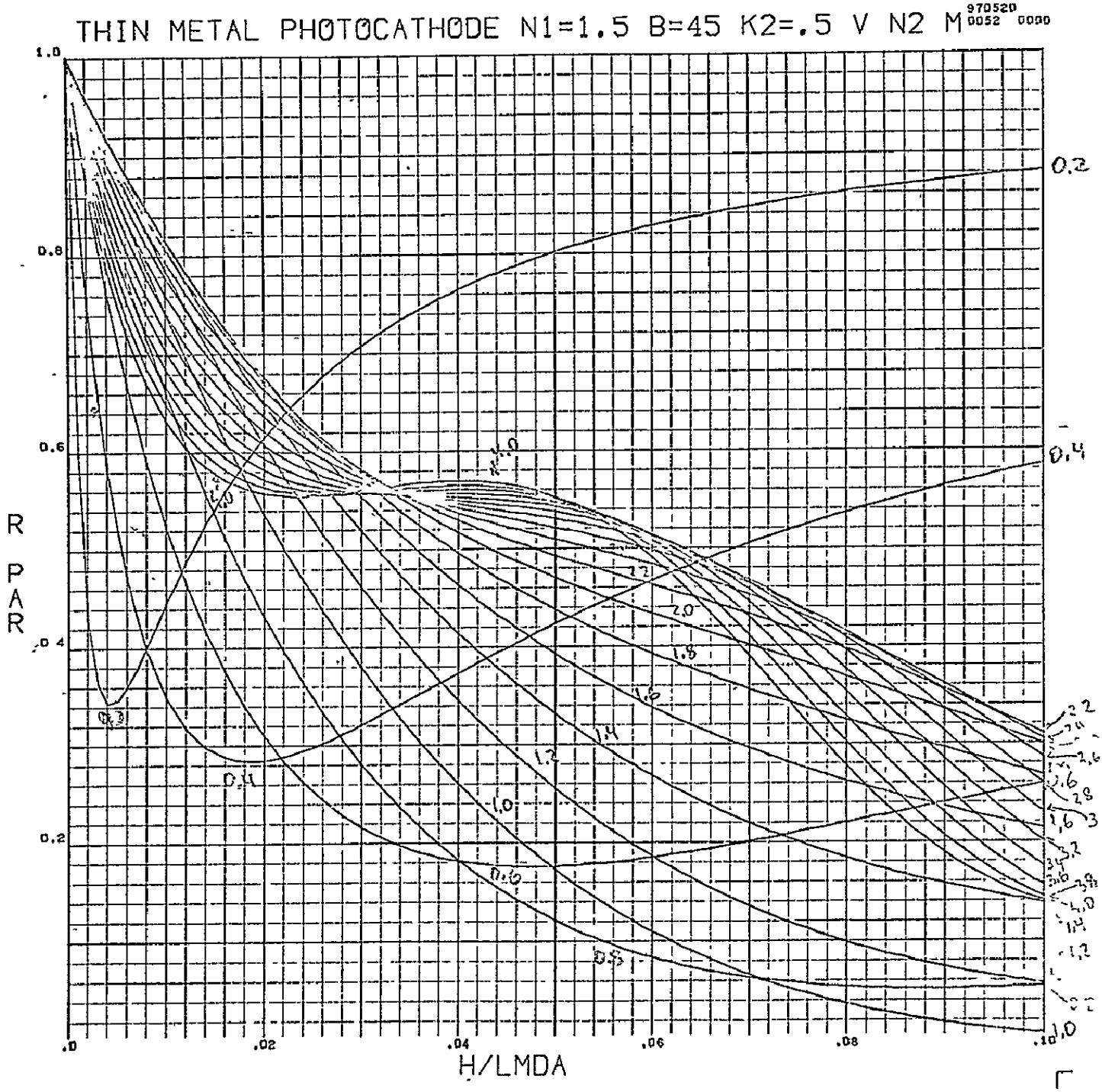

Figure 25

R_{par} versus H/Lamda, Vary N_2

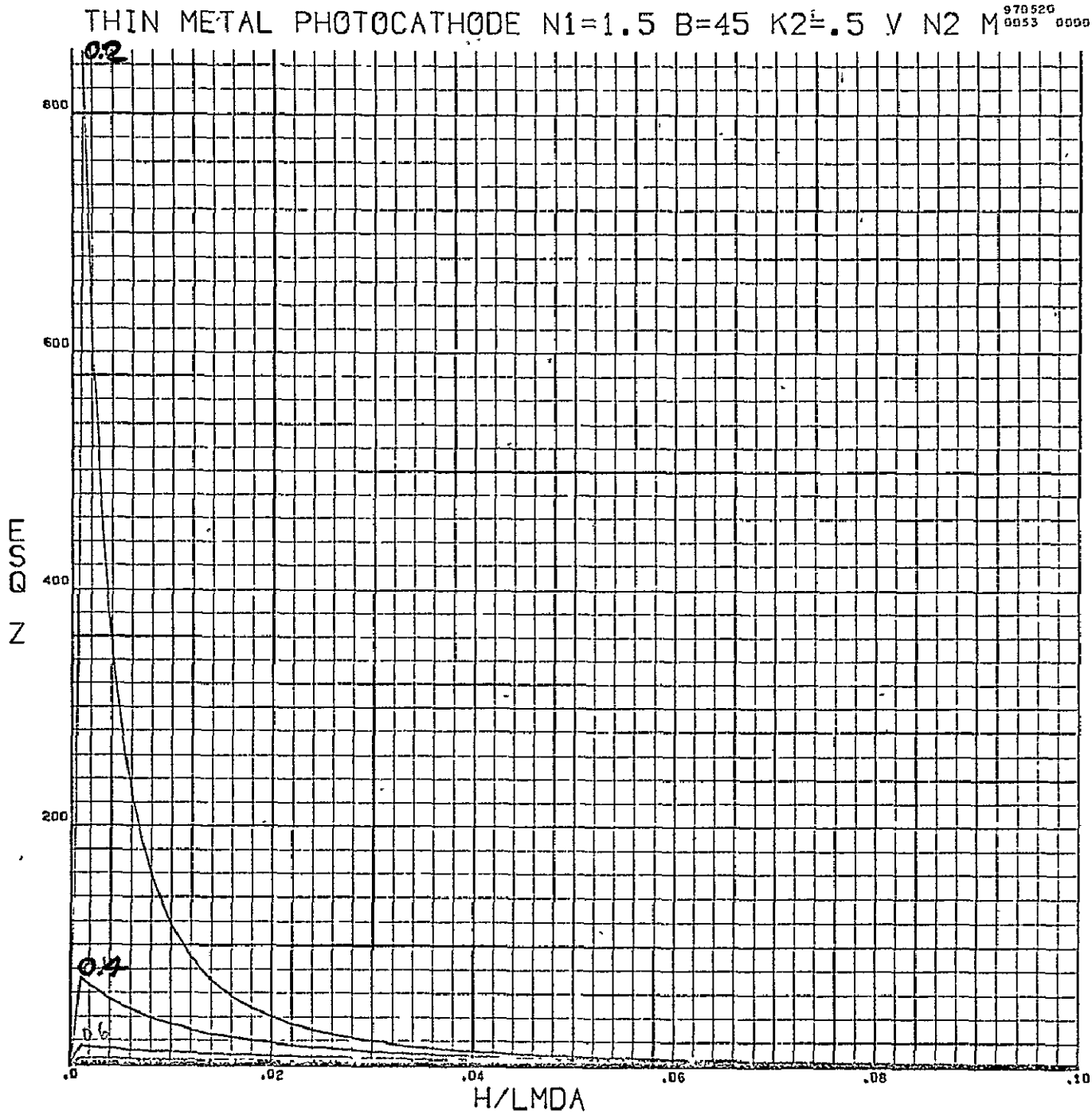

Figure 26

E_z^2 versus H/Lamda, Vary N_2

X. Calibration

Deposit Thickness Monitor

Cathodes of Gold, Platinum, Magnesium, Sodium, Potassium and Cesium were formed in layers up to 200Å thick. Quantum efficiency measurements were made after establishing the exact optical thickness of the coating on a substrate similar to that actually used for cathode testing.

Our techniques for manufacturing and testing controlled coatings have improved since the inception of the program. New optical measuring instruments have been built and used, and a complete manipulation assembly is now in use enabling a wide variety of ATR cathodes to be thoroughly tested immediately after formation.

Extensive cooperation has been obtained from the Sloan Instrument Corporation to improve and tailor the evaporation thickness monitor for the ultra thin film deposit region.

Cathode Coating Calibration

The following cathode materials have been used for calibration of the deposit thickness monitoring instrumentation.

Material	Deposition Method	Atomic Weight	Relative Density
1. Gold	Filament	196.967	19.32
2. Platinum	E.Beam Bombardment	195.09	21.45
3. Aluminum	Filament	26.9815	2.6989
4. Magnesium	Filament (Raw Material)	24.312	1.738

Material		Deposition Method	Atomic Weight	Relative Density
5a.	Potassium	Raw Material (Basket)	39.102	0.862
b.	Potassium	Complex Reaction (Basket)	39.102	0.862
6.	Sodium	Raw Material (Basket)	22.9898	0.971
7a.	Cesium	Complex Reaction (Basket)	132.905	1.873
b.	Cesium*	Raw Material*	132.905	1.873

Previously described procedures were used to calibrate thickness of deposit using a Fizeau Fringe Interferometer. Overcoatings of Aluminum were necessary to create a uniformly reflective surface and to prevent reaction of the alkali metals with the air.

A series of stepped deposits of the cathode material are coated on a quartz optical flat simultaneously with and in close geometrical proximity to the resonant crystal deposit monitor. A record of frequency deviation vs. coating thickness is then obtained for each new material. Although the calibration curves will have slopes relatively proportional to the bulk density of the material (particularly for very thick coatings near 1μ) the bulk and thin film densities of all materials are in general vastly different and so the resonant crystal must be calibrated for each material and in the same coating thickness region as will be monitored.

The stepped optical flats are examined under a Michelson interferometer with white and monochromatic light to examine surface irregularity and determine crude step height (fringes are too broad for accurate measurement). The stepped flats are then examined under a specially constructed Fizeau Fringe Interferometer which requires contact between a "proof" flat and the sample.

---

* Glass capillary system - test aborted.

In order to obtain the necessary accuracy, extremely narrow, easily resolved, high contrast fringes are necessary. These are obtained only from high reflectivity sample coatings. In the case of Gold, Platinum and even thin Magnesium coatings, their reflectivities are high enough, but Cesium, Sodium and Potassium exposed to air, oxidize rapidly and could destroy the coating of the "proof" plane unless they were overcoated. For this purpose, an overcoating of Aluminum is used immediately after depositing the alkali metals in order to increase the reflectivity and protect them from the air during thickness measurement. The Aluminum effectively shadows the step and does not introduce an error due to its own thickness (below 2000Å). Eventually the active metals discolor the Aluminum overcoat necessitating optical thickness measurements soon after coating. Thus the alkali metals present special problems in thickness determination. In particular, the vapor pressure of Cesium at room temperature necessitates close control of quartz crystal monitor temperature, otherwise erratic thickness readings will result. A recirculating thermal bath has been installed for this purpose. Potassium was evaporated first since it is easier to control and there is less danger of contamination of the vacuum system.

Three photographs showing a 500Hz, 1000Hz, and 2000Hz step of Magnesium corresponding to 445Å, 990Å and 1980Å of this material are shown for illustration in Figure 27.

MAGNESIUM STEPS

Step Height: 445 A°
Crystal Monitor Δf: 500 Hz.

Step Height: 990 A°
Crystal Monitor Δf: 1000 Hz.

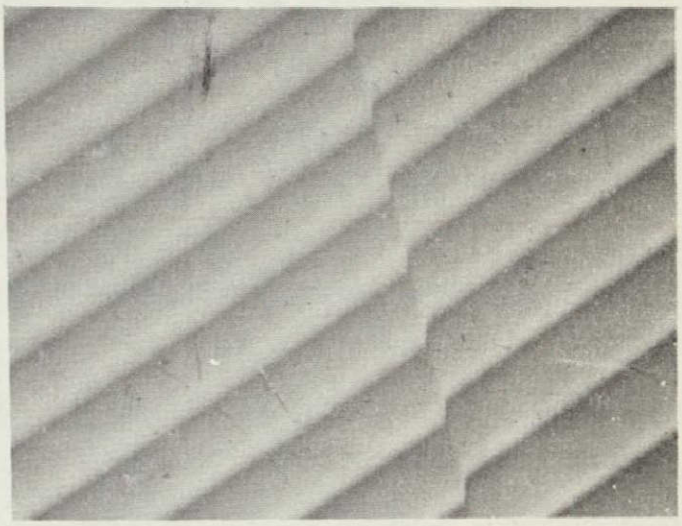

Step Height: 1980 A°
Crystal Monitor Δf: 2000 Hz.

Figure 27
Fizeau Fringe Photographs
Magnesium Steps

Film Resistance

In order to explore other possible thin film deposit controls, several slides were made which enabled us to measure the ohms-per-square resistance of the mass deposit obtained on a standard microscope slide. Extremely poor correlation between the deposit thickness or deposit mass and the resistance obtained on the surface of the slide even when using rate control. A short series of tests along these lines proved to our satisfaction that such a resistance monitor would not be suitable especially for cathodes in the ultra thin region of interest.

Optical Film Density

Figure 28 illustrates the poor correlation obtained between optical density of coatings of aluminum and the actual mass deposit. Poor correlation could be due to re-crystallization phenomena or the fact that monochromatic light was not used in the densitometer. In any case, Block feels that interferometric thickness measurement (accurate to $\pm$ 15Å) is appropriate for cathode thickness control.

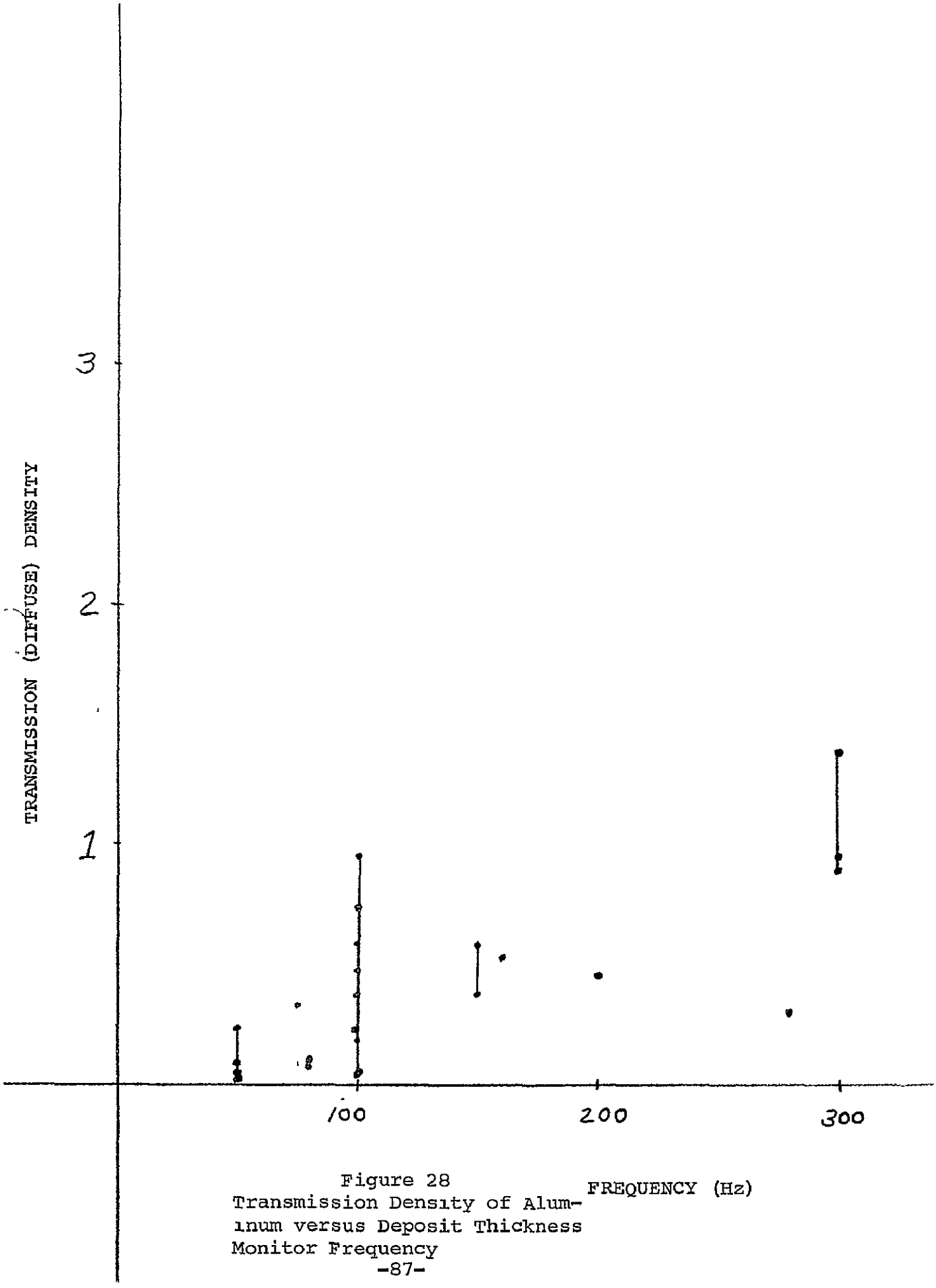

Figure 28
Transmission Density of Aluminum versus Deposit Thickness Monitor Frequency

The following curves are plots of the actual working calibration curves for the deposit monitor. Operation of the mass monitor is based on a resonant frequency shift caused in a quartz crystal as a mass deposit builds up on its surface. Details are not included here but a thorough treatment of this technique is found in reference 39. The significant point is that thicknesses of the higher density materials can be controlled more accurately than the lighter materials such as Al or Mg. The calibration points (not plotted) were obtained by coating precision optical flats to various mass readings (frequency deviations) on the monitor, and subsequently examining the optical step produced using a Fizeau fringe and Michelson interferometer. Using the Sodium D doublet for illumination, accuracies of $\pm$ 20Å obtain as a matter of routine. For most accurate results Block has assembled a Michelson interferometer using fringes of equal chromatic order (FECO) which allows accuracy of 7-10Å. This is unnecessary for most measurements and is difficult to use.

As coatings become thinner, the densities of deposit appear to vary[40] and ρ may actually approach 0.5 for 10Å films of some metals. Platinum and Gold do, however, seem to deposit almost uniformily down to monolayers.

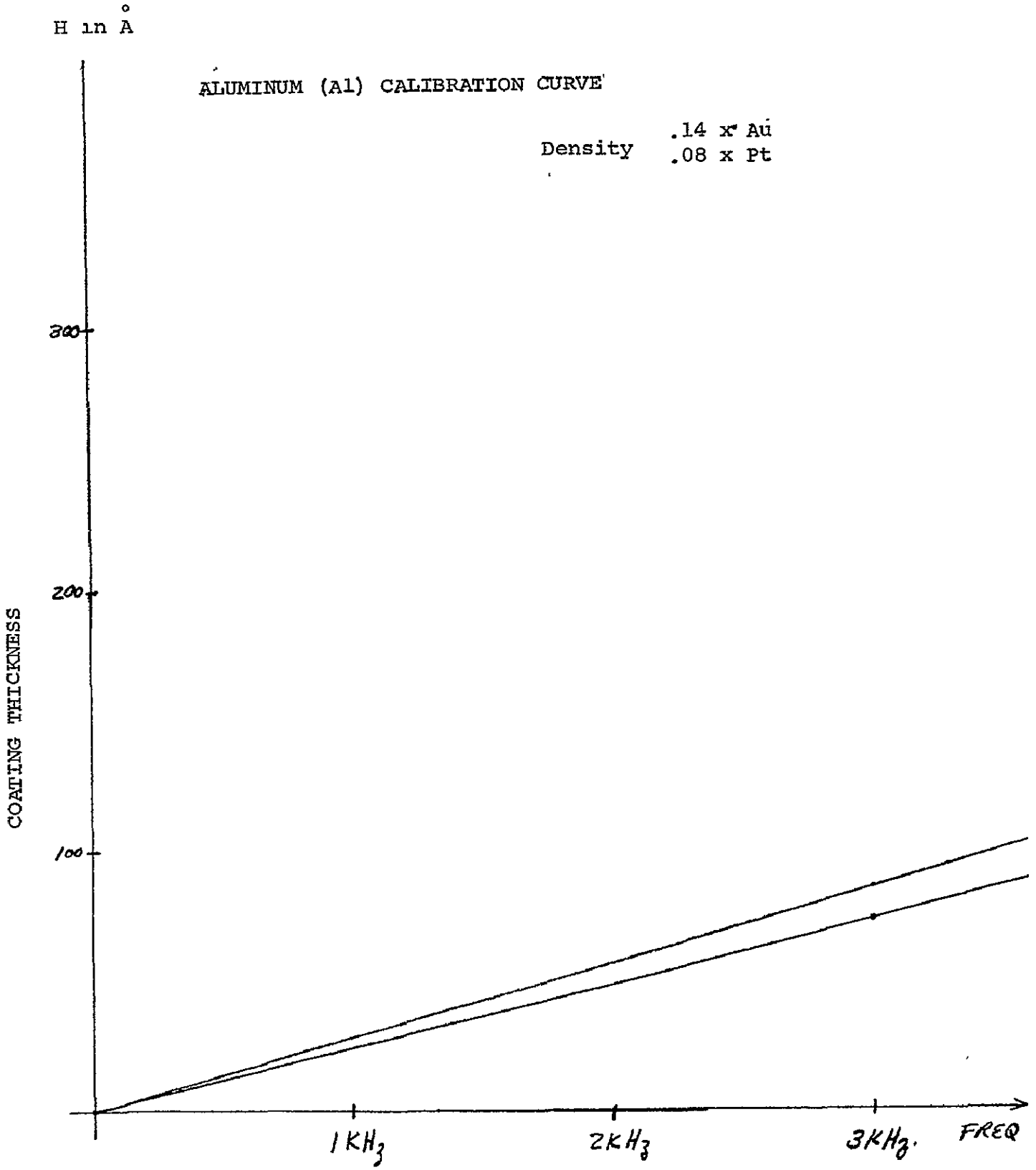

MASS DEPOSIT MONITOR

Figure 29

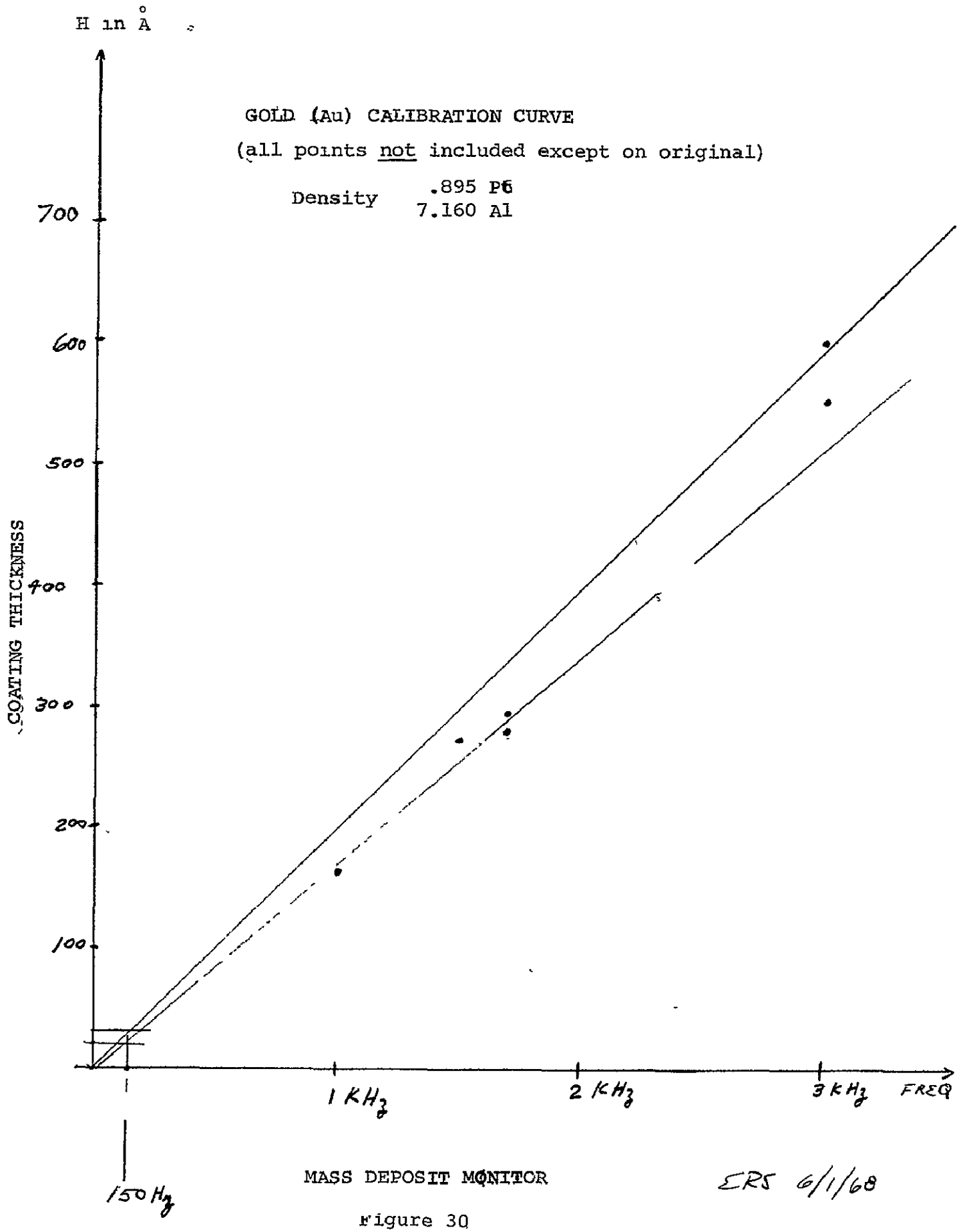
H in Å
GOLD (Au) CALIBRATION CURVE
(all points not included except on original)
Density .895 Pd
7.160 Al
700
600
500
400
300
200
100
COATING THICKNESS
1 KHz
2 KHz
3 KHz
FREQ
150 Hz
MASS DEPOSIT MONITOR
ERS 6/1/68

Figure 30

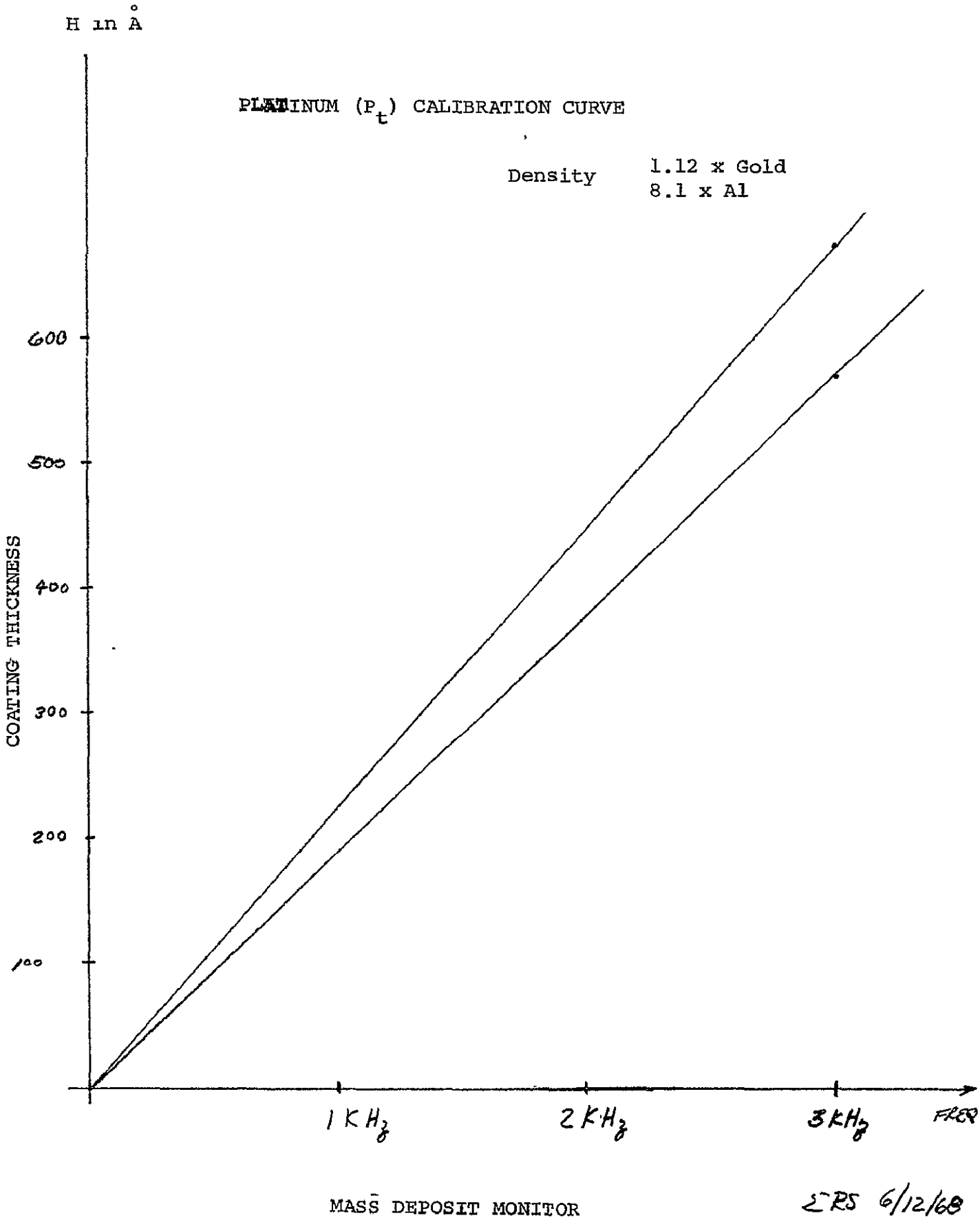

MASS DEPOSIT MONITOR

ERS 6/12/68

Figure 31

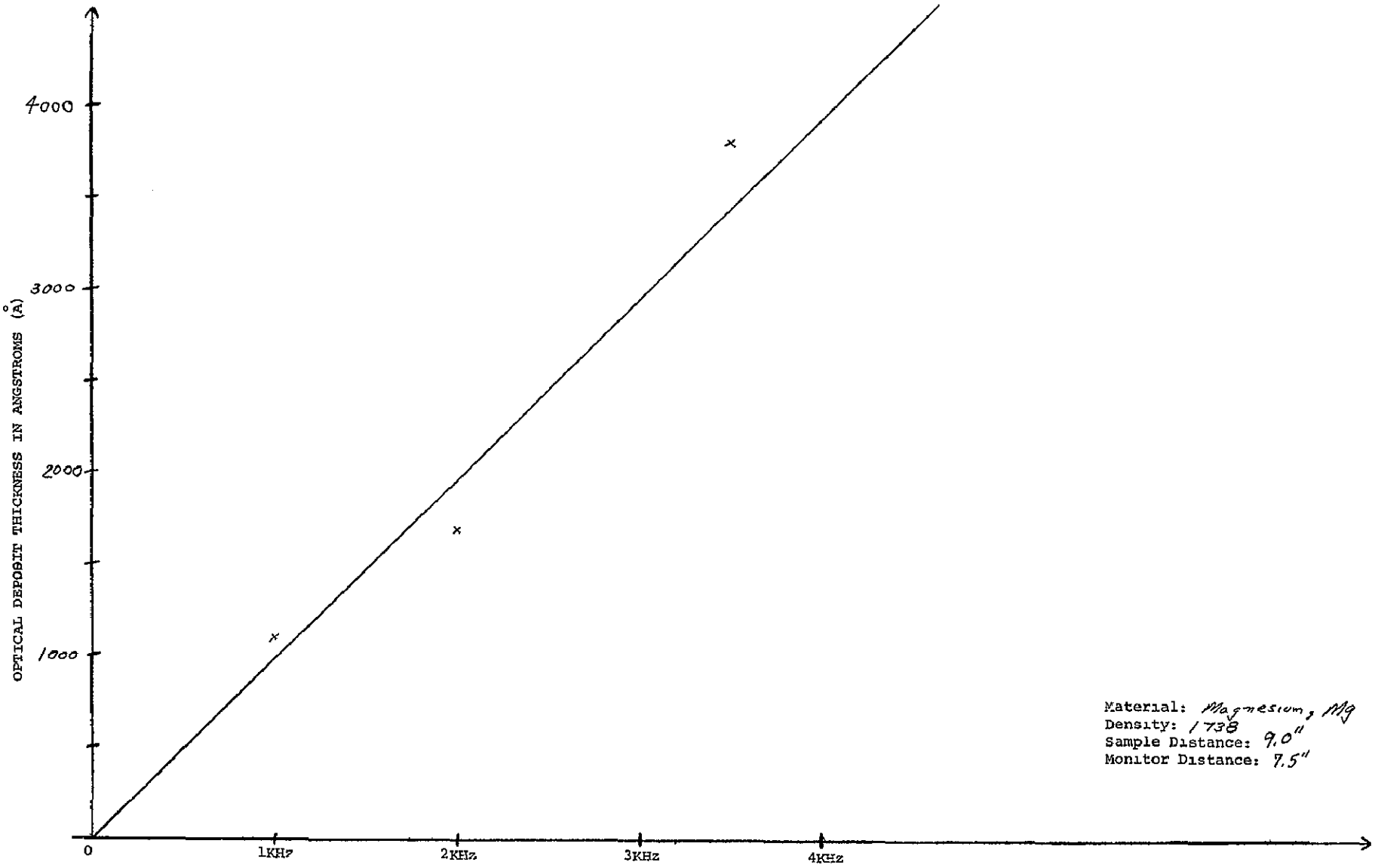

Figure 32
Magnesium - Coating Thickness
versus Monitor Frequency

Figure 32
-92-

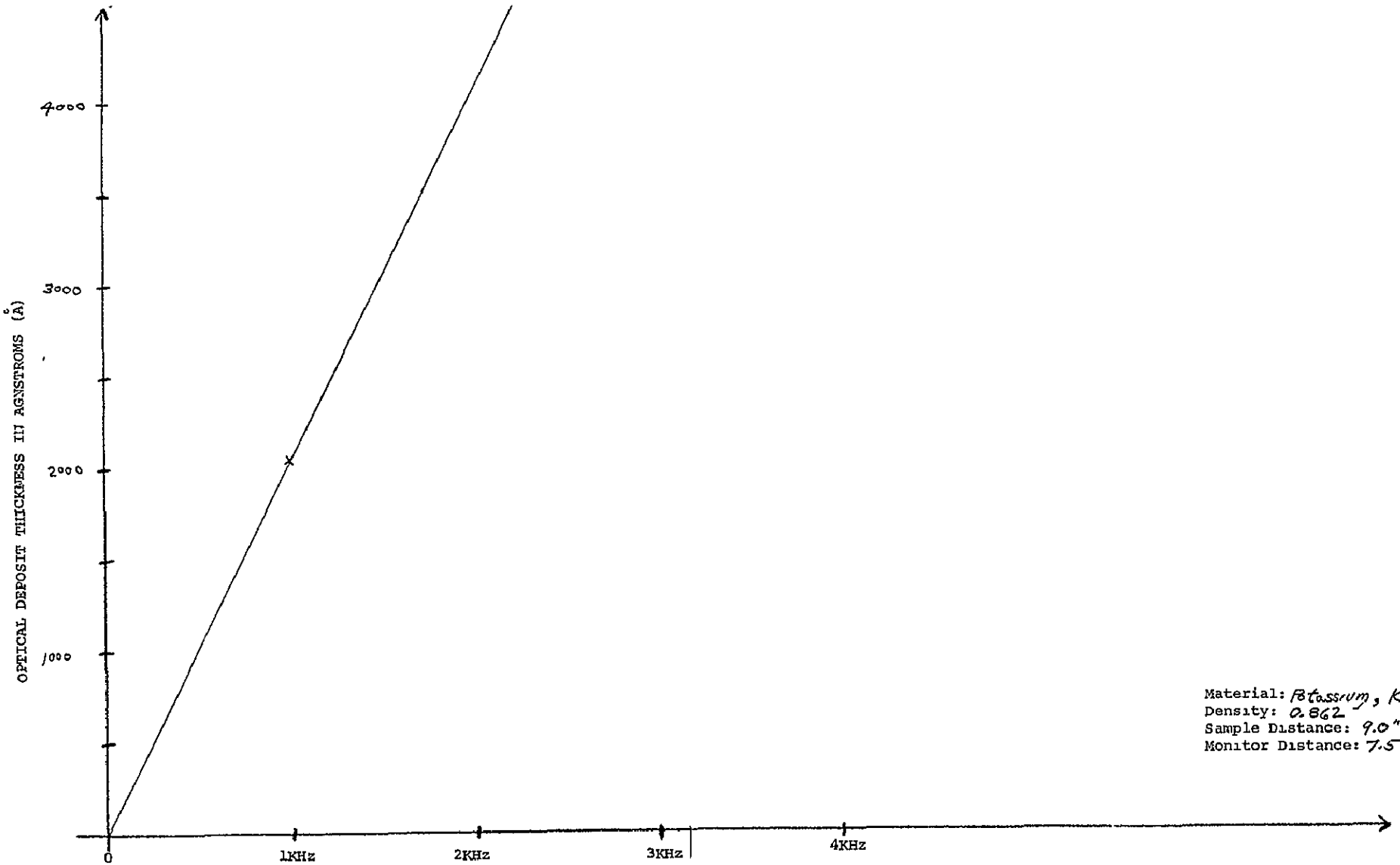

Figure 33

Potassium - Coating Thickness versus Monitor Frequency

Figure 33
-93-

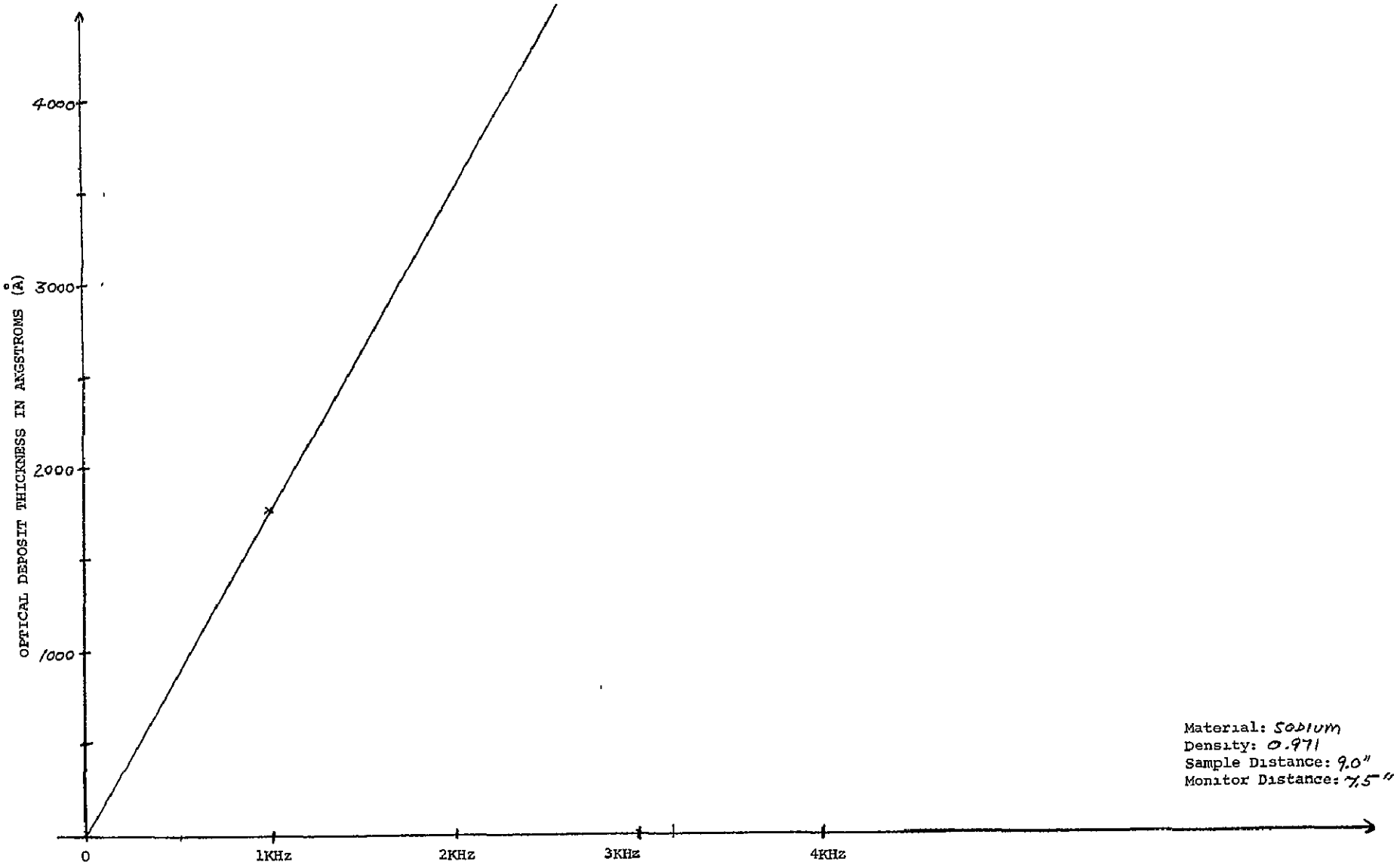

Figure 34

Sodium - Coating Thickness versus Monitor Frequency

Figure 34

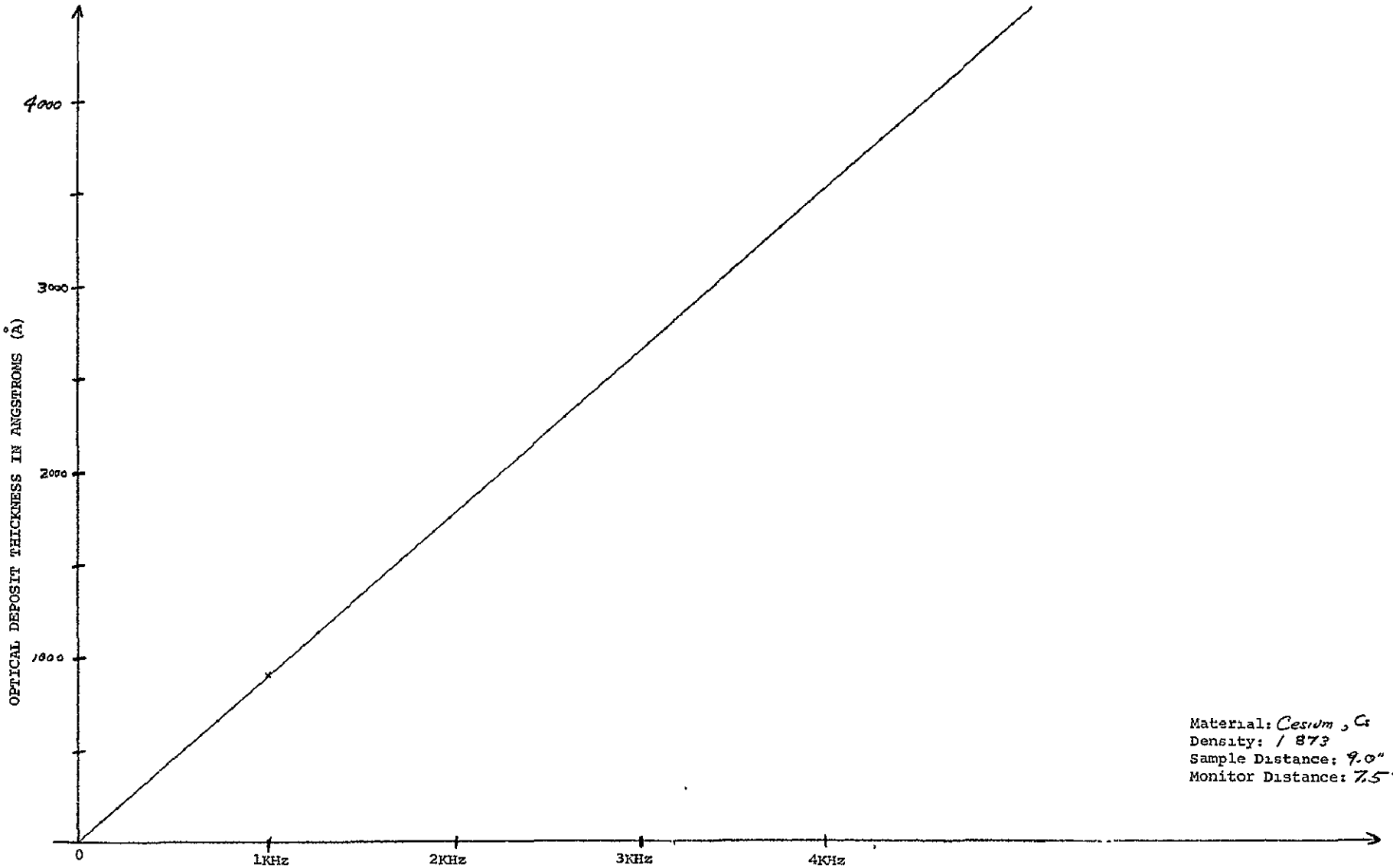

Figure 35

Cesium - Coating Thickness versus Monitor Frequency

Calibration of Detectors - Establishment of Absolute Quantum Efficiency

In order to establish the actual quantum efficiency (Q.E.) obtained by the ATR technique, it is necessary to perform absolute Q.E. measurements in the monochromator/vacuum chamber system. The establishment of standard sources and calibration in the near ultra violet has been done with great difficulty in the past and our experience is no exception.

We have obtained two calibrated thermocouples (T.C.) from Charles Reeder, Inc. These units were calibrated using a tungsten standard lamp with black body irradiance at the detector window of 46.2 watts/cm^2. The primary calibrating source had almost no U.V. output. We have assumed our thermocouples have a good blackbody absorbtion characteristic down to 1900Å which, as anyone who has tried to make UV reflectors understands, is a reasonable assumption.[43] The thermocouple window is BaF_2 and is transparent to 1500Å.

As an example one T.C. has a sensitivity of 12.98μV/μW and it has a 21Ω internal impedance.

Using the following scaling factors at 2000Å

9.93×10^{-12} ergs per photon @ λ = 2000Å

1μ watt $\cong 10^{14}$ photons/second ±2%

For our T.C. the scale factor would then be

$$\frac{12.98\mu V}{\mu W} \qquad \frac{\mu W}{10^{14}\text{photon/second}} = \frac{12.98\mu V}{10^{14}\text{photons/sec.}}$$

or $\underline{1\mu V = 7.70 \times 10^{12}}$ photons/second.

Using the T.C. to calibrate our RCA 7200 photometer, we obtained in our system: (using mercury line 2537Å)

$$1 \text{ volt} = \underline{3.16 \times 10^{7} \text{ photons/sec.}} \text{ @ } 2537\text{Å for photometer/reflectometer}$$

1μ volt = 31.6 photons/sec.

Across 1 megohm 1μ Amp = 3.16×10^{7} photons/sec.

NOTE: Since all detectors were calibrated and cross checked using the same chopper and synchronous amplifier, no scaling due to duty cycle or amplifier characteristics need be done.

Calculations-Thermocouple

0.001496 Lumens = 1 watt;

$h = 6.624 \times 10^{-27}$ erg.sec

1 Joule = 1 watt-sec $= 10^{7}$ ergs

$\lambda = 2000\text{Å} = 0.2 \times 10^{-6}$ m

$\Sigma = h\nu$;

$$\nu = \frac{c}{\lambda}$$

$$\nu h = \frac{ch}{\lambda} = \Sigma = \frac{3 \times 10^{8} \text{ m/s} \times 6.624 \times 10^{-27} \text{ meter-erg}}{2 \times 10^{-7} \text{ m}}$$

$$\Sigma_{\nu h} = 9.93 \times 10^{-12} \text{ ergs/photon}$$

$$= 9.93 \times 10^{-19} \text{ Joule/photon (watt-sec/photon)}$$

1 photon/second = 9.93×10^{-19} watts = 9.93×10^{-13} μwatts

$$P = E^2/R = E^2/21\Omega$$

$$E^2 = 21 \times 9.93 \times 10^{-13} \mu\text{watts ohms} = 209 \times 10^{-13} \mu \text{ volts}^2$$

$$E_{h\nu} = 4.57 \times 10^{-7} \mu\text{Volts/photon}$$

$1\mu watt_{T.C.} = 1.007 \times 10^{14}$ photons/sec @ 2000Å

Calculations - Photometer

Type 7200 RCA Photomultiplier

S/N U35340

Cathode Sensitivity 54.0 μA/Lumen

Anode Sensitivity 26A/Lumen @ 1KV

65×10^{3} A/watt*

Dark Current 6×10^{-9} Amp. (@20A/Lumen)

Anode sensitivity 26A/Lumen or 65000A/watt

$S_A = 0.065$ A/μwatt

Measured dark current was 200mv in $10^{7}\Omega$

$$\frac{v}{\Omega} = \frac{2\times10^{-1}}{10^{7}} = 2\times10^{-8}\text{A} = 0.02\mu\text{A}$$

which is within a factor of 4 of specified value.

$$\frac{2 \times 10^{-8}\text{A}}{0.065\text{A}/\mu\text{watt}} = 30.8\times10^{-8}\mu\text{watt} = 3.08\times10^{-7}\mu\text{watt}$$

1μ watt (@ 2000Å) = 1.007×10^{14} photons/sec.

$1.007 \times 10^{14} \times 3.08 \times 10^{-7} = 3.1 \times 10^{7}$ photons dark level

---

Since the photometer is primarily used for relative measurements of energy incident vs. energy reflected, it can operate at a higher level of illumination and the high level of dark current is not relevant.

---

* Luminous and power sensitivities are not related in UV tubes.

As a check on the stability of the calibration of the thermocouple and photometer a constant radio-active UV source was used whose output remains constant to 1½% per year. Included in this report for reference are calibration curves for our UV standard radio-active source. Sources for blue and green regions of the spectrum are being used at present.

Total radiated flux from the source is evaluated using our Reeder Thermocouple which is flat to 1400Å. Relative emittance is obtained from graph in Figures 36 and 37, which is specifically prepared for each source. Note that the source has relatively broad band emittance over a very wide range.

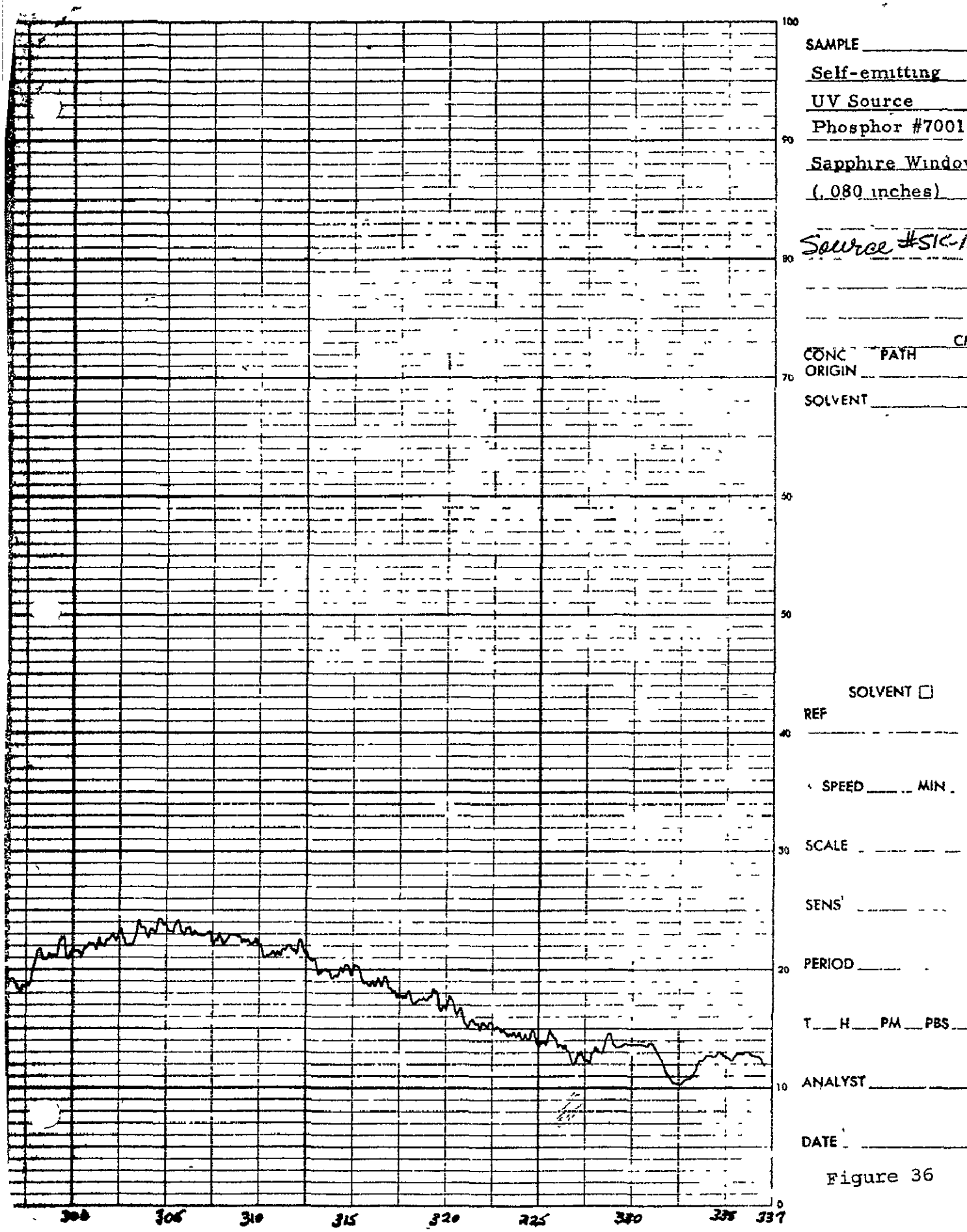
SAMPLE
Self-emitting
UV Source
Phosphor #7001
Sapphire Window
(.080 inches)
Source #SIC-10
CM
CONC PATH
ORIGIN
SOLVENT
SOLVENT
REF
SPEED MIN
SCALE
SENS
PERIOD
T H PM PBS
ANALYST
DATE
100
90
80
70
60
50
40
30
20
10
0
300
305
310
315
320
325
330
335
337
nM/M

Figure 36

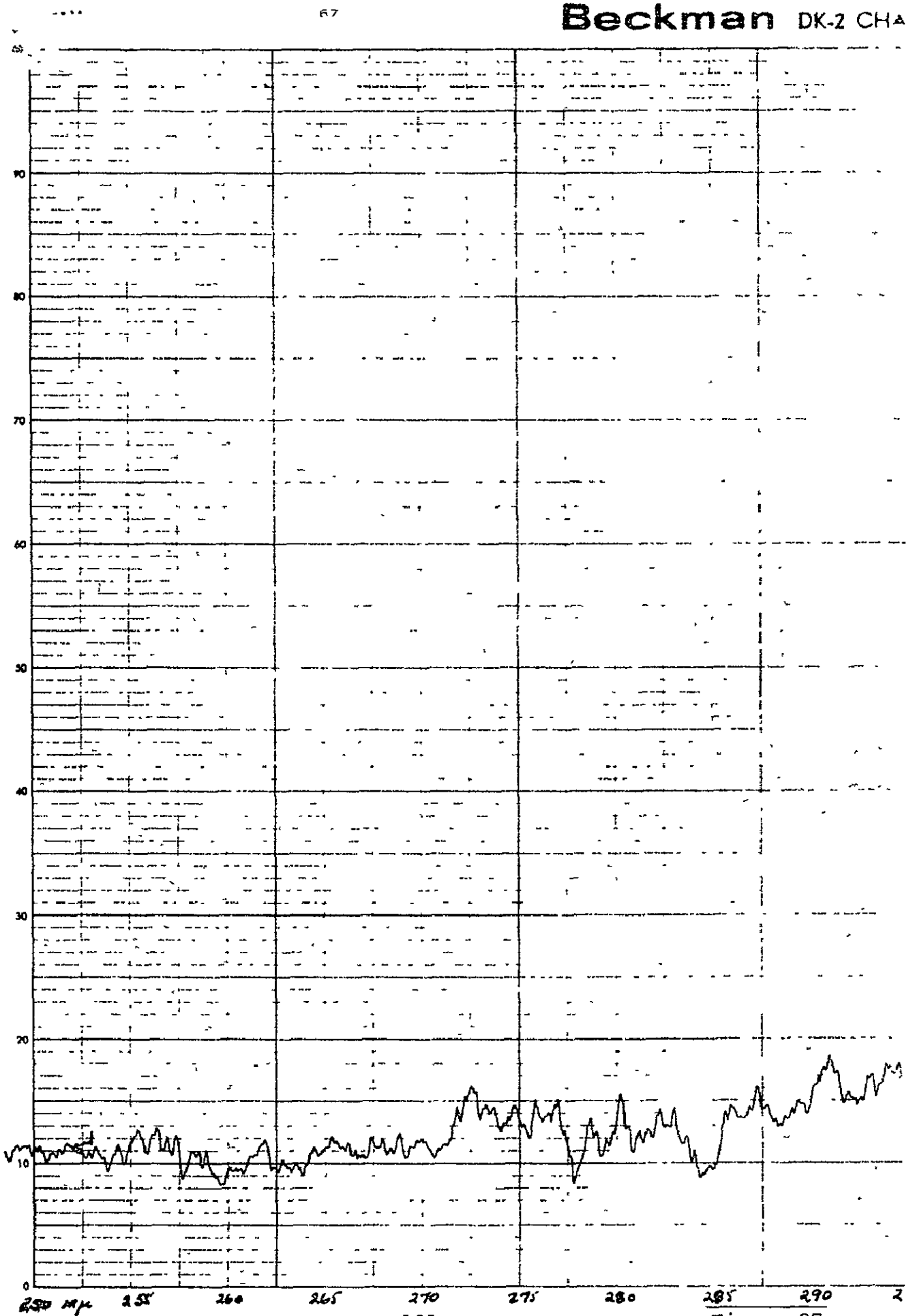
Beckman DK-2 CHA
90
80
70
60
50
40
30
20
10
0
250 mμ
255
260
265
270
275
280
285
290

Figure 37

XI. Results and Recommendations

Summary of Conclusions and Results

1. Relative quantum efficiency improvements of 100% (a factor of 2) with thin gold layers have been obtained. This corresponds to a 100% ± 20% gain in absolute quantum efficiency over commercially reported Gold cathodes in transmission or reflection (approximately 10^{-4} electrons per photon, peaked at 2000Å).

2. We have established techniques for producing monolayers and thicker coatings of Gold, Platinum, Aluminum, Magnesium, Cesium, Sodium and Potassium with accuracies of ± 5Å for the heavier metals and ± 20Å for the light metals. Preliminary techniques have also been established for coatings of Magnesium, Sodium, Potassium, and Cesium with a required accuracy inside a previously sealed envelope.

3. Our study has resulted in the fabrication of a high quantum efficiency metallic totally solar blind cathode of Magnesium.

4. Gold solar blind cathodes with extremely rapid wavelength cutoff have been produced. We feel, however, these cathodes are still far from optimum and even greater improvement is possible with further work in the ultra violet.

5. We have demonstrated some of the characteristics of ultra thin cathodes and have compared the results to date with theoretical calculations. In those areas we feel our data is most reliable (quantum efficiency vs. angle) significant agreement has resulted. Other areas (absolute absorbtion vs. angle and vs. polarization) are still undergoing refinements so that we may put more faith in our measurement technique.

6. For thin films of Gold, Aluminum, Platinum, Magnesium and the alkali metals very little uniform data is available concerning optical parameters. We have had to establish at least the approximate values of n and k by examining absorbtion of the coatings. Using the present experimental technique fore knowledge of n and k would only establish a region of coating thickness within which experiments would have to be carried on. The optimum thickness for best absorption enhancement must still be determined by experiment.

7. Alkali metal cathodes have been produced by indirect chemical reactions with peak quantum efficiencies from 1 to 5%. This approaches the quantum efficiency of the alkali antimonide cathodes with pure alkali metals. Further work on alkali metals is proceeding.

Review of Previous Results

Plots of several solar blind cathode materials, gathered from various manufacturers and recent literature, are combined to scale in Figure 38. The particular cathodes of interest for this report are Gold and Magnesium with a peak QE of 10^{-4} at 2000Å and a QE of 1.5×10^{-5} at 2500Å for Gold. Note the complete lack of visible response tail.

For an optimum solar blind cathode, Block recommends Magnesium metal over Cs_2Te for the following reasons:

1. The long "visible response tail" of Cs_2Te is thought to be due to an absence of excess Cs in the cathode.[41,42] The exact nature of the visible response is not yet completely understood by manufacturers and has yet to be uniformly controlled.

TYPICAL SOLAR BLIND CATHODES (WITHOUT ATR)

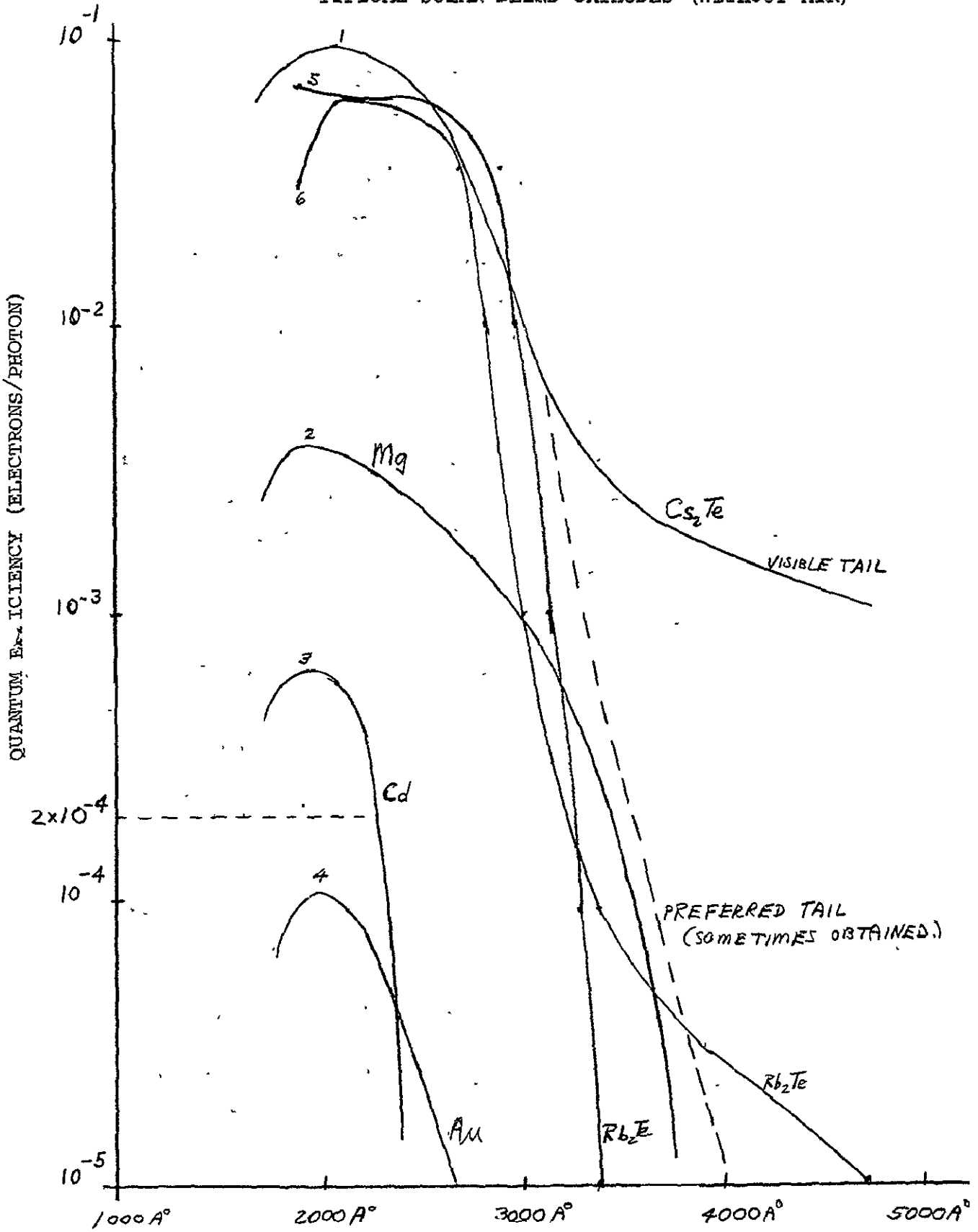

Figure 38

ERS 6/10/68

GRAPH E

2. Magnesium is amenable to theoretical ATR enhancement of almost a factor of 10 with a two pass prism system. It would have no visible tail, since enhancement can be made to scale all wavelengths almost uniformly and can be peaked at 2000-2200Å.

3. Magnesium could compete favorably with Cs_2Te in QE while being much more immune to poisoning and degradation. Our maximum enhancement is shown as dotted line on curve at 2×10^{-4}.

Reference sources: (curves)

1, 2, 3, 4, EMR Photomultiplier Division
EMR-Ascop

5, 6 Kretschmar, A Solar Blind Photodiode Having Maximum Sensitivity in the Middle Ultraviolet, NOLC, Corona, Report No. 554, 15 October 1961.

Gold Cathodes

Figure 39 illustrates the actual photoelectronic current vs. angle for a thin gold cathode. The pertinent data are indicated on the graph sheet. Only four runs, of the ten performed, are included here for clarity. Figures 40 and 41 are averages of ten runs, with a standard deviation of 3% in readings, for two different cathode thicknesses. Actual quantum efficiency level was obtained using a calibrated UV thermocouple with BaF2 window supplied and calibrated by Charles Reeder (blackbody source calibration). See calibration of detectors.

A line corresponding to a quantum yield of $10^{-4} \pm 20\%$ (our estimated calibration error) is drawn on the y axis to illustrate typical peak behavior of competitive Gold, solar blind, commercial, cathodes. Typical response curves for solar blind cathodes, and for Gold are shown in Figure 39.

The runs plotted represent the response to the band of wavelengths from 1900Å to 2537Å. The response between 0-10° cannot be measured due to vignetting of the input beam by the retro-reflecting mirror. We do not consider this a serious problem.

It should be noted, from absorption graphs and our enhancement curves for 25Å and 20Å cathodes, that the thinner coatings were superior cathodes. Here is proof that a thinner layer can be made a more efficient photoemitter by enhancing its absorption. The assumed k = 3 of the theoretical curves is probably on the low side and, in agreement with several other workers, the actual k_2 for thin Gold film in the UV may actually approach 4 or 5.

Absorption vs. angle measurements have been made and correlate roughly with the theoretical graphs. The calibration of the absorption photometer has been an extremely difficult and tedious process. The long optical paths involved in getting the light beam into and again out of the vacuum chamber have made the reliability of this measurement somewhat questionable and is included primarily since it represents a check on our optimization procedure, rather than an absolute confirmation of our theory.

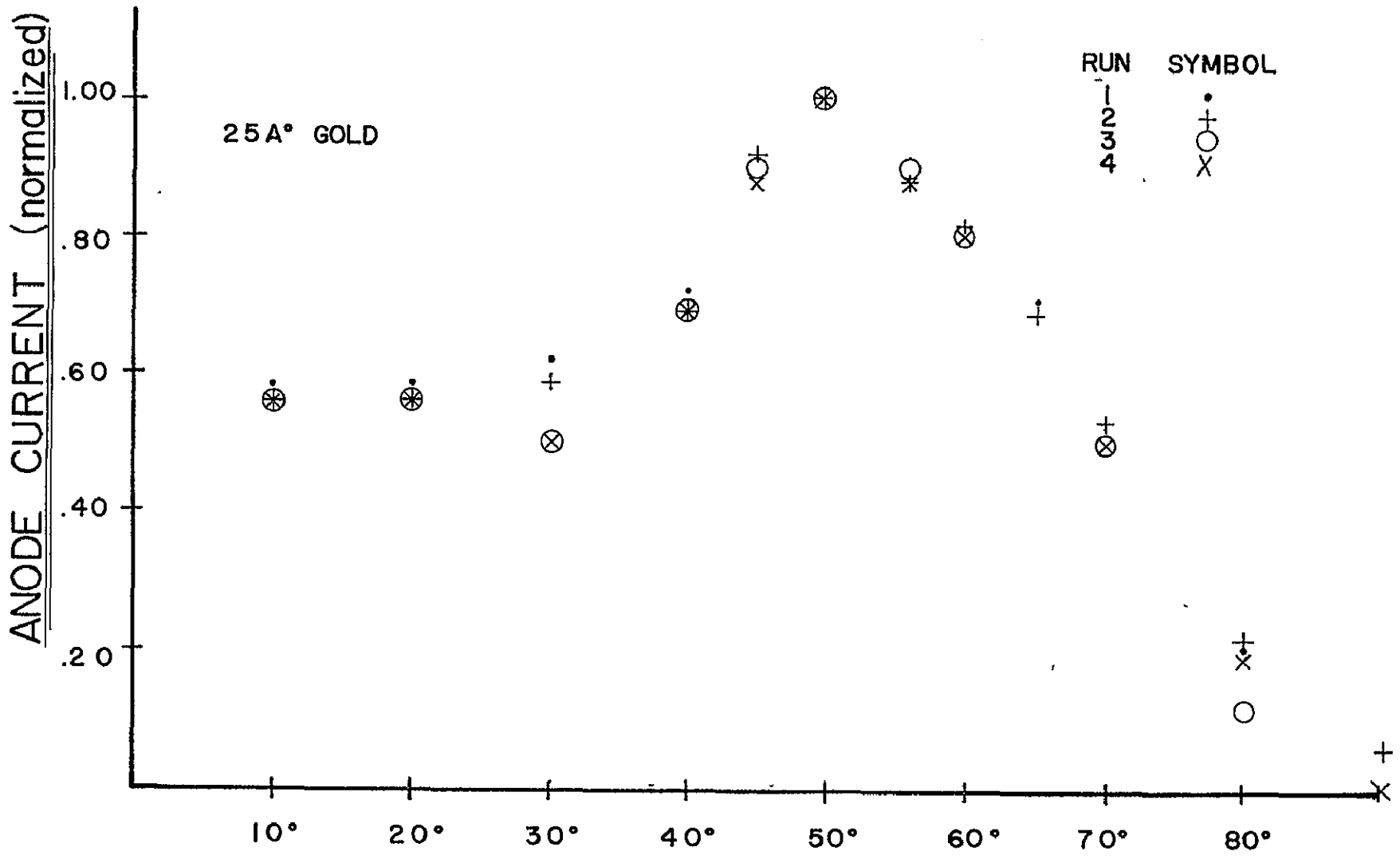

Fig. 39

-108-

NI=1.53, N2≃3, K2≃.5
H/Lmda.= 0.01 avg.
H=25A°, Lmda.=1900-2500A°

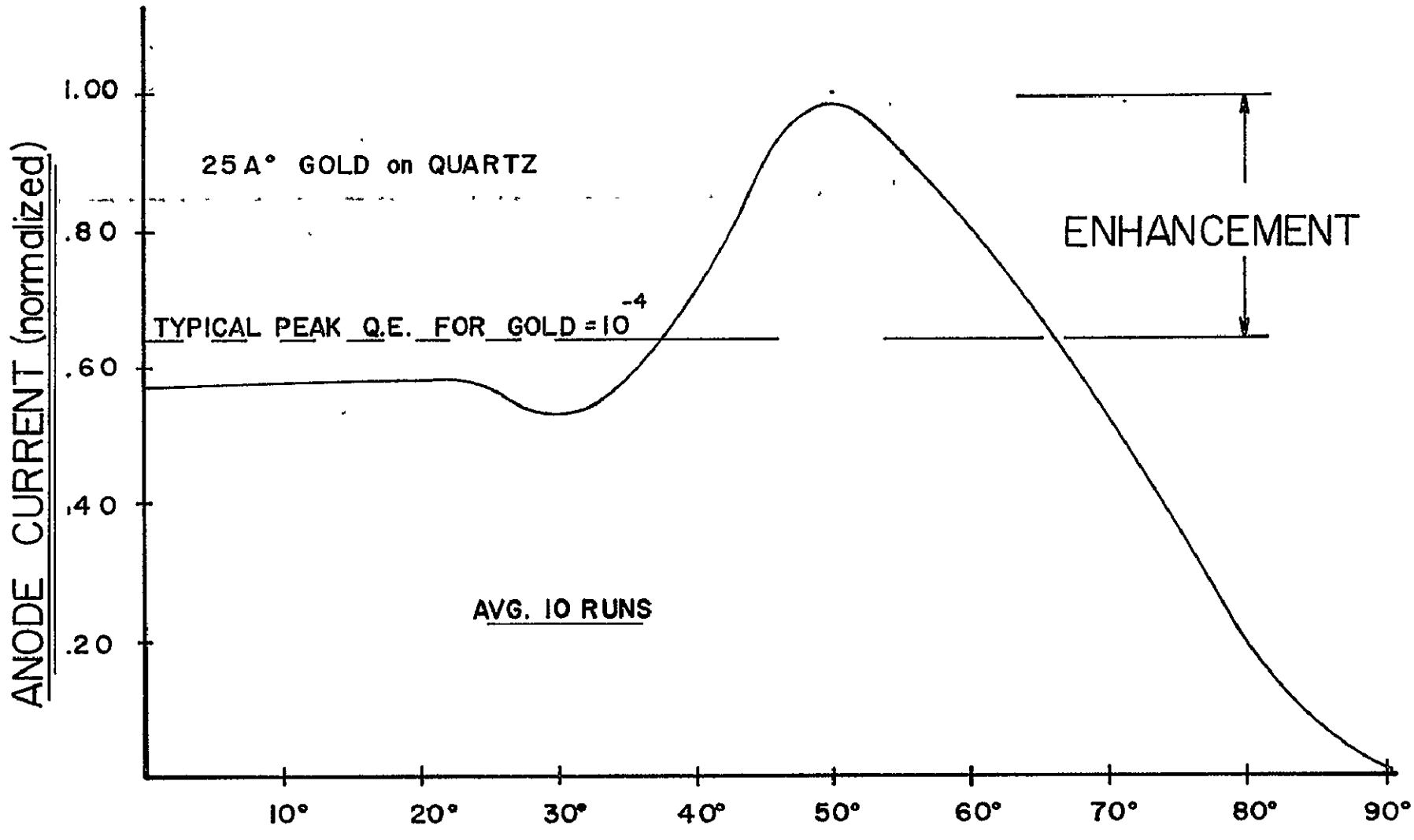

Fig. 40

N1=1.53 , N2 ≈ 3, K2 ≈ .5
H/Lmda.= .001 avg.
H = 25 A°, Lmdd. = 1900-2500A°

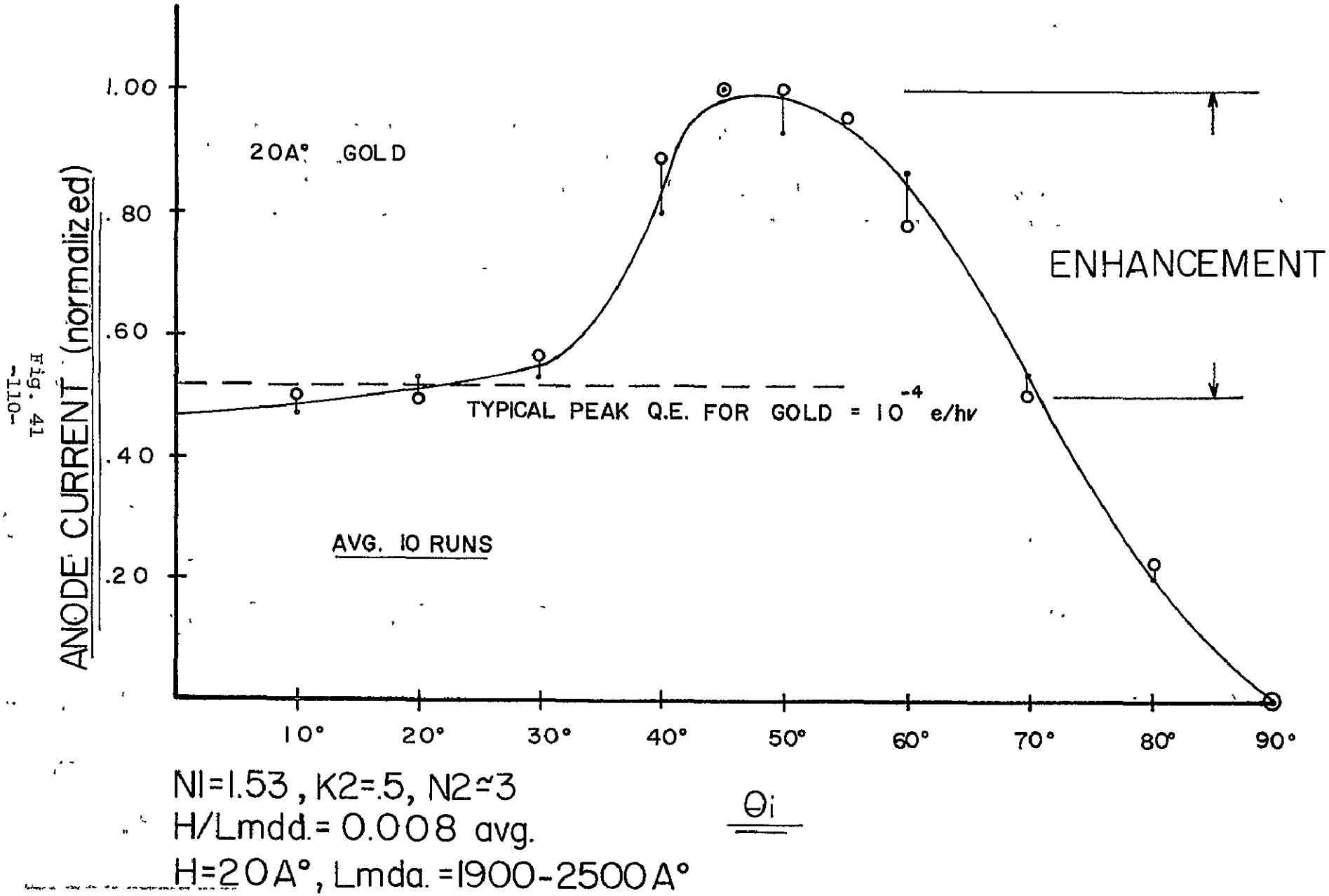

Fig. 41

N1=1.53, K2=.5, N2≃3

H/Lmdd.= 0.008 avg.

H=20A°, Lmda. =1900-2500A°

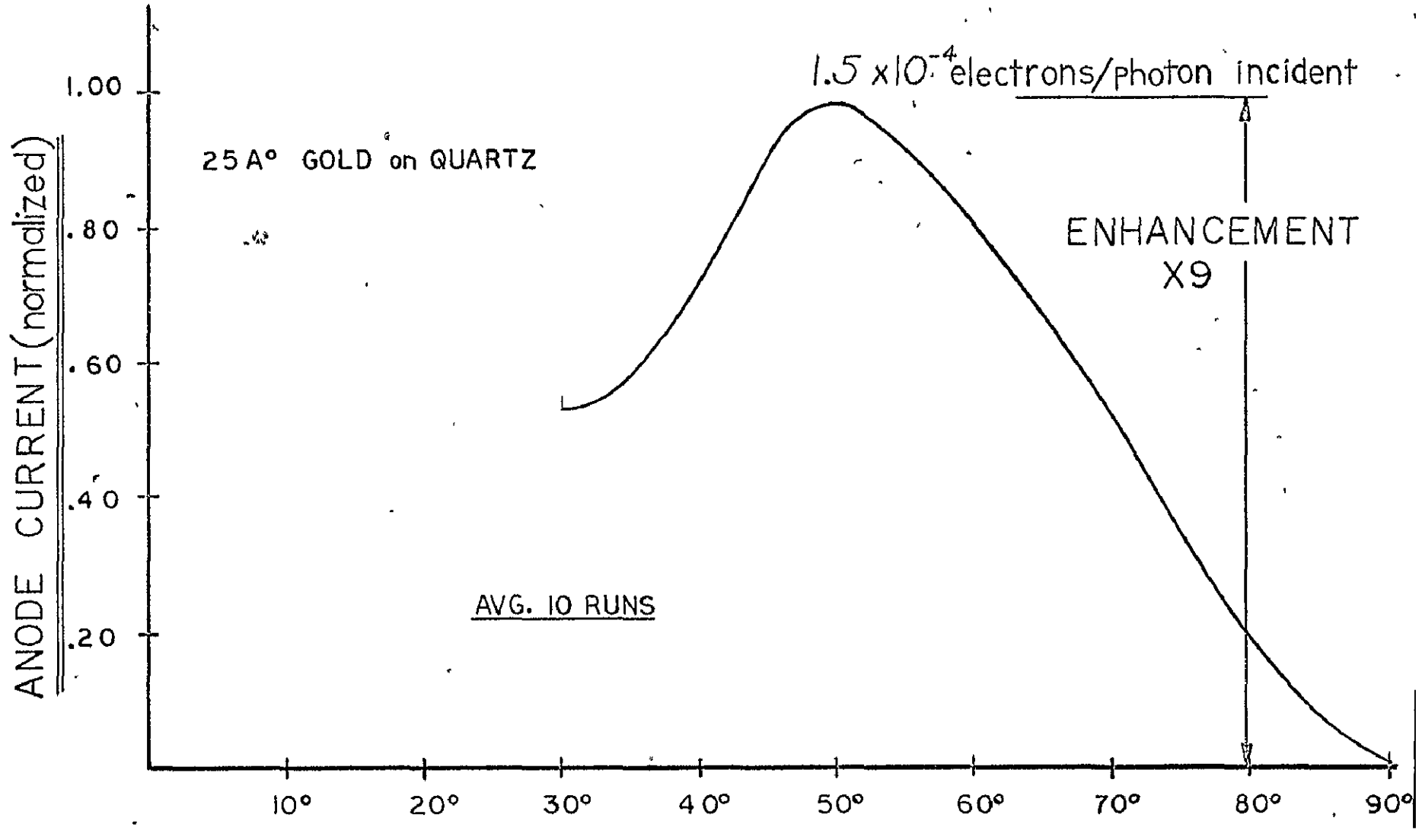

N1=1.53', N2≃3, K2≃.5
H/Lmda.= 0.01 avg.
H=25 A°, Lmda.=2537 A°

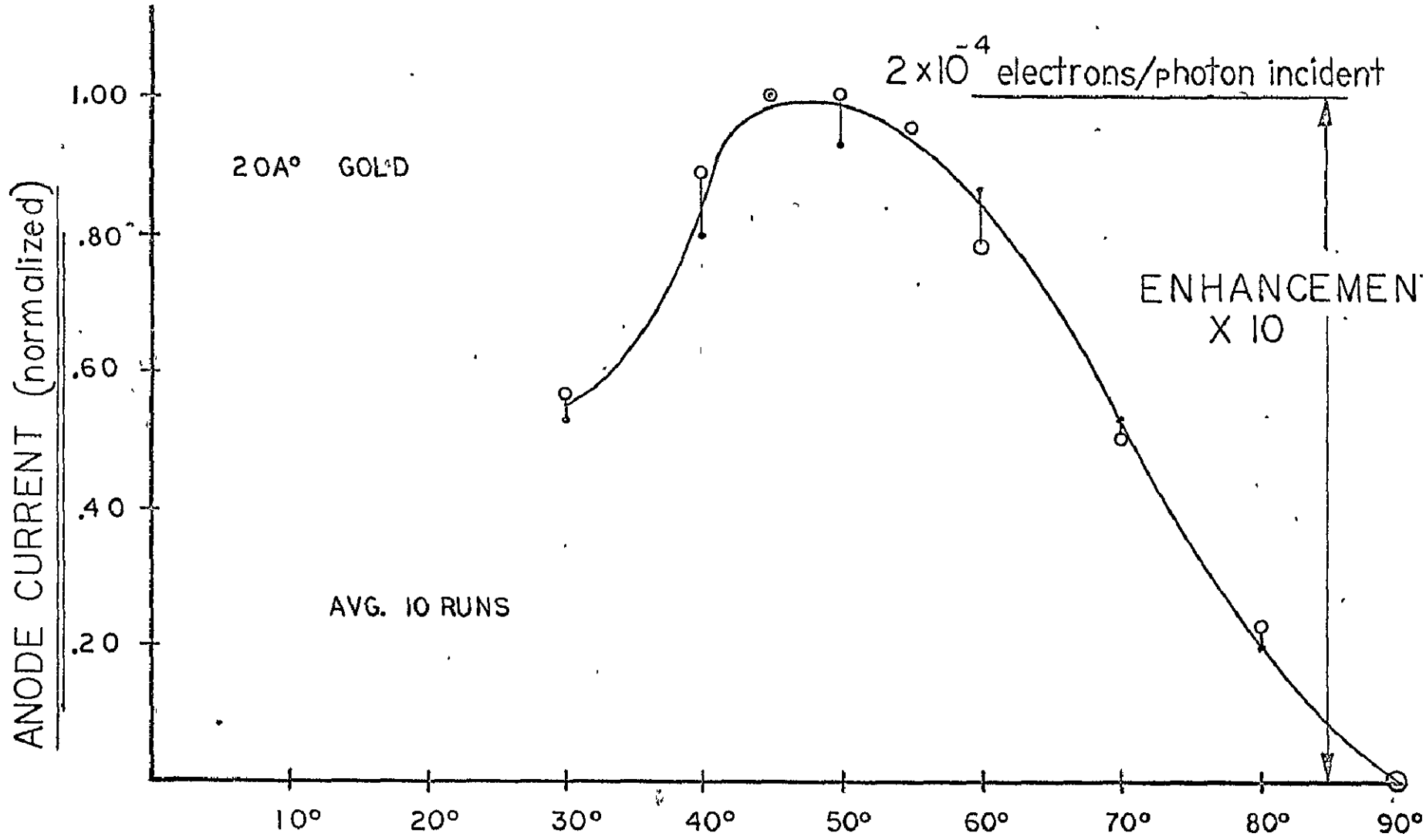

N1=1.53, K2=.5, N2≃3
H/Lmda.= 0.008 avg.
H=20A°, Lmda.=2537A°

Magnesium Cathode

As a temporary conclusion to the ultra violet phase of this work, an optimized Magnesium cathode was deposited on the quartz hemicylinder. A 40Å thickness appeared to be optimum for a single pass, however only brief measurements were made at very low illumination levels. Further optimization would certainly be possible, however this work clearly indicated no response measurable in the cathode at wavelengths longer than 3200Å. This data is being analyzed and is included in the research report along with interpreted data on the alkali metal cathodes.

Alkali Metal Cathodes

The cathode coatings for use in the violet and blue regions of the visible spectrum are considerably thicker than those which must be used in the ultra violet and vacuum ultra violet region of the spectrum. In fact, the estimated coating thicknesses progress from 75 to 200Å in thickness for the blue and visible regions, compared to 5, 10 and 50Å thicknesses in the ultra violet region of the spectrum. Optimum thickness must be determined by experiment.

We have on hand computer plotted graphs for all of the previously described cathodes, coated on a material of index 1.3 such as the fluorides. Such materials are unnecessary in the visible spectral region and are needlessly expensive. The possibility of contamination and cathode poisoning are also increased by the use of halogen substrates and we have been given to understand by manufacturers that the possibility of coating multi-alkali cathodes on such substrates is extremely remote. A program for generating curves for sapphire substrates (where $n_1 = 1.7$) has been completed in order to evaluate input aperture improvements possible due to the higher index of the substrate.

Calibration

In order to establish actual quantum efficiencies at various wavelengths, a Reeder thermocouple was used to calibrate the input energy in watts per cm^2 at the cathode. A quartz iodine source (2900°K) and monochromator (grating blazed for 3000Å) were used during this procedure and the calibration curve in Figure 46 takes into account the combined output response of the entire illumination system. All spectral curves shown in the data section have been normalized to the curve illustrated in Figure 46.

ALKALI METALS

Sodium

Only one preliminary curve of sodium is shown and it is for a relatively thick (200Å) cathode. The response peak is well into the ultra-violet and indicates the cathode thickness is far above optimum for sodium even though the peak quantum efficiency, 5×10^{-3}, is relatively high. A typical work function for sodium is 2.29 electron volts corresponding to a λ_{max} of about 5800Å. Our cutoff at 3250Å definitely indicates an ATR cathode which is much too thick. Most materials, metals in particular, become less transparent in the ultra-violet and the shift of the peak response toward the UV indicates that the cathode is absorbing significantly more radiation at the short wavelengths and hence the cathode thickness is well past the optimum absorbtion thickness for this material. Figure 47 further illustrates the typical extremely rapid cutoffs we have obtained with almost all thin cathodes in general. Since the expected response of sodium would have extended well out to at least 5000Å (if optimum response was obtained), it was not anticipated

that the UV source would be needed for this particular work and consequently the curve appears severely skewed to the short wavelength side of the available spectral response range. Only the incandescent source was used for the alkali metals.

Potassium

Figure 48 and 49 illustrate spectral response for two different coating thicknesses of potassium on quartz. The thicknesses illustrated are 100 and 200Å respectively with the 100Å thickness of potassium exhibiting the higher peak quantum efficiency. The flatening of the response tail toward the ultraviolet illustrated in Figure 49 is probably due to the fact that the material is becoming more effective an absorber as the illumination extends further into the UV.

The increase in response at longer wavelengths in the thinner cathode indicates the approach toward an optimum thickness, which is probably somewhat less than 100Å for potassium. The cathode is not thin enough to illustrate an extended red response of any significant magnitude. We expect that this extended red response would begin to make itself apparent at thicknesses from 50Å down to 10Å. Again, as with most of the ATR cathodes, the response curve becomes more broad as the optimum thickness is approached. This broadening is present in spectral response and angular response.

Cesium

In Figure 50 we illustrate an average of several runs obtained with a 200Å thick coating of cesium. We experienced great difficulty in coating cesium in controlled layers due to instabilities noted in the deposit thickness monitor. These instabilities took some time to correct and in the time remaining

for useful work under this program we made as many runs as possible using a relatively thick cesium cathode. Again our peak quantum efficiency of 3×10^{-2} is significantly higher than has been reported before with cesium cathodes of a much thicker nature. An additional series of tests performed using deposited monolayers of cesium on a quartz substrate proved fruitless, either because the lateral resistence of such a cathode is so high or because the monolayer of cesium may possibly have become contaminated due to adsorbed impurities on the surface of the quartz. This is less of a problem as the cathode grows thicker and may not have been noticed with the thicker cathodes. It is interesting to note that the major deviation in data from run to run occurred at the relatively low angles of incidence between 25° and 45° and that the uniformity of response with angle from 45° to 75° was significantly greater. This is illustrated by the 3 cross marks superposed on the graph in Figure 50, located on the 35°, 40°, and 45° lines. These illustrate the lowest response obtained during any run, and serve to indicate the type of deviation between tests which was typically present during this series. Further details on the interpretation of the cesium, potassium, and sodium data are available in the Research Report which has been forwarded to NASA Ames under separate cover.

QUANTUM EFFICIENCY MEASUREMENT

Material: Mg

Thickness: 30 A°

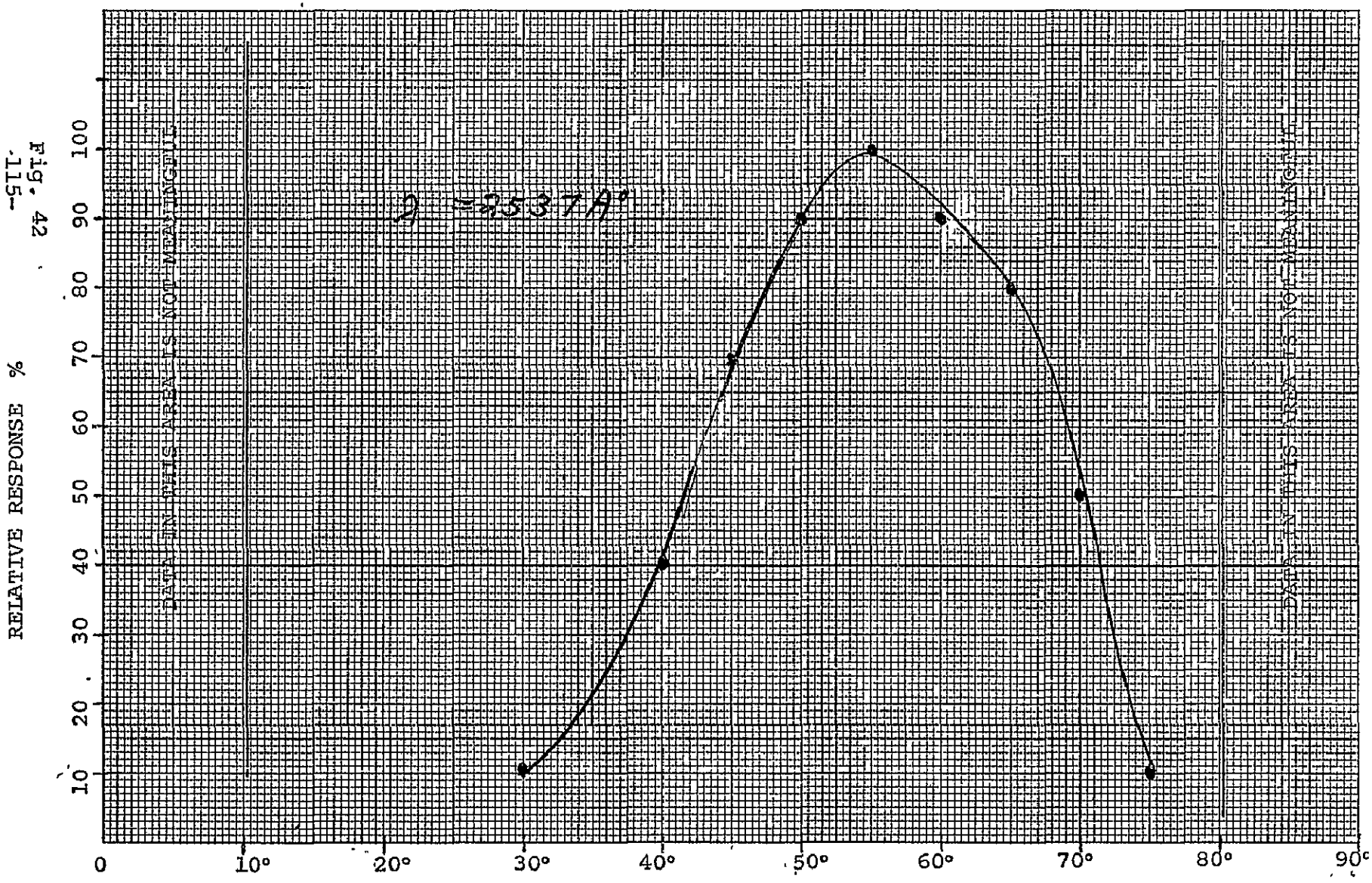

100%= 1×10^{-2} $e^-/h\nu$

Fig. 42

QUANTUM EFFICIENCY MEASUREMENT

Material: Mg

Thickness: 40A°V

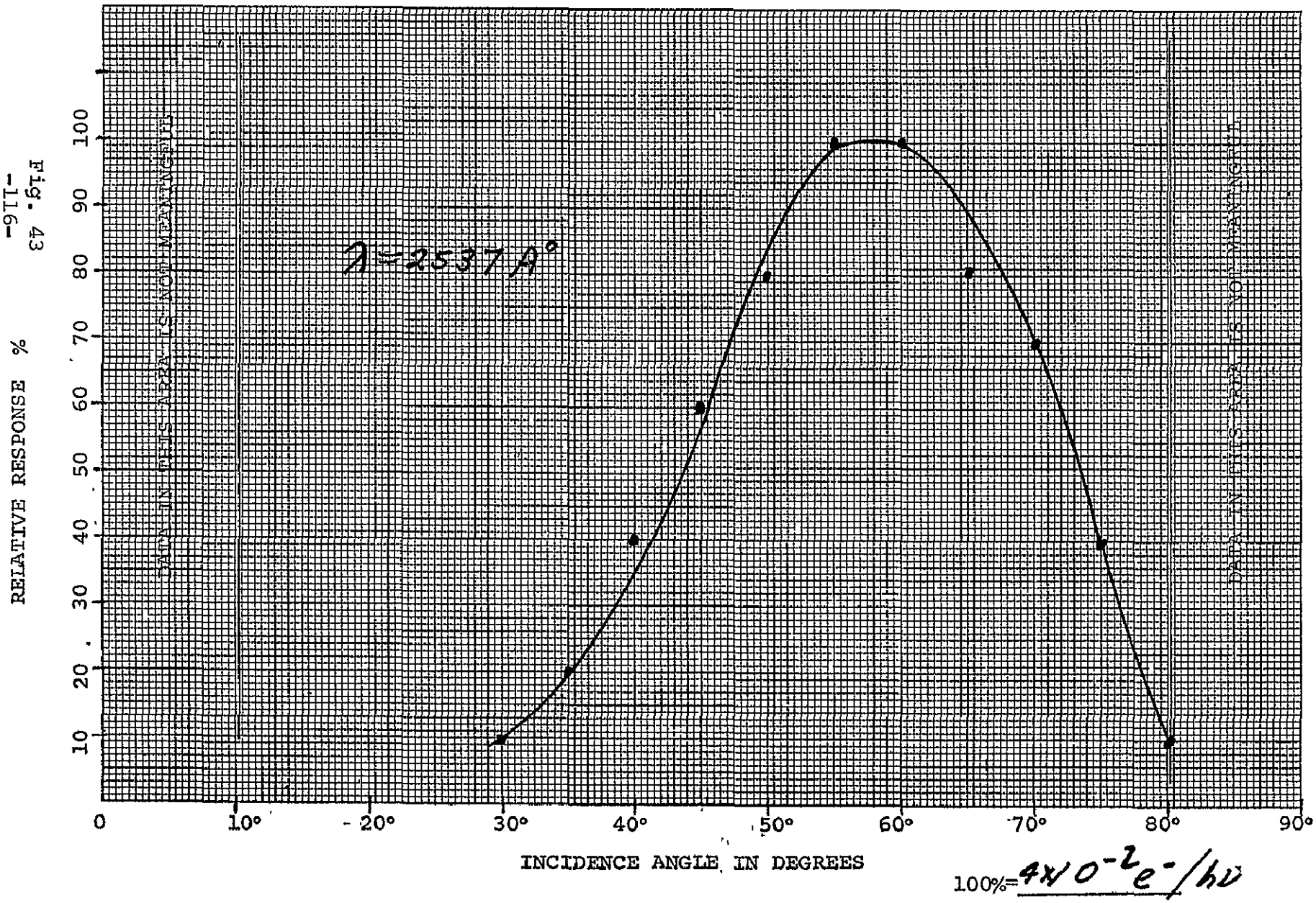

Fig. 43

QUANTUM EFFICIENCY MEASUREMENT

Material: Mg

Thickness: 60 A°

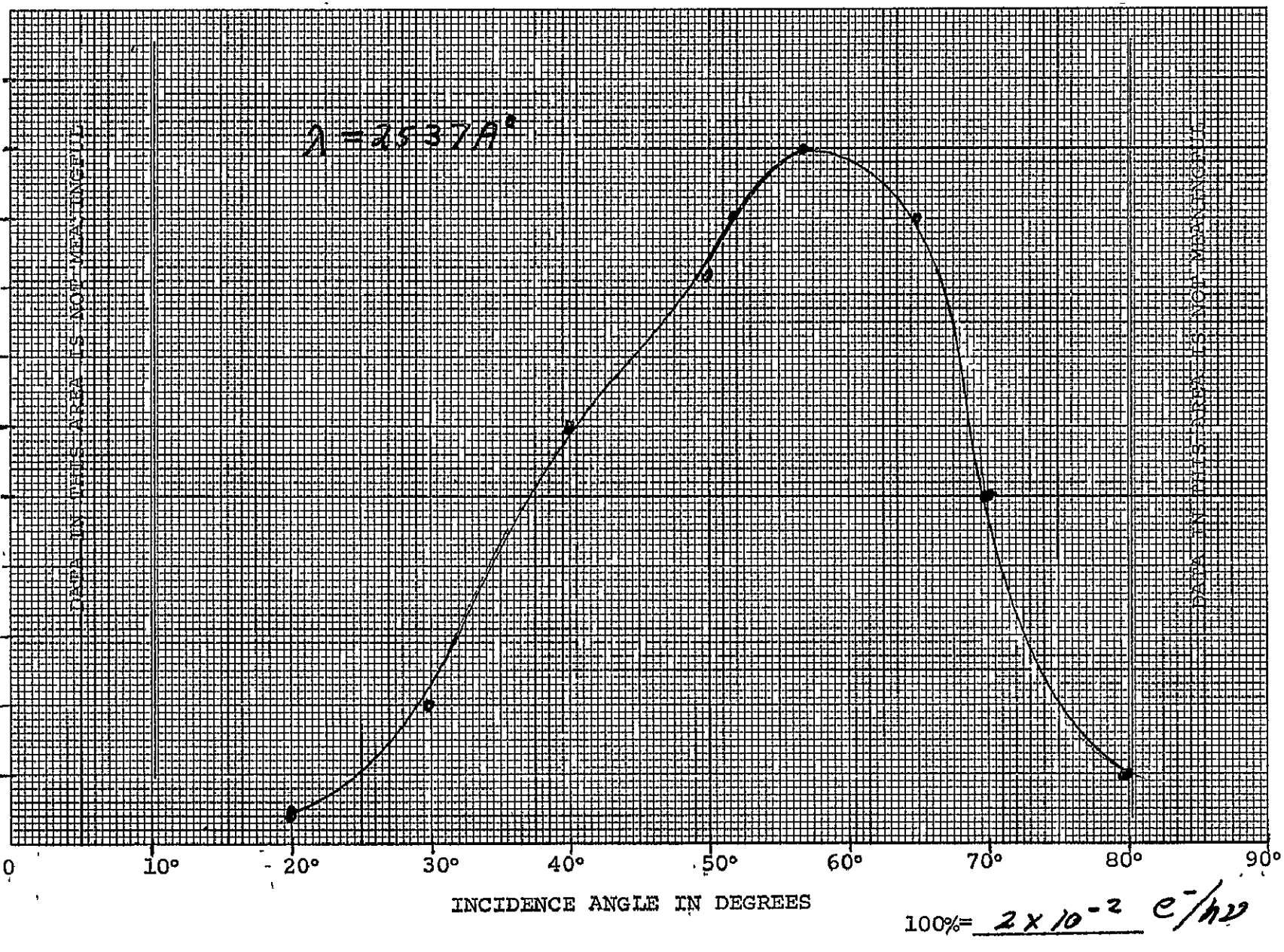

100%= 2 x 10⁻² e⁻/hν

Fig. 44

WAVELENGTH RESPONSE TEST

Incidence Angle: 50°

Source: Hg High pressure

Dynode: RCA 10^6

Material: Mg

Thickness: 40 A°

Peak Q° E°: 3×10^{-2} $\epsilon^-/h\nu$

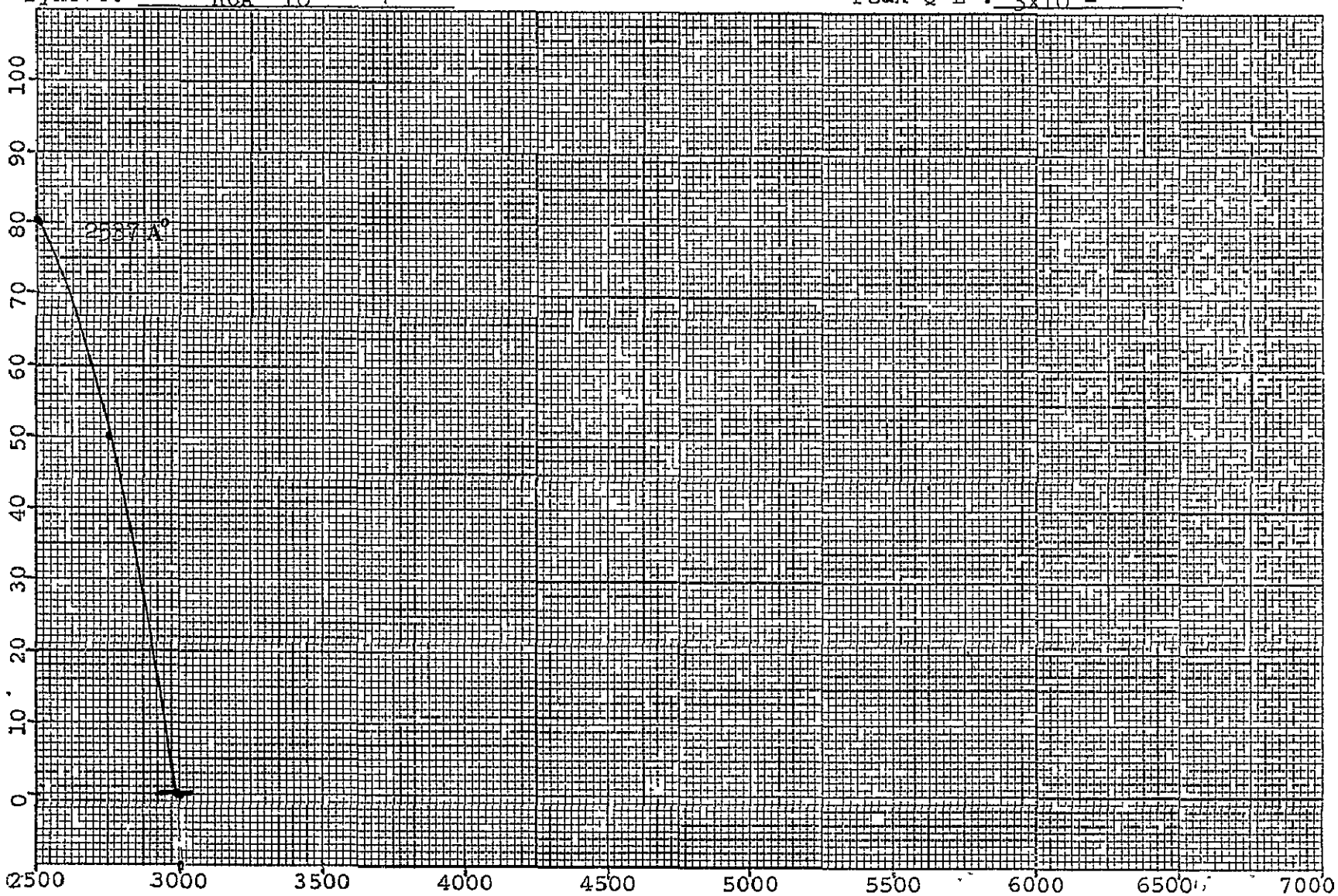

Technician: ERS

Date: 6/18/69

Fig. 45

WAVELENGTH RESPONSE TEST

Incidence Angle: _____

Source: CALIBRATION

Dynode: _____

REEDER THERMOCOUPLE

Material: _____

Thickness: _____

Peak Q° E° : _____

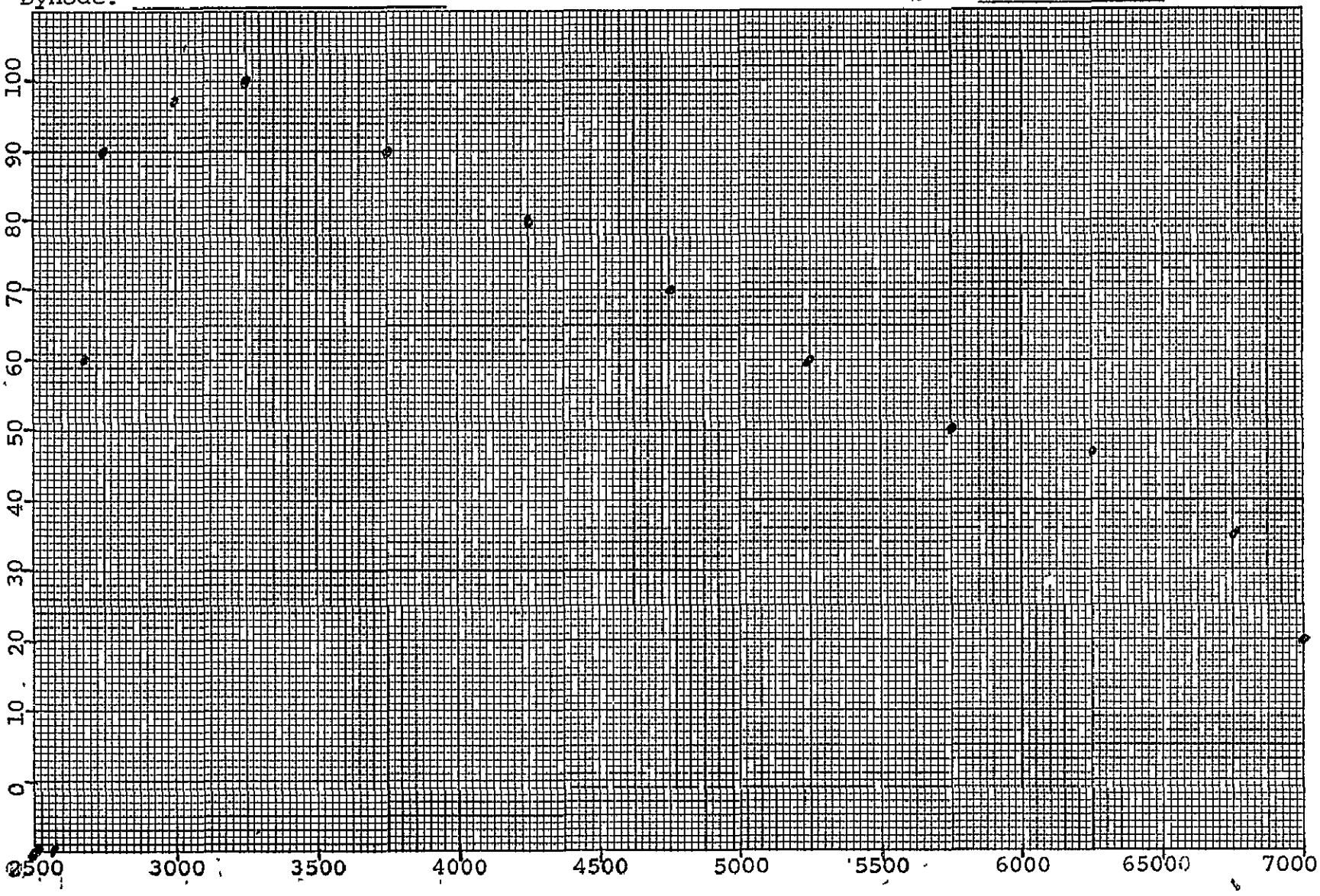

Fig. 46

Technician: ERS

Date: 6/3/69

File: Cal.

WAVELENGTH RESPONSE TEST

Incidence Angle: 60°

Source: Quartz I

Dynode: 1 A x 10^6

Material: Na

Thickness: 200 A°

Peak Q°E°: 5 x 10^{-3} $e^-/h\nu$

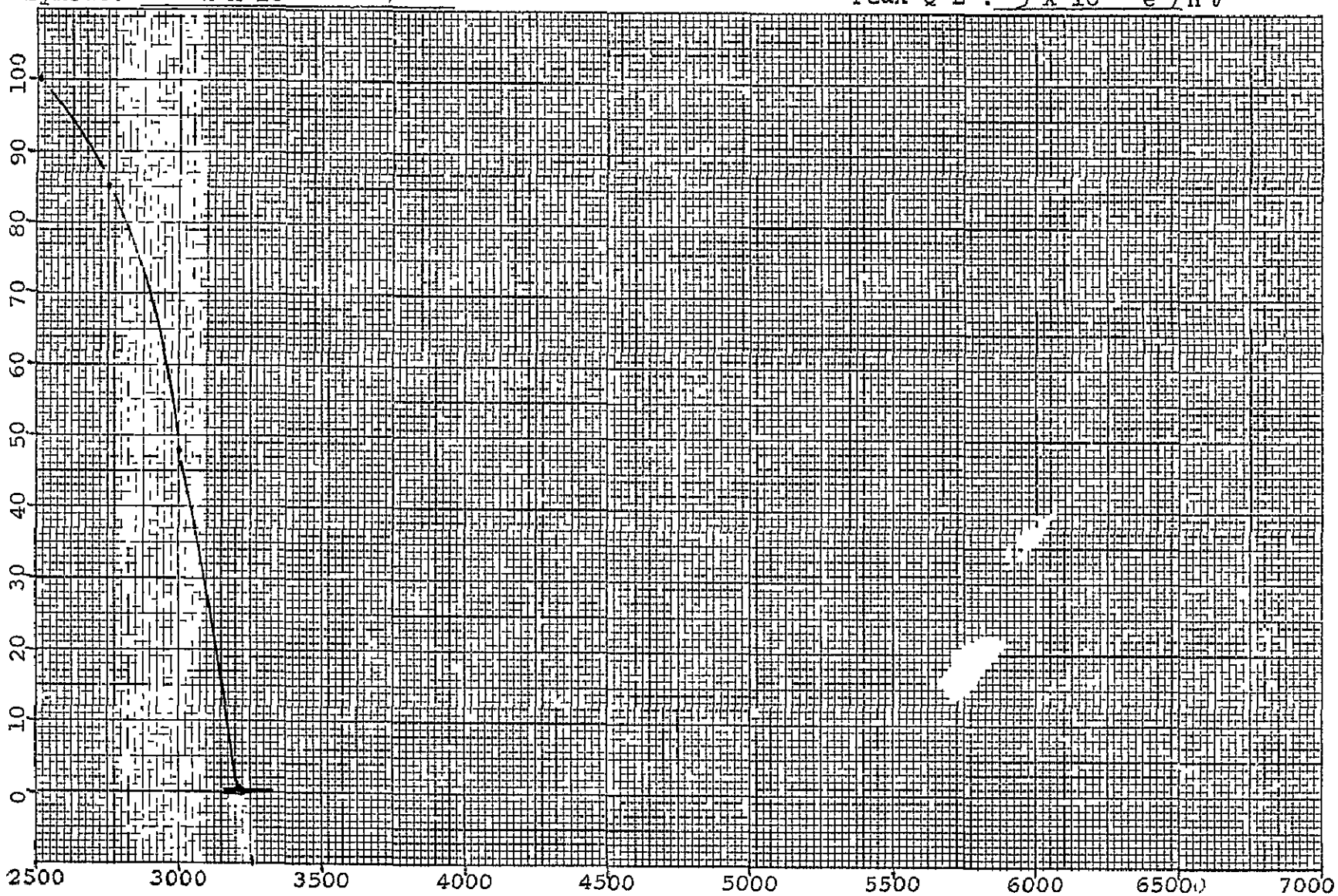

Technician:

Date: 6/13/69

File:Na

Fig. 47

WAVELENGTH RESPONSE TEST

Incidence Angle: 58°

Source: Quartz I

Dynode: RCA 106

Material: K

Thickness: 100 A°

Peak Q°E°: 1 x 10^{-2} $e^-/h\nu$

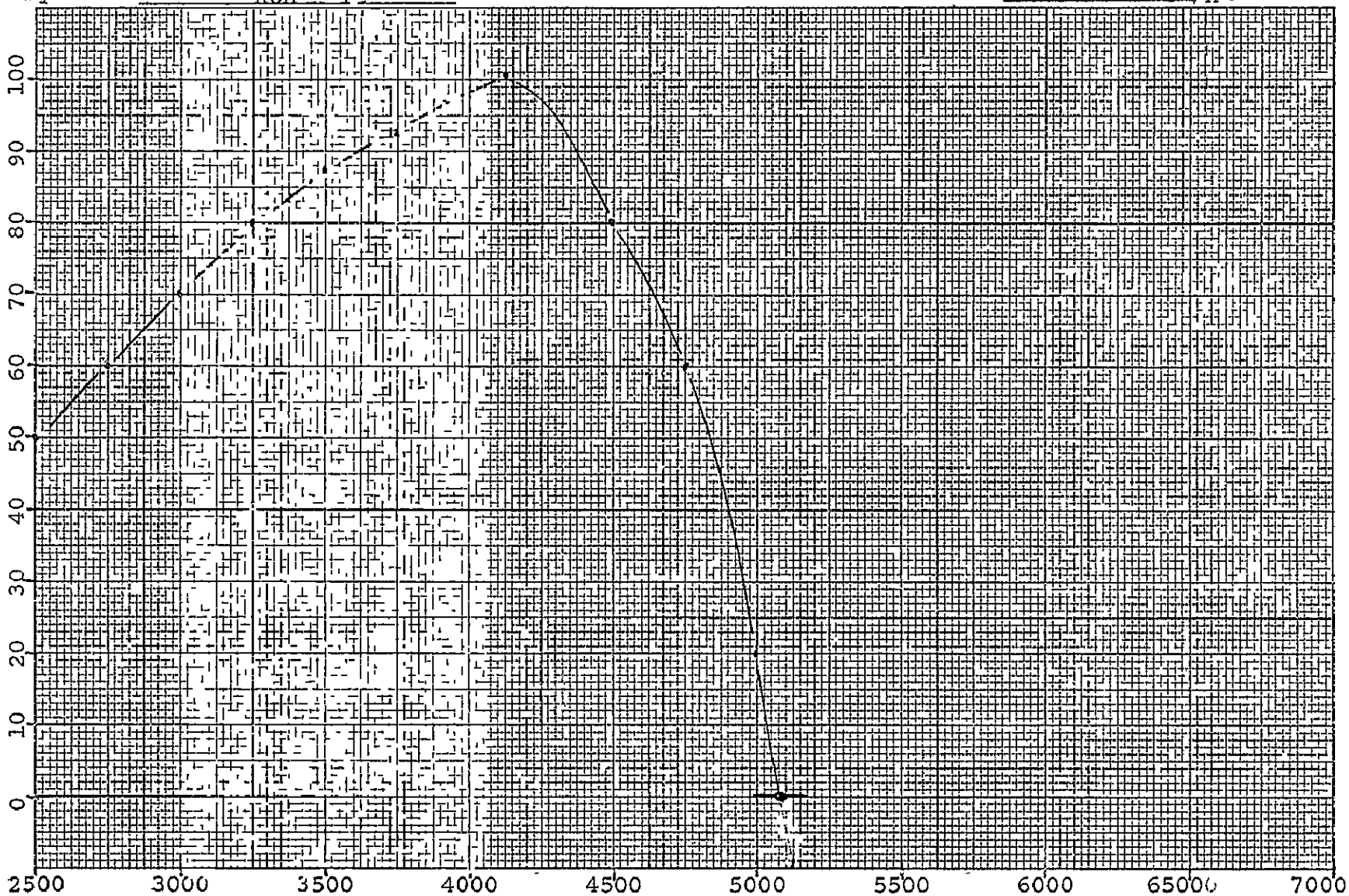

Technician:

Date: 6/10/69

File: K

Fig. 48

WAVELENGTH RESPONSE TEST

Incidence Angle: 58°

Source: Quartz I

Dynode: RCA 10^6

Material: K

Thickness: 200 A°

Peak Q° E°: 7×10^{-3} $e^-/h\nu$

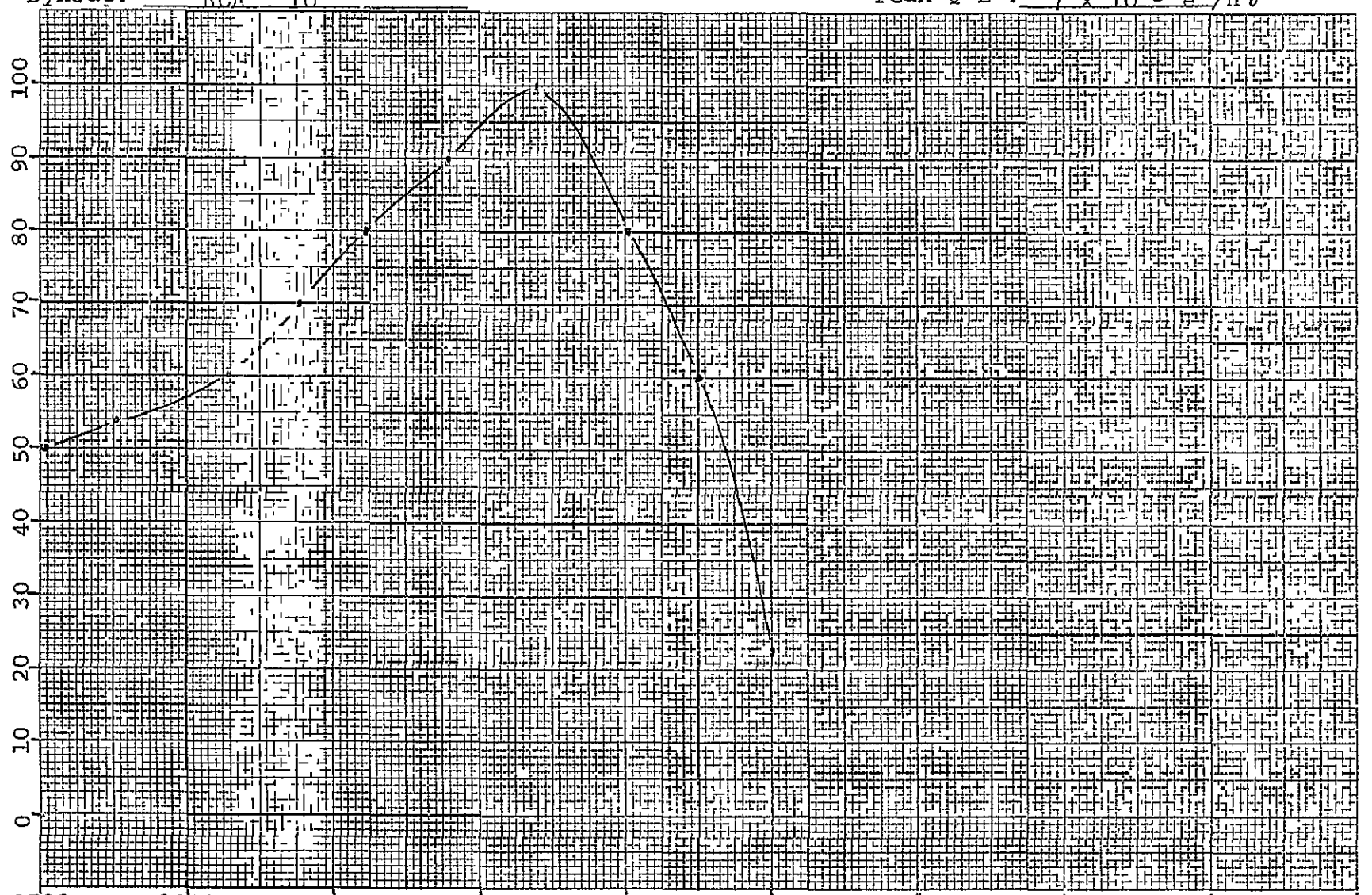

Technician: _____

Date: 6/11/69

File: K

Fig. 49

QUANTUM EFFICIENCY MEASUREMENT

Material: Cs

Thickness: 200 A°

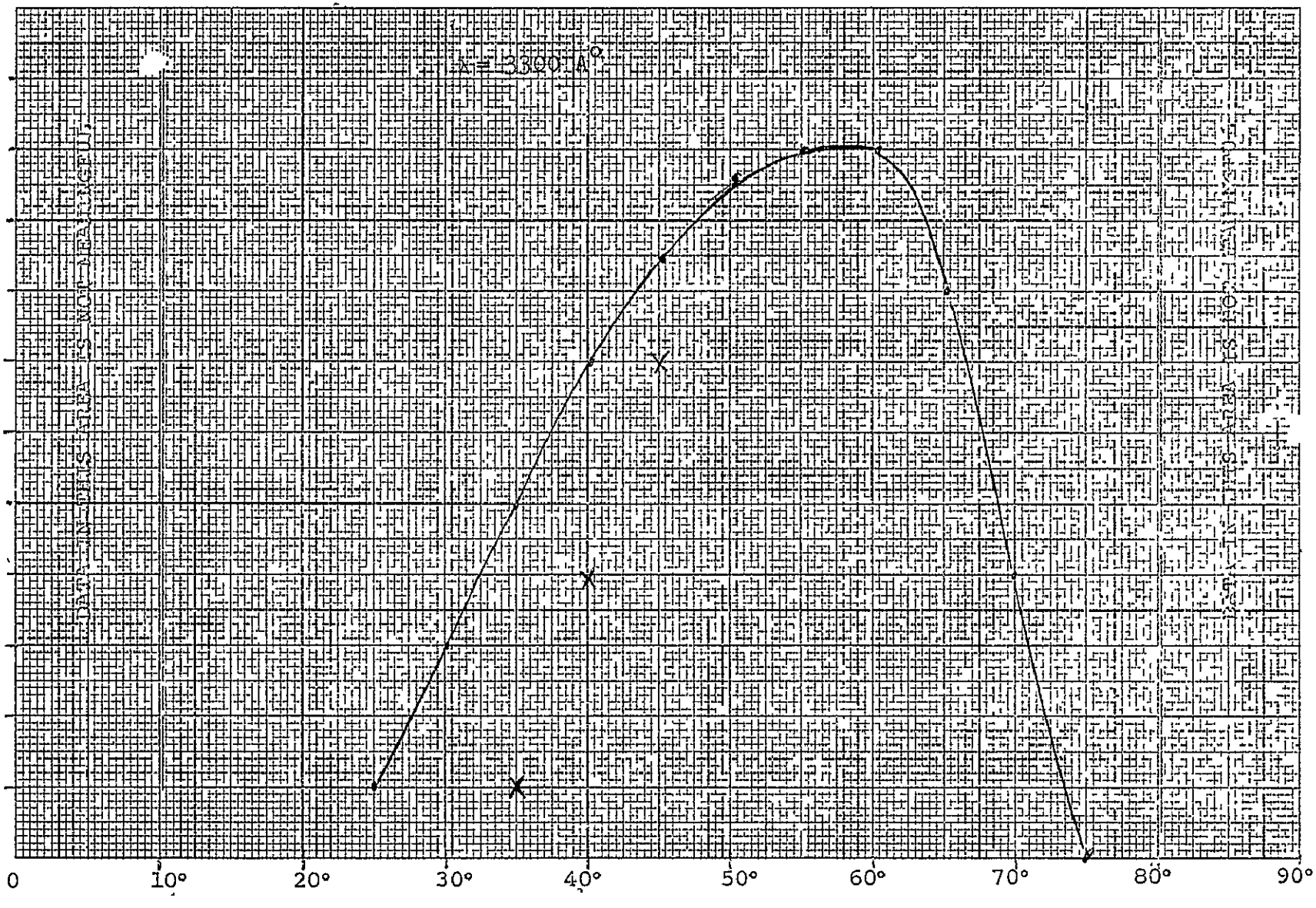

100%= 3×10^{-2} e⁻/hv

Fig. 50
-123-

Conclusions and Recommendations for Future Work

At the conclusion of this report period, Block Engineering, Inc. has demonstrated the applicability of the ATR technique successfully applied to photoemissive cathodes in the ultra violet and blue-visible regions of the spectrum. While these measurements have not led to a final design for a production photomultiplier tube employing such cathodes, they have proven the feasibility of the technique and indicated agreement between the experimental results and the theoretical equations which predict enhanced absorption of the incident radiation.

Confirmation of the different behavior of parallel and prependicularly polarized incident light add further confirmation to the theory and indicate that the present method for obtaining computer plots of absorption vs. h/λ is a sound procedure.

Difficulties in the construction of equipment to manufacture and subsequently test photocathodes without breaking vacuum took considerable effort during the program although these problems were expected. Photometer measurements of the absorption of incident radiation, even at the conclusion of the program, were not of comparable accuracy to the quantum efficiency measurements. A recommendation for future design in this area would be to incorporate a moving photomultiplier within the vacuum housing which could be moved to the appropriate angle to sense the remaining reflected light after a single pass through the hemicylindrical photocathode substrate. This would eliminate the use of the retro-reflecting quadrant mirror and its associated optical problems. Any difficulty of moving such a photomultiplier

at twice the angle of rotation of the cathode is far outweighed by the difficulty in aligning a retro-reflecting system and the difficulty in obtaining retro-reflecting components. We would recommend that future programs carrying this work further into the visible and the infrared region would utilize such a movable photomultiplier arrangement in order to confirm, with much greater accuracy than was possible during the present program, the absorbtion of the parallel and perpendicularly polarized rays vs. angle of incidence and vs. wavelength.

Block recommends retention of the present experimental equipment and technique which allows coating and immediate testing of the cathodes. A measurement of absorption of parallel and perpendicularly polarized rays could also be made versus cathode thickness. The use of hemicylinders, diffused quartz, enables the spectral range from ultra violet through the visible to be used while assuring a minimum probability of poisoning the cathode after deposition. Although the hemicylinder is not the most convenient shape to work with mechanically, it does represent probably the optimum research geometry for work on ultra thin cathodes in the ATR mode.

Further work on metal oxide cathodes of the S-1 type and a few alkali antimonides* should be carried on, if possible, with the assistance of a competent vendor for such cathodes in order to avoid the common pitfalls inherent in learning photocathode technology. Silver-oxygen-Cesium cathodes can also be investigated in thin films. In the manufacture of

---

* Cesium antimonide is the easiest semiconducting photoemissive cathode to manufacture. We recommend it be attempted first.

oxide type cathodes, Block Engineering, Inc. believes that the Attenuated Total Reflection technique and the associated accuracies required in deposition are incompatible with typical cathode manufacture, and in fact, can only be successfully carried on by people who have specialized in very accurate thin film measurements. It is for this reason that we recommend such work be carried on by ourselves although we must learn the multi-alkali cathode technology rather than cathode specialists, who must then learn ATR theory and thin film control technology, which we believe to be far more complicated.

More work should be conducted on the complex multiple internal reflection geometries. Complex geometries are possible as stated previously which allow multiple passing of the incident beam through the cathode. Among these geometries are the multi-reflection Uniline system illustrated here and the multiple reflection Unipoint system shown next which allows the use of extremely small and hence noise free cathodes

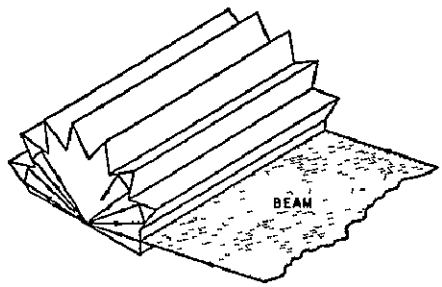

Multiple internal reflection uniline system.

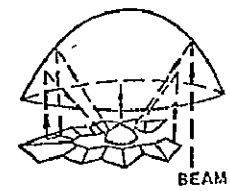

MULTIPLE INTERNAL REFLECTION UNIPOINT SYSTEM

Materials heretofore too transparent for use as cathodes can be enhanced in absorption and used as cathdoes efficiently. Such materials should be tested.

Reduced transit time dispersion results from the use of ultra thin cathodes since energy loss of emitted photoelectrons is less and consequently there is a smaller spread in their kinetic energies as they cross the cathode/vacuum interface. This effect should be investigated.

Extended infrared response may be possible if it is feasible to utilize the lower work functions found in ultra thin cathodes by other workers. ATR offers a method for effectively coupling to these cathodes.

An extension of response of the S-1 type surface to 1.6 and even 1.7 has been reported.[44] The lowering of work function is apparently due to dipole layer effects when cathodes are made so thin that the substrate surface affects their polarization. New work in Gallium Arsenide thin films has shown response to 1.6 .[45] Both references report difficulty in obtaining adequate absorption of incident photons for practical use at present.

In summary, the ATR technique offers a method for enhancing the absorption of very thin or non-absorbing cathode materials without reducing their spectral sensitivity or field-of-view.

APPENDIX I

XII. Optics

One of the main problems associated with the photometer measurement was obtaining an adequate retro-reflecting mirror for use with the optical system. The mirror must have an extremely high surface polish, be relatively rugged and of an extremely accurate figure in order that the exit beam be displaced laterally and remain exactly parallel to the entrance beam. Several vendors have tried to make this mirror, but none of the mirrors we have obtained from outside sources have exceeded the specifications which we were able to achieve in-house. Since the main purpose of this component is to achieve accurate absorbtion vs. incidence angle measurements and since the mirror is not used in the determination of absolute quantum efficiency, we have decided that extensive further investigation with this geometry is not warranted or desirable due to the large expense of obtaining additional optics in this geometry. We suggest to other workers in this field that an alternate arrangement be used whereby the reflection photometer photomultiplier be actually moved at twice the angular rate of the cathode itself. The photometer tube then monitors the reflected beam inside the vacuum chamber without attempting to re-exit the beam onto an external photometer.

XIII. Retro-reflecting Quadrant Mirror

The Retro-reflecting Quadrant Mirror (RQM) serves the purpose of redirecting the light beam, reflected from the cathode, back through the hemicylinder-displaced ¼" laterally. This redirected ray emerges from the hemicylinder parallel with the entrance beam but displaced by ¼ inch and then travels to the photometer. Although the RQM can be cut into one quadrant of the hemicylinder, this increases the cost of the hemicylinder by a large factor. Since each hemicylinder can be stripped and recoated only a few times without repolishing, it is more economical to use only one RQM and a less expensive set of hemicylinders, although alignment between the two is more tedious.

The RQM is manufactured from cut and polished type 404, or 304 stainless steel or 2024-T6 Aluminum. An overcoat of 800Å of freshly evaporated Aluminum on either substrate serves to improve UV reflectance and completes the operation. No overcoating of Silicon Monoxide can be tolerated for short wave UV work. The particular geometry used is illustrated in Figure 45.

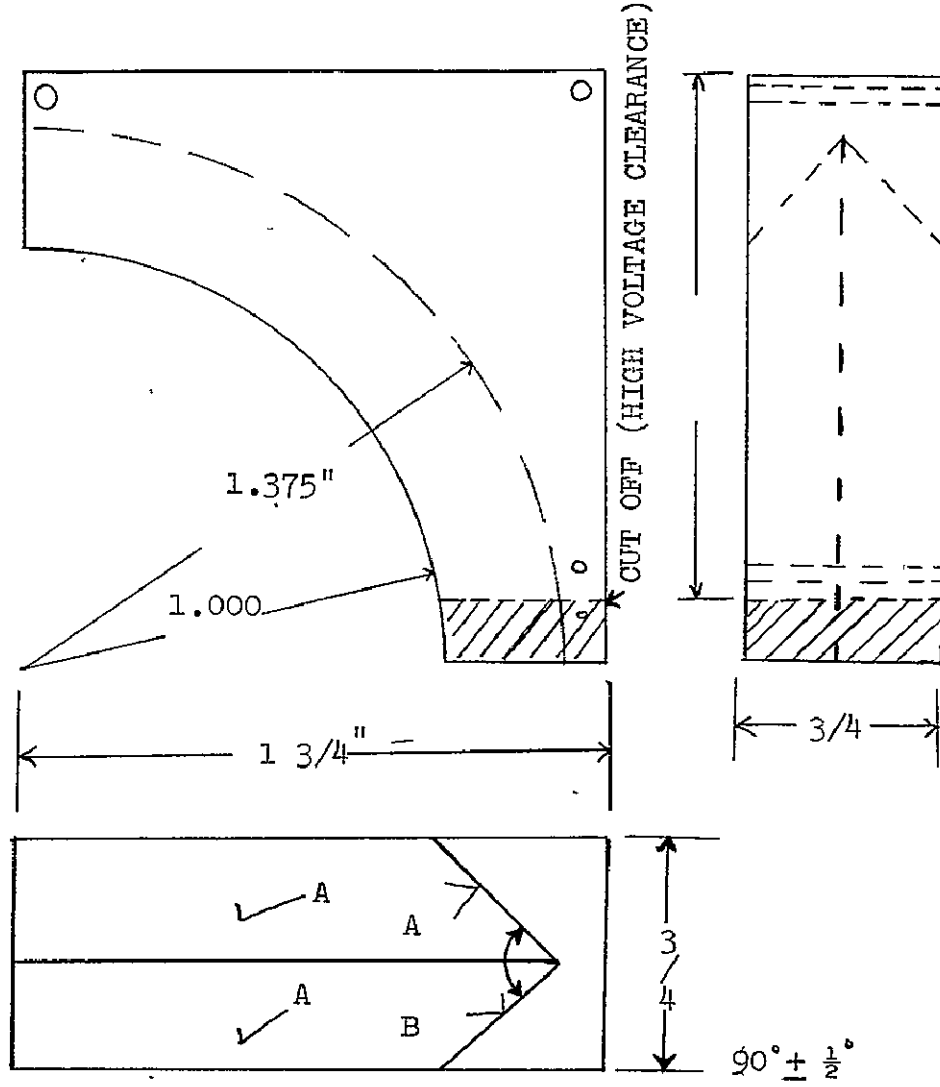

THE FINISH ON INSIDE SURFACES A&B IS CRITICAL; IT MUST TAKE ON AN OPTICAL QUALITY POLISH WITH NO SCRATCHES OR NICKS. BOTH SURFACES SHOULD BE FLAT TO ± .0001"

MATL:
304 STAINLESS OR EQUIVALENT.
LAP AND POLISH SURFACE A&B TO MIRROR FINISH.

ROUGH CUT SURFACE A&B WITH 90° MILLING CUTTER 2 3/4" DIAMETER.

RETROREFLECTING QUADRANT MIRROR

Fig. 51

XIV. Hemicylinder

Figure 46, included for reference and completeness, illustrates the working sketch used to manufacture two ATR hemicylinders inexpensively from one striation free (G.E. type 151) UV quartz window.

We have found that these specifications have provided all the necessary optical quality while retaining maximum economy. This data is included as an economy aid and suggestion for those doing similar work.

ATR HEMICYLINDRICAL LENS (UV QUARTZ)

TRIATION FREE
GE #151 QUARTZ
MADE FROM L$\frac{1}{4}$"
WINDOW 1" THICK

2 PIECES CUT AND
POLISHED FROM
BLANK SUPPLIED

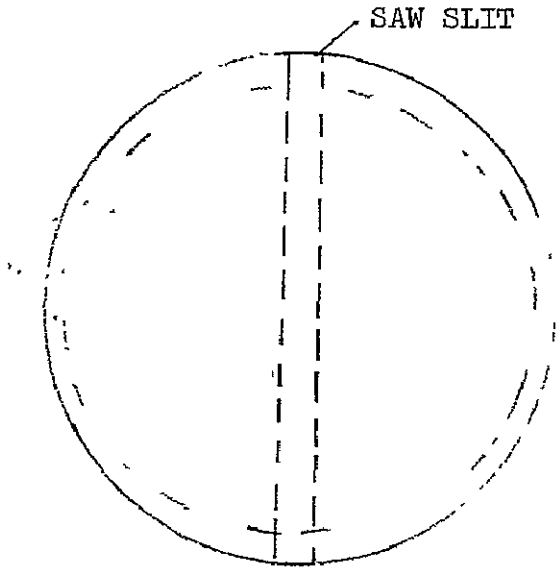

BLANK DISC
SUPPLIED

A SMOOTH OPTICAL
POLISH
NO FLATNESS
SPEC.

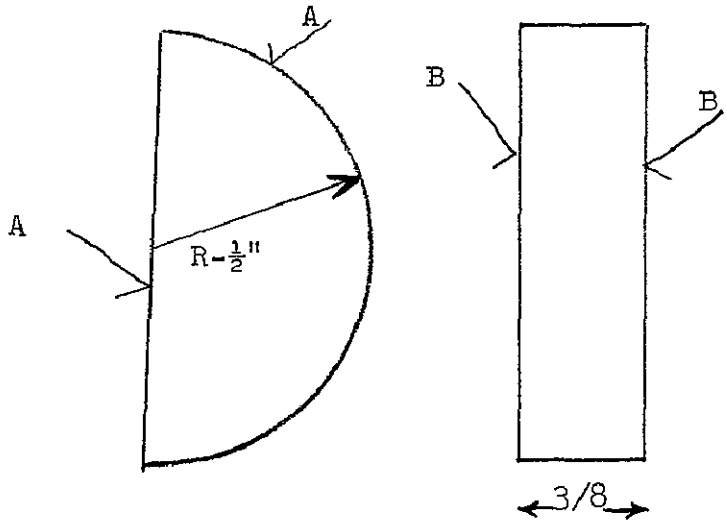

B NO FINISH SPEC.

RADIUS R = MAXIMUM DIMENSION OBTAINABLE AFTER SLITTING
MUST BE LARGER THAN ½".

XV. Multiple Internal Reflection Cathode (Multipass)

As part of the current effort, a multiple reflection substrate (Internal Reflection Element) has been proposed for the present experiments. A Calcium Fluoride prism would be optimum in the UV region, but for visible response cathodes, quartz, or even glass is more suitable. Quartz with its higher index and inert properties is unlikely to poison complex or alkali metal cathodes, but glass with a Calcium ion concentration reduces the mobility of cathode ions and hence may be a better substrate for complex multi-alkali cathodes. The proposed geometry, which is compatible with our present dynode string and coating system, is outlined in Figure 47 on the following page.

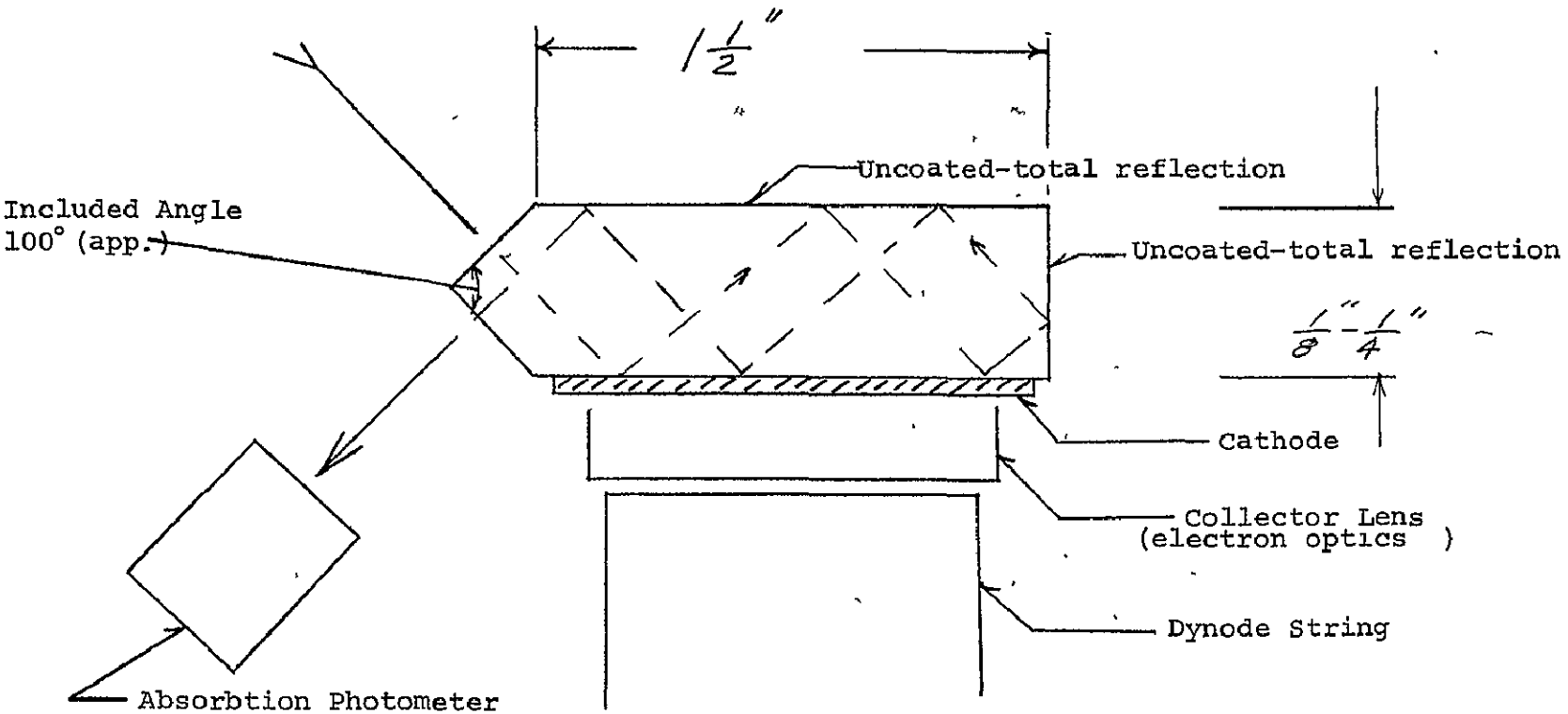

MULTIPLE INTERNAL REFLECTION ELEMENT CATHODE

Fig. 53
-134-

REFERENCES

1. Harrick, N.J., Internal Reflection Spectroscopy, Interscience, John Wiley, NY 1967, p15.

2. Ibid 1, p19.

3. Hirschfeld, Tomas, Improvements in Photomultipliers with Total Internal Reflection Sensitivity Enhancement, Applied Optics 7, 443, March 1968.

4. Ibid 3.

5. Gunter, W.D. Jr., Erickson, E.F., and Grant G.R., Enhancement of Photomultiplier Sensitivity by Total Internal Reflection, Applied Optics 4, 512(1965).

6. Hirschfeld, T., Modification in Photomultipliers with Total Internal Reflection Enhanced Sensitivity, Applied Optics 5, 1337(1966).

7. Ibid 3.

8. Tove, R.J., Personal Communication.

9. Behrndt, K.H., The Microbalance and its Evolution Since 1886, Z. Angew Physik 8, 453(1956).

10. Schildkraut, E.R., Coating Control of Oligatomic Films, Block Engineering, Inc., Internal report to be submitted as NASA Contractor Report.

11a. Hass & Thun, Physics of Thin Films, Volume IV, Academic Press 1967, p31.

b. Tolansky S., Microstructures of Surfaces Using Interferometry, American Elsevier, NY. 1968, p11-13.

12. Schildkraut , E.R., The Michelson Interferometer at Zero Order for Measurement of Film Thickness, Block Engineering, Inc., Special Report to be submitted to NASA as a Contractor Report.

13. Harrick and DuPre, "Effective Thickness of Bulk Materials and of Thin Films for Internal Reflection Spectroscopy", Applied Optics 5, 1739.

14. Stirn, R.J. and Hermann, W.A., Device for Metering a Variety of Metals for High Vacuum "Flash" Evaporation, Rev. Sci. Inst., Vol. 38, #10, pp1522, October 1967.

15. Hirschfeld Ibid 3.

16. Grant, G.R., W.D. Gunter Jr.,and E.F. Erickson, High Absolute Photocathode Sensitivity, Rev. Sci. Inst. Vol. 36 #10, 1511-12, October 1965.

17. Ibid 1, p90, 95.

18. Gold, Platinum, Magnesium, Cesium, Potassium and Sodium - See Merck Index.

19. Ibid 3.

20. Ibid 11a, p7-36.

21. Huber, E.E. Jr., The Effect of Mercury Contamination on the Work Function of Gold, Applied Physics Letters Vol. 8, #7, pp1169-72, 1 April 1966.

22. Heavens, O.S., Optical Properties of Thin Solid Films, Dover S1523, Dover NY 1955, p8.

23. Ibid 22, p25.

24. Ibid #1, p98.

25. Larach, Simon, Photoelectric Materials and Devices, D. VanNostrand NYC, p199-201, (1965).

26. Ibid. p199.

27. Ibid p199.

28. Ibid 1, p17, 27.

29. Ibid 1, p19.

30. Ibid 1, p27.

31. Krautkramer J. Ann der Phys., 32(1938) 537.

32. Ibid 13.

33. Hansen, W. T., Private Communication.

34. Jackson, John David, Classical Electrodynamics, John Wiley, NY 1962, p227,337.

35. Simon, Ivan, Infrared Radiation, VanNostrand Momentum #12, D. Van Nostrand NY 1966, p54.

36. Ibid 35.

37. Ibid 34.

38. Sutherland, J.C., Arakawa, E.T., Hamm, R.N., Optical Properties of Sodium in the Vacuum Ultra-Violet, JOSA 57, #5, May 1967, pp645-50.

39. Riegert, Richard P., Optimum Usage of Quartz Crystal Monitor-Based Devices, Sloan Instrument Corp., Alexandria, Va.

40. Ibid 22.

41. Sommer, A.H., UV-Sensitive Photoemitters, RCA Review, March 1967, Vol XXVIII, No. 1 Publication number ST-3257.

42. Taft, E. and Apker, L., Photoemission from Cesium and Rubidium Tellurides, JOSA, Vol. 43, p.81, Feb. 1953.

43. Metzger, P.H. and Cook, G.R.,"Flux Distribution of the Hopfield Helium Continuum From the Photoionization of Ar, Kr, and Xe., JOSA, Vol. 55, p.516, May 1965.

44. Von Suso Weber, "Einflus der Caesium-Komponente auf die Eigenshaften von Ag-O-Cs-Photokathoden, Zeitschrift für Augewendte Physik 19 Bond, 3, Heft, 1965, 5193-196.

45. Phillips Laboratories, H.J. Lemmens, "Cold Cathode Studies and Surface Effects During Cold Cathode Emission".